2mf

N74-28287

NASA TECHNICAL TRANSLATION NASA TT F-15,412

APPLIED PROBLEMS OF SPACE BALLISTICS

P. Ye. El'yasberg, et al., editors

(NASA-TT-F-15412) APPLIED PROBLEMS OF SPACE BALLISTICS (Scientific Translation Service) 205 p HC $13.25 CSCL 22C

N74-28287 THRU N74-28297 Unclas G3/30 42008

Translation of "Prikladnyye zadachi kosmicheskoy ballistiki," Nauka Press, Moscow, 1973, 143 pages.

NATIONAL AERONAUTICS AND SPACE ADMINISTRATION
WASHINGTON, D. C. 20546 APRIL 1974

N74-28288

STANDARD TITLE PAGE

1. Report No. NASA TT F-15,412	2. Government Accession No.	3. Recipient's Catalog No.
4. Title and Subtitle: APPLIED PROBLEMS OF SPACE BALLISTICS		5. Report Date: April, 1974 6. Performing Organization Code
7. Author(s): P. Ye. El'yasberg, et al., editors		8. Performing Organization Report No. 10. Work Unit No.
9. Performing Organization Name and Address: SCITRAN, Box 5456, Santa Barbara, CA 93108		11. Contract or Grant No. NASw-2483 13. Type of Report and Period Covered: Translation
12. Sponsoring Agency Name and Address: National Aeronautics and Space Administration, Washington, D.C. 20546		14. Sponsoring Agency Code

15. Supplementary Notes

Translation of "Prikladnyye zadachi kosmicheskoy ballistiki", Nauka Press, Moscow, 1973, 143 pages.

16. Abstract

Papers of seminars of the Institute of Space Research, Academy of Science USSR are presented in this collection. Papers of the seminar, "Theory of the Flight and Control of Spacecraft" are collected in the first part, which is devoted to problems of determining and correcting space trajectories and to problems of investigating optimum trajectories. Papers of the seminar, "Study of the Upper Atmosphere of the Earth for Braking Artificial Earth Satellites" are collected in the second part. These papers are devoted to an analysis of the effect of atmospheric drag on the evolution of satellite orbits, to a study of variations of atmospheric density and to questions of predicting atmospheric density for calculating artificial Earth satellite orbits.

17. Key Words (Selected by Author(s))	18. Distribution Statement
	Unclassified - Unlimited

19. Security Classif. (of this report)	20. Security Classif. (of this page)	21. No. of Pages	22. Price
Unclassified	Unclassified	205	

ANNOTATION

Papers of seminars of the Institute of Space Research, Academy of Science USSR are presented in this collection. Papers of the seminar, "Theory of the Flight and Control of Spacecraft" are collected in the first part, which is devoted to problems of determining and correcting space trajectories and to problems of investigating optimum trajectories. Papers of the seminar, "Study of the Upper Atmosphere of the Earth for Braking Artificial Earth Satellites" are collected in the second part. These works are devoted to an analysis of the effect of atmospheric drag on the evolution of satellite orbits, to a study of variations of atmospheric density and to questions of predicting atmospheric density for calculating artificial Earth satellite orbits.

This edition is intended for specialists in the area of space technology.

TABLE OF CONTENTS

	Page
ANNOTATION	ii
ANALYSIS OF FLIGHT TRAJECTORIES USING THE GRAVITATIONAL FIELD OF JUPITER B. Ts. Bakhshiyan, N. G. Khavenson, P. Ye. El'yasberg	1
ENTRANCE CORRIDORS INTO THE ATMOSPHERE OF A PLANET WITH EXECUTION OF THE SPACECRAFT CAPTURE MANEUVER BY AERODYNAMIC BRAKING N. A. Eysmont	13
ON CALCULATING THE PARALLAX OF A DISTANT ARTIFICIAL SPACE OBJECT V. I. Belenko, Z. S. Shilkina	31
AN A POSTERIORI ALGORITHM FOR FILTERING INTERFERING PARAMETERS FOR INDEPENDENT SPACE NAVIGATION G. A. Mersov	37
METHODS FOR DETERMINING AND PREDICTING ARTIFICIAL EARTH SATELLITE (AES) ORBITS WITH ERRORS PRESENT IN THE MATHEMATICAL DESCRIPTION OF THE MOTION A. I. Nazarenko, L. G. Markova	52
STATISTICAL ANALYSIS OF THE DAILY MEAN FLUCTUATIONS OF THE PARAMETERS FOR THE UPPER ATMOSPHERE OF THE EARTH V. Ye. Chertoprud	96
EVALUATION OF THE ACCURACY IN PREDICTING SHORT-PERIOD VARIATIONS OF THE ATMOSPHERIC DENSITY M. I. Voyskovskiy, I. I. Volkov, N. I. Gryazev, B. V. Kugayenko, V. M. Sinitsyn, P. Ye. El'yasberg	134
SEMIANNUAL VARIATIONS OF THE ATMOSPHERIC DENSITY AT ALTITUDES OF 200 — 300 km A. M. Alferov	151

Page

AERODYNAMICS OF SATELLITES AND THE DETERMINATION OF THE SURFACE-FLUX INTERACTION PARAMETERS FROM AES "KOSMOS-166" AND "KOSMOS-230" DRAG IN THE UPPER ATMOSPHERE OF THE EARTH
G. I. Zmiyevskaya 170

MODIFICATIONS OF JACCHIA'S STATIC DIFFUSION MODELS OF THE UPPER ATMOSPHERE
M. A. Degtyarev 187

N74-28289

ANALYSIS OF FLIGHT TRAJECTORIES USING THE GRAVITATIONAL FIELD OF JUPITER

B. Ts. Bakhshiyan, N. G. Khavenson, and P. Ye. El'yasberg

ABSTRACT. Spacecraft (SC) trajectories using the gravitational field of Jupiter for flight in the immediate vicinity of the Sun and leaving the plane of the ecliptic are investigated. The optimal nominal trajectories are selected with an inclination to the plane of the ecliptic of 90° (after the flight around Jupiter) and a given perihelion distance. The possibilities of observing the SC after loss of radio communications with it during the flight around Jupiter are investigated.

The possibility of using the gravitation of Jupiter (passive gravitational maneuver) for flight in the immediate vicinity of the Sun (at a minimum distance R_π) and leaving the plane of the ecliptic is investigated in this work. It is necessary in this case to observe the spacecraft (SC) after loss of radio communications with it during the flight around Jupiter. The accuracy of fixing the SC position after the maneuver is determined, and the possibility of determining the mass of Jupiter more precisely from the measured data is also considered. The energetically optimum trajectories are selected from the investigated ones, under the condition that the heliocentric orbit of the SC after the flight by Jupiter has a perihelion distance equal to the given value of R_π and inclination to the plane of the ecliptic is $i = 90°$. /3*

*Numbers in the margin indicate the pagination of the original foreign text.

1. Selection of the Spacecraft Trajectory

For solution of the problem, the following model of SC motion is considered: all trajectories are divided into four nonoverlapping successive portions, within each of which the motion occurs in a central force field along a Keplerian orbit (Earth, Sun, Jupiter, Sun). The boundaries of the portions are determined by the dimensions of the spheres of influence of the Earth and Jupiter. The technique for calculating the initial conditions of the SC motion in each portion of the trajectory is given below.

The initial conditions $\vec{r}_0^{(1)}, \vec{v}_0^{(1)}$ for the heliocentric trajectory of the flight from the Earth to Jupiter, the geocentric velocity $\vec{v}_1$ of the SC exit from the sphere of influence of the Earth, and the Joviocentric velocity $\vec{v}_2$ of the SC entrance into the sphere of influence of Jupiter are determined from the solution of the Lambert equation. The search for the optimum trajectory for the flight from the Earth to Jupiter is carried out by the sorting method over the parameters τ, T (τ — starting date, T — time of flight to Jupiter). Isolines of the velocity v_1 and the boundaries for the region in which the solution exists are constructed in the plane of these parameters. The isolines tangent to the boundary correspond to the minimum value of v_1, and the position of the point of tangency determines the starting date and the duration of the flight of Jupiter along the optimum trajectory.

For the selected velocity vector $\vec{v}_1$, the SC position can be determined at the starting time from the circular orbit for given values of geocentric inclination $i_\oplus$, radius $r_\oplus$, and coordinates of the starting point at the Earth. To determine the ascending node of the orbit $\Omega_\oplus$ in the geocentric equatorial /4

coordinate system ξ, η, ζ, one has the equation:

$$a\sin\Omega_{\oplus} - b\cos\Omega_{\oplus} + c = 0,$$
$$a = v_{1\xi}\sin i_{\oplus}, \quad b = v_{1\eta}\sin i_{\oplus}, \quad c = v_{1\zeta}\cos i_{\oplus}, \tag{1.1}$$

which follows from the perpendicularity of the angular momentum vector and the velocity vector $\bar{v}_1$. When the condition $a^2+b^2-c^2>0$ is satisfied, Equation (1.1) has two solutions:

$$\sin\Omega_{\oplus 1} = \frac{-ac + b\sqrt{a^2+b^2-c^2}}{a^2+b^2},$$
$$\cos\Omega_{\oplus 1} = \frac{bc + a\sqrt{a^2+b^2-c^2}}{a^2+b^2}; \tag{1.2}$$

$$\sin\Omega_{\oplus 2} = \frac{-ac - b\sqrt{a^2+b^2-c^2}}{a^2+b^2},$$
$$\cos\Omega_{\oplus 2} = \frac{bc - a\sqrt{a^2+b^2-c^2}}{a^2+b^2}. \tag{1.3}$$

The longitude $\omega_{\oplus}$ of the perigee of the hyperbolic orbit in the geocentric portion of the trajectory can be determined by a simple geometric construction. Knowing $i_{\oplus}$, $\Omega_{\oplus}$, $\omega_{\oplus}$ and the radius of the intermediate circular geocentric orbit makes it possible to calculate the initial conditions for the SC at the pericenter of its hyperbolic trajectory.

We place the initial conditions for the heliocentric trajectory for the flight from Jupiter equal to the SC coordinates and velocity components at its exit from the sphere of influence of Jupiter.

We turn to the determination of the initial conditions for the Joviocentric portion of the SC trajectory. We consider the heliocentric and Joviocentric velocity vectors v_3^a and v_3 of the

SC ($v_3 = v_2$), the position R_J and velocity V_J vectors of Jupiter relative to the Sun at the time of the SC exit from the sphere of influence of Jupiter. We also introduce the Joviocentric coordinate systems $\tilde{x}, \tilde{y}, \tilde{z}$ and $\hat{x}, \hat{y}, \hat{z}$. The unit vectors of the $\tilde{x}, \tilde{y}, \tilde{z}$ system are expressed through the unit vectors of the heliocentric ecliptic coordinate system x, y, z by the equations

$$\tilde{x}^0 = \frac{z^0 \times R_J}{|z^0 \times R_J|}, \quad \tilde{y}^0 = z^0 \times \tilde{x}^0, \quad \tilde{z}^0 = z^0. \tag{1.4}$$

The coordinates of the $\hat{x}, \hat{y}, \hat{z}$ and $\tilde{x}, \tilde{y}, \tilde{z}$ systems are interlinked by the relations: /5

$$\begin{Vmatrix} \tilde{x} \\ \tilde{y} \\ \tilde{z} \end{Vmatrix} = \begin{Vmatrix} 1 & 0 & 0 \\ 0 & -\frac{R_{J\tilde{y}}}{R_J} & -\frac{R_{J\tilde{z}}}{R_J} \\ 0 & \frac{R_{J\tilde{z}}}{R_J} & \frac{R_{J\tilde{y}}}{R_J} \end{Vmatrix} \begin{Vmatrix} \hat{x} \\ \hat{y} \\ \hat{z} \end{Vmatrix}. \tag{1.5}$$

To achieve a SC orbit with an inclination of 90° to the plane of the ecliptic, the velocity v_3^a must lie in the plane $\tilde{y}\tilde{z}$ ($v_{3\tilde{x}}^a = 0$). This condition corresponds to the relation:

$$(v_{3\tilde{y}}^a - V_{J\tilde{y}})^2 + (v_{3\tilde{z}}^a - V_{J\tilde{z}})^2 = v_2^2 - V_{J\tilde{x}}^2. \tag{1.6}$$

Accomplishing the condition of the SC flight at the given distance at perihelion R_π from the Sun (after the exit of the SC from the sphere of influence of Jupiter) leads to the equation:

$$\frac{R_J(R_\pi + R_J)}{2\mu_S R_\pi}(v_{3\hat{z}}^a)^2 - \frac{R_\pi R_J}{2\mu_S(R_J - R_\pi)}(v_{3\hat{y}}^a)^2 = 1, \tag{1.7}$$

(μ_S is the solar gravitational parameter), which follows from the integrals of energy and areas of the Keplerian heliocentric motion.

The solution of the system of equations (1.6), (1.7) is not unique. We limit ourselves to the case $v^a_{3\hat{y}} > 0$, which corresponds to flight with minimum time (flight angle less than 180°). The sign of the component $v^a_{3\hat{z}}$ determines the direction of motion to the Sun: exit to the northern latitudes of the ecliptic $(v^a_{3\hat{z}} \geq 0)$, or to the southern $(v^a_{3\hat{z}} \leq 0)$.

The initial conditions $r_0^{(2)}, v_0^{(2)}$ of the Joviocentric orbit at the time of entrance into the sphere of influence of Jupiter can be calculated from the velocities of the SC entrance into the sphere of influence of Jupiter v_2 and exit from it $v_3 = v_3^a - V_J$. To solve this problem, we introduce the Joviocentric coordinate system x', y', z', whose unit vectors are determined by the formulas:

$$(x')^0 = \frac{v_2 \times v_3 \times v_2}{|v_2 \times v_3 \times v_2|}, \quad (y')^0 = \frac{v_2}{|v_2|}, \quad (z')^0 = \frac{v_2 \times v_3}{|v_2 \times v_3|}. \tag{1.8}$$

In the x', y', z' system, we obtain the following formulas for calculating the initial conditions:

$$v_0^{(2)} = v_2 = \begin{Vmatrix} 0 \\ v_2 \\ 0 \end{Vmatrix}, \tag{1.9}$$

/6

$$r^{(2)}_{0x'} = \mu_J \cos\frac{f}{2}\left(\frac{\mu_J^2}{r_J} - 2\frac{\mu_J}{r_J}v_2^2\sin^2\frac{f}{2} + v_2^4\sin^2\frac{f}{2}\right)^{-1/2},$$
$$r^{(2)}_{0y'} = -\sqrt{r_J^2 - r_{Jx}^2}, \quad r^{(2)}_{0z'} = 0, \tag{1.10}$$

where f is the angle between the vectors v_2, and v_3, r_J is the radius of the sphere of influence of Jupiter, μ_J is the gravitational parameter of Jupiter.

2. Optimum Strategy for Predicting the Trajectory of Spacecraft

The accuracy of predicting several of the parameters of the selected flight trajectory to Jupiter are estimated below. We first discuss the technique for calculating these estimates.

Let the SC trajectory be uniquely determined by the vector $q = (q_1, q_2, \ldots, q_k)^T$ (T denotes the transposition operation; all the vectors to be introduced are to be considered as column vectors) and the estimate $\hat{l}$ of some parameter $l(q)$ be calculated by the formula:

$$\hat{l} = l(q^0) + Z^T (D - \tilde{D}(q^0)), \tag{2.1}$$

where q^0 is the a priori value of the vector q (or its value obtained by analysis of the trajectory measurements); $D(q) = D_1, D_2, \ldots, D_N)$ is the vector of the measured functions; $\tilde{D}$ is the measured value of the vector $D(q)$; $Z = (z_1, z_2, \ldots, z_N)^T$ is the vector determining the method of analysis of the measurements.

It is not difficult to see from (2.1) that the error $\delta l = \hat{l} - l(q^*)$ in determining the parameter l is expressed with an accuracy of the order of $|q^0 - q^*|^2$ (q^* is the true value of the vector q) by the formula:

$$\delta l = Z^T \rho + (B - \tilde{A}Z)^T (q^0 - q^*), \tag{2.2}$$

where $\tilde{\rho} = \tilde{D} - D(q^*)$ is the vector of the errors in the measurements;

$$B = \left(\frac{\partial l(q)}{\partial q}\right)^T_{q=q^0}; \quad \tilde{A} = \left\| \frac{\partial D(q)}{\partial q} \right\|_{q=q^0}$$

is a matrix of dimension k × N.

By introducing the notation:

$$\rho = (\rho_1, \rho_2, \ldots, \rho_{N+k})^T = \left\| q^0 \overset{\sim}{\rho} - q^* \right\| \text{ — component vector,} \quad (2.3)$$

and $\tilde{A} = \|\tilde{A} E\|$ the component matrix of dimension $k \times (N+k)$, (E is the unit matrix), we rewrite (2.2) in the form:

$$\delta l = X^T \rho, \quad (2.4)$$

$$AX = B \quad (2.5)$$

[the identity (2.5) follows from the notations (2.3)].

Denoting the maximum a priori errors in the trajectory measurements and a priori data by σ_i $(i=1, 2, \ldots, N+k)$, we have: /7

$$|\rho_i| \leqslant \sigma_i \quad (i = 1, 2, \ldots, N+k). \quad (2.6)$$

We consider the problem of the optimum prediction of the parameter l for the case of the most unfavorable correlation among the errors ρ_i under the condition (2.6):

$$L = \min_X \max_{\rho_i} \delta l = \sum_{i=1}^{N+k} \sigma_i |x_i|, \quad (2.7)$$

$$AX = B. \quad (2.8)$$

One can show that the solution of the problem (2.7), (2.8) is found from the solution of the problem of linear programming:

$$L = \min \sum_{i=1}^{N+k} \sigma_i (x_{1i} + x_{2i}), \quad (2.9)$$

$$A(X_1 - X_2) = B, \quad (2.10)$$

$$x_{1i} \geqslant 0,\ x_{2i} \geqslant 0, \qquad (2.11)$$

where $X_1 = (x_{11}, x_{12}, \ldots, x_{1(N+k)})^T$, $X_2 = (x_{21}, x_{22}, \ldots, x_{2(N+k)})^T$.

It follows from the properties of the problem (2.9) — (2.11) of linear programming [1] and its correspondence to the problem (2.7), (2.8) that the vector X has k (and with degeneracy no more than k) nonzero components of which, generally speaking, the components $x_1^{(1)}, x_2^{(1)}, \ldots, x_m^{(1)}$ $(0 \leqslant m \leqslant k)$ correspond to the trajectory measurements $D_1^{(1)}, D_2^{(1)}, \ldots, D_m^{(1)}$, and the components $x_1^{(2)}, x_2^{(2)}, \ldots, x_{k-m}^{(2)}$ correspond to the a priori data.

Since the quantities $x_i^{(2)} = (B - \tilde{A}Z)_i^{(2)}$ do not equal zero, then the corresponding components $q_i^{(2)}$ of the vector q are taken equal to their a priori values $(q_i^{(2)})^0$ when calculating the estimate of the prediction accuracy (2.2). The remaining m of quantities q_i, which correspond to the components $x_{i+N} = (B - \tilde{A}Z)_i$ equaling zero, are determined from the the data of the trajectory measurements $D_1^{(1)}, D_2^{(1)}, \ldots, D_m^{(1)}$.

Thus, the solution of the problem (2.9) — (2.11) determines the optimum [in the sense of predicting the parameter $l(q)$] separation of the vector q into quantities "refined" and "unrefined" in the process of measurement analysis. This result was obtained in [2] from other considerations.

In applying the discussed estimation technique for flight trajectories to Jupiter, we take as components of the vector q the following set of constants: the initial conditions $x_0, y_0, z_0, v_{0x}, v_{0y}, v_{0z}$ of the SC motion at the time of its start from the circular geocentric orbit; the gravitational parameter of the Earth μ_E and the initial conditions $x_E, y_E, z_E, v_{Ex}, v_{Ey}, v_{Ez}$ of its motion at the time of the SC start from the circular geocentric orbit; the gravitational parameter of Jupiter μ_{Jup} and the initial conditions

/8

$x_G, y_G, z_G, v_{Gx}, v_{Gy}, v_{Gz}$ of its motion at the time of the SC entrance into the sphere of influence of Jupiter; the components v_{kx}, v_{ky}, v_{kz} of the SC trajectory correction vector, which are included in **q** if the correction occurs at a given moment of time t_k. We associate the numbers i = 1, 2, ..., 23 and the maximum values σ_i^a of the a priori accuracy to the components of the vector **q** corresponding to the order of their enumeration.

We consider the measurement of distance D and radial velocity $\dot{D}$ of the SC relative to a measuring point on the Earth as trajectory measurements. It is assumed that the measurements can be carried out at intervals of 1 hour, 2 days, 1 day on the geocentric, heliocentric, Joviocentric portions of the trajectory, respectively, and the precision characteristics σ_i for measuring the distance or radial velocity remain equal to the constants σ_D and $\sigma_{\dot{D}}$ during the flight. The accuracy of predicting the parameter $\dot{D}_n$ and SC coordinates η_n, ζ_n in the η, ζ system, whose origin is at the point $\bar{r}(q^0, t_n)$, and the directions of whose axes are determined by the unit vectors:

$$\bar{\zeta}^0 = \frac{(\bar{r}(q^0, t_n) - \bar{r}_r(t_n)) \times \bar{v}(q^0, t_n)}{|\bar{r}(q^0, t_n) - \bar{r}_r(t_n)|\, v(q^0, t_n)}, \quad \bar{\eta}^0 = \frac{\bar{\zeta}^0 \times (\bar{r}(q^0, t_n) - \bar{r}_r(t_n))}{|\bar{r}(q^0, t_n) - \bar{r}_r(t_n)|}, \tag{2.12}$$

where $\mathbf{r}_r(t_n)$ is the vector of the measuring point coordinates, is investigated at some moment in time t_n during the flight around Jupiter.

A sufficiently accurate prediction of the parameters $\dot{D}, \eta, \zeta$ will make it possible to detect the SC during communications during the flight around Jupiter.

For the considered scheme, the SC motions derived from the initial conditions of the SC and planet (matrix $\tilde{A}$ and vector B) are calculated from the final formulas of [3].

For the case of the Keplerian SC motion in the time interval $[t_0, t]$ about the attracting object with the gravitational parameter μ, one can obtain the formula

$$\frac{\partial \left\| \begin{matrix} r(t) \\ v(t) \end{matrix} \right\|}{\partial \mu} = \frac{1}{3\mu} \left(\left\| \begin{matrix} r(t) \\ v(t) \end{matrix} \right\| - \Phi(t, t_0) \left\| \begin{matrix} r(t_0) \\ v(t_0) \end{matrix} \right\| \right) \qquad (2.13)$$

[$\Phi(t, t_0)$ is the transition matrix], with which it is not difficult to calculate the isochronous derivatives from the SC trajectory parameters by the gravitational constants of the Earth and Jupiter in any portion of the orbit.

Results of calculations for a trajectory which exits after /10
the flight around Jupiter into the northern latitudes of the ecliptic and passes at a distance of 0.1 au from the Sun are presented below. For the SC flight along this trajectory, the time interval during which radio communications with the Earth are not possible is that from 448.3 to 449 days. For example, we take the following values for the a priori precision characteristics:

$$\sigma_D = 1 \text{ km}, \ \sigma_{\dot{D}} = 10^{-4} \text{ km/sec}^{-1}, \ \sigma_1^a = \sigma_2^a = \sigma_3^a = 100 \text{ km},$$

$$\sigma_4^a = \sigma_5^a = \sigma_6^a = 0.1 \text{ km/sec}^{-1}, \ \sigma_7^a = 0.5 \text{ km}^3/\text{sec}^{-2},$$

$$\sigma_8^a = \sigma_9^a = \sigma_{10}^a = 500 \text{ km}, \ \sigma_{11}^a = \sigma_{12}^a = \sigma_{13}^a = 10^{-2} \text{ km/sec}^{-1},$$

$$\sigma_{14}^a = 10^4 \text{ km}^3/\text{sec}^{-2}, \ \sigma_{15}^a = \sigma_{16}^a = \sigma_{17}^a = 10^3 \text{ km},$$

$$\sigma_{18}^a = \sigma_{19}^a = \sigma_{20}^a = 10^{-2} \text{ km/sec}^{-1}, \ \sigma_{21}^a = \sigma_{22}^a = \sigma_{23}^a = 10^{-4} \text{ km/sec}^{-1}$$

In this case, sufficient accuracy in the SC coordinates in the figure plane of the target planet (the order of its radius) can be obtained with analysis of the measurements after t_Σ = 330 days of the flight.

TABLE 1*

t_Σ days	Prediction error	Unrefined parameters number	Time of measurements, distance and radial velocity (*), days
	$\delta\dot{D}_n 15=50$ m/sec	3 7 8 10 14 15 16 17 18 19 20	0,7 17,4 57,4 108,0 178,0 252,0 318,0 348,6 350,6 410,6 412,6
415,6	$\delta\eta_n=6{,}2\cdot10^4$ km	3 7 8 10 14 15 16 17 18 19 20	0,7 17,4 57,4 108,0 178,0 252,0 318,0 348,6 350,6 382,6 410,6 412,6
	$\delta\zeta_n=1{,}3\cdot10^5$ km	6 7 8 10 14 15 16 17 18 19 20	0,7 17,4 57,4 108,0 178,0 252,0 318,0 348,6 350,6 382,6 410,6 412,6
	$\delta\dot{D}_n=147$ m/sec	7 10 15 16 17 20	0,7 1,4 21 4 59,4 112,0 178,0 2 6, 318,6 348,6 356,6 388,6 410,6 426,6 442,6 446,6 447,6 447,6*
447,6	$\delta\eta_n=8980$ km	3 7 8 10 15 16 17	0,7 19,4 65,4 122,0 124,0 224,0 290,0 348,6 350,6 392,6 410,6 912,6 439,6 445,6 447,6 447,6*
	$\delta\zeta_n=7{,}4\cdot10^4$ km	7 10 15 16 17 20	0,7 1,4 21,4 59,4 105,4 180,0 254,0 318,0 348,6 350,6 390,6 410,6 427,6 441,6 446,6 447,6 447,6*

TABLE 2*

t_Σ days	$\frac{\delta\mu_J}{\sigma_{14}}$	Unrefined parameters number	Time of measurements, distance and radial velocity (*), days
455,3	1,00	2 5 7 8 10 14 15 17	411,3 416,3 418,3 440,3 446,3 448,3 448,3* 449,3 450,3 453,3 455,3
465,3	0,66	1 2 5 7 8 15 17	411,3 419,3 433,3 446,3 447, 3 447, 3* 448,3 449,3 450,3 455,3 461,3 463,3
475,3	0,55	1 2 5 7 8 15 16	465,3 411,3 421,3 439,3 445,3 446,3* 448,3* 448,3 449,3 451,3 458,3 468,3 470,3 474,3
485,3	0,38	3 5 7 15	411,3 416,3 429,3 440,3 446,3 447,3 448,3 449,3 451,3 460,3 464,3 468,3 472,3 480,3 482,3 485,3

* Translator's Note: Commas in numbers indicate decimals.

Results of the calculations for t_k = 348.57 days, t_n = 449.27 days are presented in Table 1.

Results of the calculations for the case of a SC flight without orbit correction in order to measure the mass of Jupiter more precisely from the data of the trajectory measurements in the Joviocentric portion with σ_D = 10 m, $\sigma_{\dot{D}}$ = 0.1 cm/sec are presented in Table 2.

LITERATURE

1. Yudin, D. B. and Ye. G. Gol'shteyn. Lineynoye programmirovaniye (Linear Programming). Moscow, State Physics and Mathematics Press, 1963.

2. Bakhshiyan, B. Ts. and P. Ye. El'yasberg. Avtomatika i telemekhanika, No. 3, 1970, p. 16.

3. Bettin, R. Navedeniye v kosmose (Guidance in Space). Moscow, "Mashinostroyeniye" Press, 1966.

N74-28289

ENTRANCE CORRIDORS INTO THE ATMOSPHERE OF A PLANET WITH EXECUTION OF THE SPACECRAFT CAPTURE MANEUVER BY AERODYNAMIC BRAKING

N. A. Eysmont /11

ABSTRACT. The possibilities of spacecraft transfer from a pre-entrance trajectory to a satellite orbit of a planet using aerodynamic braking in the atmosphere of the planet are analyzed in the article. The available entrance corridors are determined depending on the aerodynamic characteristics of the craft and the parameters of the pre-entrance trajectories. Evaluations of the possibilities of accomplishing the transfer maneuvers depending on the errors in determining the pre-entrance trajectory are given.

As was shown in [1 — 4], the transition of spacecraft (moving relative to a planet along a hyperbolic trajectory) to an orbit as a satellite of the planet by using aerodynamic braking in the atmosphere can give a significant advantage of payload in comparison with dynamic rocket braking. However, this method is more complicated technically, since it requires the use of heat shields and increased accuracy in determining and correcting the trajectory. Estimates of the possibilities of various navigation systems in the sense of increased accuracy in determining trajectories are given in the cited works. These estimates are compared with the available entrance corridors for craft with various lift-drag ratios. The width of the entrance corridor also depends on the entrance velocity and on the assumed constraints. A systematic analysis of entrance corridors for craft braking in the atmospheres of Venus and Mars in order to transfer

to satellite orbits depending on the control method, the lift-drag ratio, and velocity of the craft at infinity relative to the planet is carried out in this work.

1. Regions of Variation of the Pre-Entrance Trajectory Parameters

We take the value of the velocity at infinity relative to the planet V_∞ as the characteristic of the pre-entrance trajectory. The range of possible values of V_∞ is determined in the following manner. The trajectory with the minimum exit velocity from the satellite orbit of the Earth is selected from the family of flight trajectories along the minimum arc. Trajectories with launch data in the vicinity of the optimum and with flight times giving the minimum exit velocity are considered further.

In the vicinity of the optimum launch date, a range of dates is taken, within which at launch the exit velocity at infinity does not exceed the velocity corresponding to the optimum date by more than 0.5 km/sec. The range of velocities at infinity relative to the target planet obtained thus is taken as the possible range. According to calculations carried out at IKI (Institute of Space Research) AN SSSR by G. A. Mersov and V. A. Filippov, this range is defined by values of V_∞ equalling 2.5 — 6.5 km/sec for Mars and 3 — 7 km/sec for Venus.

2. Aerodynamic Characteristics of Spacecraft Entering an Atmosphere and Models of Planetary Atmospheres /12

The flight velocities of spacecraft in an atmosphere with completion of the transfer maneuver from the hyperbolic trajectory to the satellite orbit correspond to Mach numbers significantly greater than M = 3 — 4, beginning with which the modes

of streamline flow are considered hypersonic, and the aerodynamic characteristics of the craft do not depend on the Mach number [5]. For Reynolds numbers Re > 1000, these coefficients do not depend on Re either [6]. At the range of altitudes where the dependence of the aerodynamic coefficients on Re does appear, the aerodynamic forces themselves are small enough to consider the aerodynamic coefficients as constant with satisfactory accuracy.

Present space engineering is familiar with descent craft of the capsule type ("Soyuz," "Apollo") having a maximum lift-drag ratio $k_{max} = 0.5$. Spacecraft with support frames having $k_{max} \approx 1$ at hypersonic velocities are in the stage of experimental research. Increasing the lift-drag ratio leads to serious deterioration of the weight characteristics due to the increasing weight of the heat shielding [5]. This is caused by the fact that the weight of the heat shielding and structure of the craft are proportional to the surface of the craft, and with increasing lift-drag ratio, the so-called volume efficiency (ratio of the volume to the 2/3 power to the surface area) drops, decreasing from 0.2 for a sphere ($k = 0$) to approximately 0.1 for $k = 1.5$ and approximately 0.05 for $k = 3$ [7].

Another cause of increasing weight of the craft structure with the quality is the decrease of the aerodynamic drag coefficient C_D due to increasing quality k, since decreasing C_D leads to increasing thermal flux to the craft [5].

In connection with this discussion, the calculations in this work are carried out for craft with lift-drag ratio $k \leq 2$.

The dependence of atmospheric density on altitude corresponding to the model developed in [8] is taken for calculating the motion in the atmosphere of Venus.

Motion in the atmosphere of Mars is considered for two atmospheric models [9] corresponding to the maximum and minimum density at the altitudes where the flight occurs ($h > 10$ km).

3. Optimum Execution of the Spacecraft Transfer Maneuver from the Hyperbolic Trajectory to the Satellite Orbit

The requirement of craft exit from the atmosphere is general for any method of accomplishing the maneuver. In addition, it is necessary to turn on the engine to raise the pericenter to prevent re-entry into the atmosphere.

Let us assume that it is required that the satellite transfer /13 to an orbit with given altitudes for the apocenter and pericenter and the number of atmopsheric immersions must be no more than one. In this case, the optimum control problem arises, which consists of selecting the control for motion in the atmosphere for which the velocity impulse at the apocenter ΔV_α required to raise the pericenter is minimum. Let the control occur by changing the bank angle, so that the projection of the lift in the vertical direction L_e varies from L_{min} to L_{max} and, correspondingly, the effective lift-drag ratio $k_e = L_e/D$ varies from k_{min} to k_{max} (D is the aerodynamic drag remaining constant with changing bank angle).

If the apocenter altitude of the orbit obtained after exit from the atmosphere is fixed, then, as was proven in [10] for an atmosphere with constant scale height and in [11] for an arbitrary atmosphere, the optimum control must be of the relay type with one switchover. The requirement of a sufficiently small inclination angle of the trajectory to the local horizon θ, so that $\theta \approx \theta$ and $\cos\theta \approx 1$, is set for this in [10, 11].

In addition, it is assumed in [11] that the velocity at exit from the atmosphere is not less than the circular. Calculations carried out by numerical integration of the equations of motion for a planet with a central gravitational field and non-rotating atmosphere have show that, even for cases when the angle θ is fairly large and the exit velocity is less than circular, control with one switchover remains optimum.

It is evident that, for unfixed apocenter altitude of the orbit after exit from the atmosphere, the structure of optimum control remains the same.

As calculations have shown, the mangitude of the impulse ΔV_α for trajectories of motion with optimum control increases with decreasing radius of the nominal pericenter of the pre-entrance trajectory. Thus, the maximum allowable value of ΔV_α corresponding to the available fuel supply on board the craft determines the lower boundary of the entrance corridor. The minimum radius of the nominal pericenter $r_{\pi ent}$ for which the impulse ΔV_α for raising the pericenter to a fixed altitude equals the prescribed value is achieved for control with one switchover. This follows from the structure of the optimum control giving min ΔV_α and the fact of increasing ΔV_α with decreasing $r_{\pi ent}$.

4. Calculation Procedure for Determining the Entrance Corridor

The requirement of spacecraft exit from the atmosphere reduces to the condition of attaining a given value of apocenter radius r_α osculating with an orbit at an altitude taken beyond the boundary of the atmosphere. It is evident that, to obtain a fixed r_α, the minimum value of $r_{\pi ent}$ for craft with given lift-drag ratio k and ballistic coefficient is achieved for $k_e = k_{emax}$, /14

and the maximum for $k_e = k_{e\,min}$. Thus, to determine the entrance corridor for craft transfer to an orbit with fixed r_α for various k_e, it is sufficient to have the curve for the dependence $r_{\pi ent} = r_{\pi ent}^{(k)}$ obtained for each k from the solution of the equation:

$$r_\alpha(r_{\pi ent}) = r_{\alpha g}, \tag{1}$$

where $r_{\alpha g}$ is the given apocenter radius.

In the limiting case, when it is necessary to accomplish spacecraft capture by atmospheric braking for transfer to an orbit with an apocenter radius unbounded from above, the value of the maximum allowable $r_{\pi ent}$ is found from the solution of the equation:

$$E(r_{\pi ent}) = 0, \tag{2}$$

where E is the energy of the orbit obtained after exit from the atmosphere.

The apocenter altitude is limited from above in many cases for reasons of convenience in solving the problems accomplished by the satellite, and also of its control in flight. The values r_α = 72,500 and 37,580 km are taken in this work as the maximum allowable apocenter radii for satellites of Venus and Mars, respectively. Such values of r_α and the values of pericenter radii cited below determine orbits with a period of approximately 1 day. The values r_α = 6,650 and 3,988 km are taken as the minimum allowable. The last two values are also taken as the required pericenter radii obtained by the impulse ΔV_α of the engine at the apocenter of the orbit at which the craft arrives after braking in the atmosphere.

The radius of the nominal pericenter satisfying the condition of (1) is calculated by solving the transcendental equation:

$$E(r_{\pi ent}) = E_g, \tag{3}$$

where the value of E_g is determined from the relation

$$E_g = -\frac{\mu}{r_{\alpha g} + r_\pi} \tag{4}$$

(μ is the gravitational constant of the planet).

Substitution of Equation (1) into (3) is carried out to the extent that the entrance of $r_{\pi ent}$ into the region where the function $r_\alpha(r_{\pi ent})$ does not exist is possible in the iteration process for solving Equation (1).

The left part of the equations are calculated from the formulas of conic sections as a function of the orbital elements at the exit from the atmosphere. The latter are determined by numerical solution of the differential equations of motion of the craft as a point mass, which are written for a planet with a central gravitational field and nonrotating atmosphere. The lift-drag ratio and ballistic coefficient along the trajectory are taken as constant. /15

For manned flight, the maximum allowable overloads n_{max} can determine the lower boundary of the entrance corridor. The minimum allowable radius of the nominal pericenter is found, in this case, from the condition:

$$n_{max}(r_{\pi ent}) = n_g, \tag{5}$$

where n_g is the maximum allowable total overload.

Three possible values for the maximum allowable total overload: 5, 7.5, and 10 are taken in this work.

The left part of Equation (5) is determined by numerical integration of the equations of motion from the initial conditions at entrance into the atmosphere to the moment when the maximum overload is reached, i.e., when the derivative dn/dt becomes zero.

In the case when the available impulse ΔV_α is limited, the lower boundary of the entrance corridor is determined by the radius of the nominal pericenter $r_{\pi ent}$, for which

$$\Delta V_\alpha(r_{\pi ent}) = \Delta V_g, \tag{6}$$

where ΔV_g is the given value of the available impulse. The value of $r_{\pi ent}$ satisfying Equation (6) depends on the control and, as noted in the preceding paragraph, the minimum value of $r_{\pi ent}$ is achieved with optimum control.

Equation (6) is solved for two versions of control: with constant effective lift-drag ratio along the whole trajectory and with optimum switchover of the lift-drag ratio. It is assumed for this that $k_{e\ max} = k = -k_{e\ min}$. The left part of Equation (6) is calculated in a manner analogous to that for Equations (2) and (3).

For the case of flight with optimum control, the optimum value of the apocenter radius r_α is also selected, i.e., Equation (6) is replaced by the relation:

$$\min_{r_{\alpha g} < r_\alpha} \Delta V_\alpha(r_{\pi ent}) = \Delta V_g, \tag{7}$$

where $r_{\alpha g}$ is the minimum allowable apocenter radius.

Since the optimum control is control with one switchover, then for fixed $r_{\pi ent}$, the switchover time has a one-to-one relation with r_α of the orbit obtained after exit from the atmosphere. /16 Thus, the relation:

$$\min_{t_s} \Delta V_\alpha (r_{\pi ent}) = \Delta V_g \qquad (8)$$

with the condition $r_\alpha > r_{\alpha g}$, where t_s is the switchover time, is taken in place of (7) for the calculations.

5. Results of the Entrance Corridor Calculations

The results of the entrance corridor calculations are presented in Figures 1 — 4 for the transfer to a satellite orbit of Venus and in Figures 5 — 7 — of Mars.

The dependencies $r_{\pi ent} = r_{\pi ent}(k)$ for V_∞ = 3, 5, 7 km/sec obtained from the condition that the craft transfer to an orbit with r_α = 6,650 km after exit from the atmosphere are shown in Figure 1a. The lift-drag ratio for the craft motion is considered constant. The quantity m/SC_D is also assumed constant and, for all cases of braking in the atmosphere of Venus, equals 200 kg/m^2 (m is the mass of the spacecraft, S is the area of the midship cross section, C_D is the aerodynamic drag coefficient). The indicated dependencies determine the lower boundary of the entrance corridor. Curves obtained from the condition that r_α = 72,500 km under the same assumptions as for the dependencies presented in Figure 1a are shown in Figure 1b. The functions

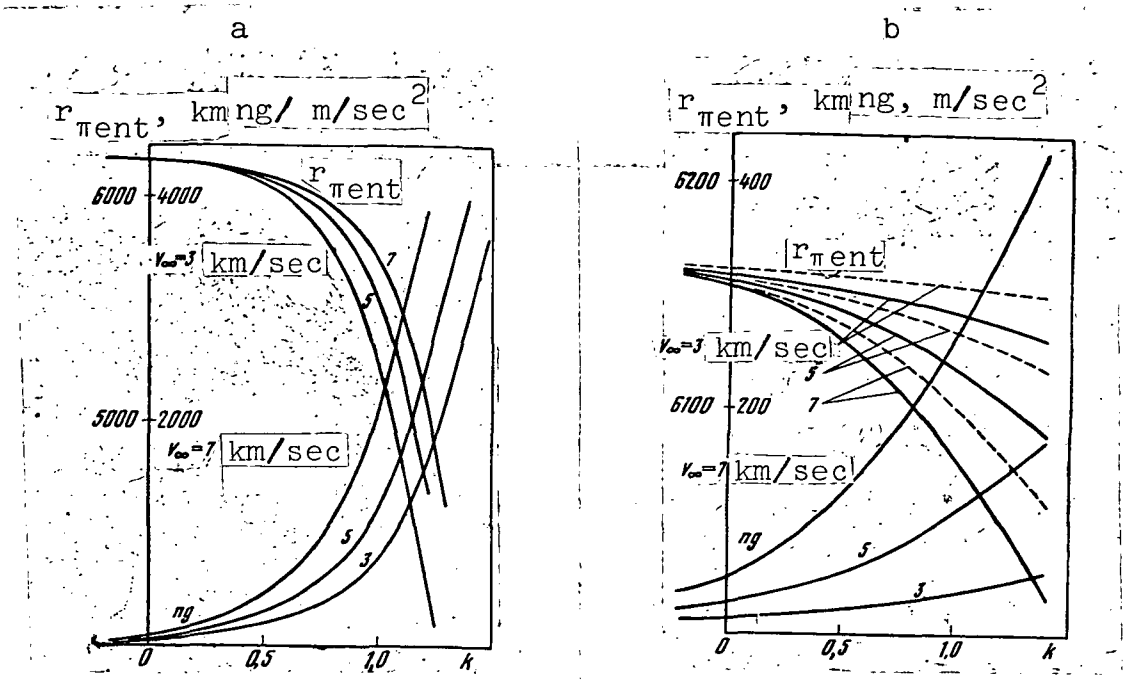

Figure 1. Dependence of the maximum overload ng and the nominal pericenter radius $r_{\pi ent}$ of the entrance trajectory into the atmosphere of Venus on the lift-drag ratio of the craft for r_α = 6,650 km (a), r_α = 72,500 km, and E = 0 (b).

$r_{\pi ent}(k)$ for the cases when it is required that E = 0 at exit from the atmosphere are indicated here by dashed lines. In addition, the curves for the dependencies of the maximum overload ng on the lift-drag ratio are given in Figure 1 for the trajectories obtained under the described conditions.

The dependence of the entrance corridor width on the lift-drag ratio is presented in Figure 2, which is determined as the interval of values of nominal pericenter radii $r_{\pi ent}$ which ensure for constant lift-drag ratio that the values of apocenter radius fall in the interval [6,650, 72,500] km at exit from the atmosphere. Here also the dashed lines show the corridor width for the case when the upper boundary is determined under the condition that E = 0 at exit from the atmosphere.

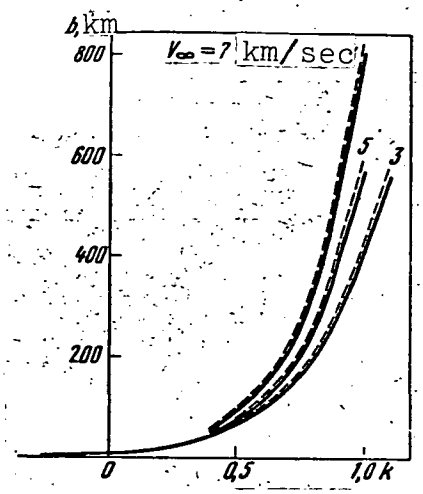

Figure 2. Dependence of the entrance corridor width b into the atmosphere of Venus on the lift-drag ratio.

It is clear from consideration of Figure 2 that the transition from the limitation at exit of r_α = 72,500 km to the limitation E = 0 does not give a significant broadening of the entrance corridor, if the lower boundary is determined by the condition r_α = 6,650 km. Thus, for V_∞ = 3 km/sec and lift-drag ratio k = 0.5, the corridor width increases by 6.5 km, i.e., by less than 10%. For craft with larger lift-drag ratio, the relative corridor broadening is even less: for V_∞ = 3 km/sec and k = 1, the entrance corridor is broadened by 13 km for a width of 415 km.

It is also evident from Figure 2 that the entrance corridor is wider for larger V_∞ and k. For k = 1 and V_∞ > 5 km/sec, the entrance corridor width exceeds 570 km, which according to [4], is sufficient to span the possible errors in guiding a craft to an atmospheric braking trajectory even for trajectory prediction with Earth-bound radio techniques. However, the maximum overload level for motion at the lower boundary of the corridor exceeds /17 the crew endurance limits, if the lift-drag ratio is greater than the values determined easily from Figure 1. For k = 1 and V_∞ = 3 km/sec, the overload reaches 80, and for V_∞ = 7 km/sec, it increases to 210.

To evaluate the entrance corridor width with maximum loading limitations, the dependencies of $r_{\pi ent} = r_{\pi ent}(k)$ obtained under the conditions $n_{max} = n_g$ for n_g = 5, 7.5, and 10 are presented /18

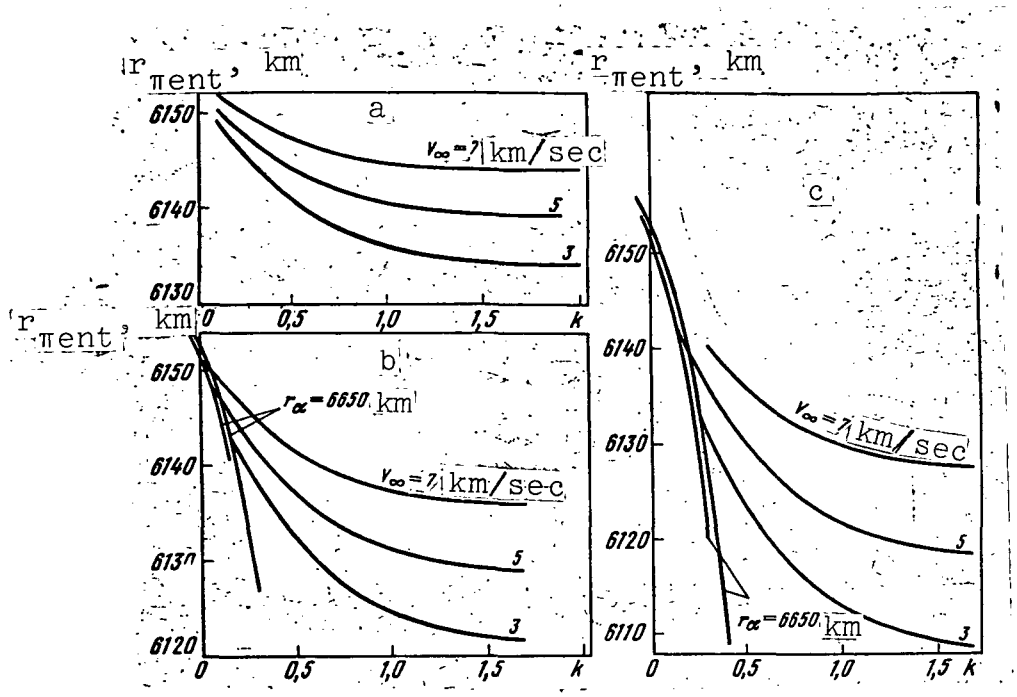

Figure 3. Dependence of $r_{\pi ent}$ of the entrance trajectory into the atmosphere of Venus on the lift-drag ratio of the craft with maximum overload.

a- $n_{max} = 5$; b- $n_{max} = 7.5$; c- $n_{max} = 10$..

in Figure 3. The dependence $r_{\pi ent}(k)$ obtained under the condition $r_\alpha = 6{,}650$ km is shown for values of the lift-drag ratio determining the given overload level for trajectories with $r_\alpha \leq 6{,}650$ km. It is clear from consideration of Figure 3 that the overload limitation sharply reduces the width of the entrance corridor, the increase of lift-drag ratio lowering the lower boundary of the corridor only for values of $k \leq 1.6 — 1.8$.

Limitation by the available impulse ΔV_α also reduces the corridor width. The dependencies $r_{\pi ent}(k)$ under the condition $\Delta V_\alpha = \Delta V_g$ for a number of values of ΔV_g are shown in Figure 4. The dependencies $r_{\pi ent}(k)$ under the condition that $r_\alpha = 6{,}650$ km at exit from the atmosphere and the corresponding values of $\Delta V_\alpha(k)$

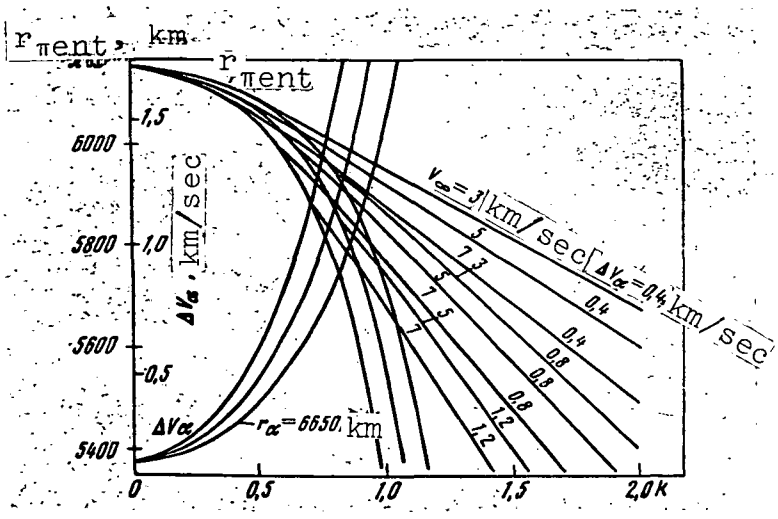

Figure 4. Dependence of $r_{\pi ent}$ of the entrance trajectory into the atmosphere of Venus on the lift-drag ratio of the craft for a fixed value of the velocity impulse at apocenter ΔV_α.

are shown in the same figure for comparison. The curves for $\Delta V_\alpha = \Delta V_g$ are constructed for the values of k for which $r_\alpha \geq$ 6,650 km. The lift-drag ratio is assumed constant in calculating these dependencies.

The quantity m/SC_D is taken equal to 50 kg/m^2 in calculating the transfer trajectories to satellite orbits of Mars.

The dependencies $r_{\pi ent}(k)$ for transfer trajectories to satellite orbits of Mars with apocenter radii r_α equaling 3,988 and 37,580 km, respectively, are shown in Figure 5. These dependencies are obtained for the three values of velocity at infinity V_∞ = 2.5; 4.5; 6.5 km/sec and for the model of minimum atmospheric density at altitudes above 10 km [9]. The variations in maximum overloading are presented in the same figures.

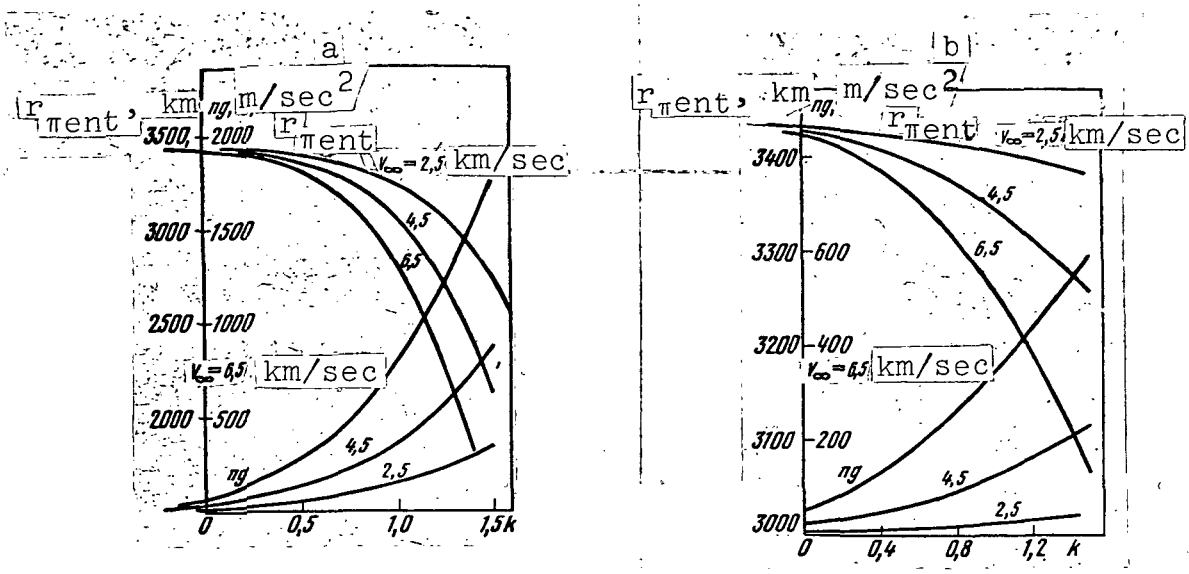

Figure 5. Dependence of the maximum overload and $r_{\pi ent}$ of the entrance trajectory into the atmosphere of Mars on the lift-drag ratio of the craft for r_α = 3,988 km (a) and r_α = 37,580 km (b).

The dependencies $r_{\pi ent}(k)$ obtained for the model of maximum atmospheric density of Mars [9] under the condition that the maximum total overload n_{max} = 5, 7.5, and 10 are shown in Figure 6. These curves are constructed for values of k for which the condition on n_{max} is satisfied in trajectories with values of r_α at exit from the atmosphere of no less than 3,988 km. The dependencies $r_{\pi ent}(k)$ under the condition that r_α = 3,988 km at exit from the atmosphere are constructed in the same figures for smaller values of k. /20

The dependence $r_{\pi ent}(k)$ for the model of maximum atmospheric density under the condition that ΔV_α = 0.2 km/sec is shown in Figure 7a. The solid lines indicate the dependencies for trajectories with constant lift-drag ratio, and the dashed — for

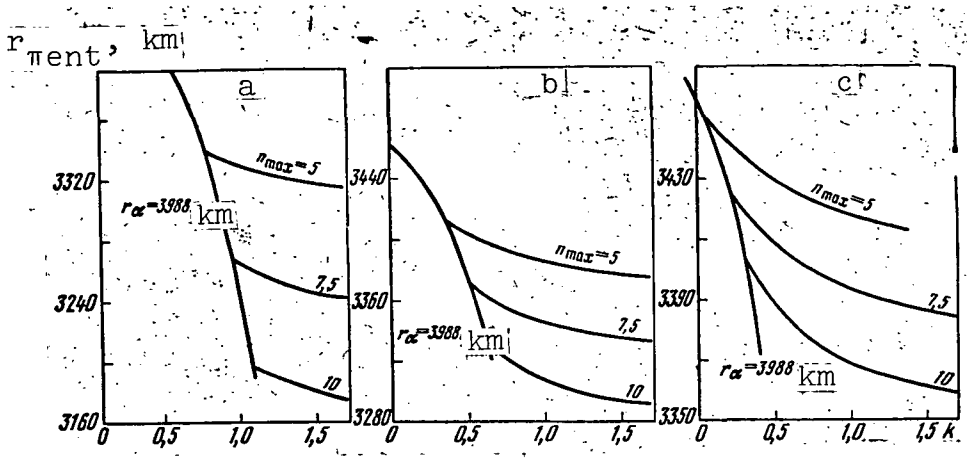

Figure 6. Dependence of $r_{\pi ent}$ of the entrance trajectory into the atmosphere of Mars on the lift-drag ratio for fixed values of the maximum overload for V_∞ = 2.5 km/sec (a); for V_∞ = 4.5 km/sec (b); for V_∞ = 6.5 km/sec (c).

optimum control. It is evident from the figure that, for a lift drag ratio k = 0.5, which is attainable with present-day space technology, limiting ΔV_α to the value 0.2 km/sec does not /21 permit using the whole width of the entrance corridor whose lower boundary is determined by the minimum $r_{\pi ent}$, ensuring entrance to an orbit with r_α = 3,988 km after exit from the atmosphere.

Application of optimum control permits lowering the lower boundary and thereby broadening the entrance corridor. For V_∞ = 6.5 km/sec and k = 0.5, 1, and 1.4, the broadening is 8, 65, and 157 km, respectively, which — under the conditions $r_\alpha \leq$ 37,580 km — $\Delta V_\alpha \leq$ 0.2 km/sec for k = 0.5, 1, and 1.4 is 18, 78, and 150%, respectively, of the corridor width obtained for flight with constant lift-drag ratio.

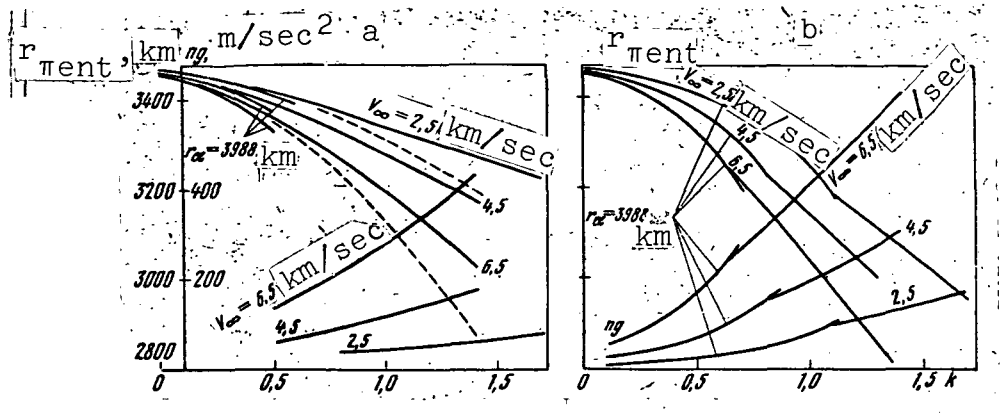

Figure 7. Dependence of $r_{пent}$ of the entrance trajectory into the atmosphere of Mars on the lift-drag ratio for the velocity impulse at apocenter ΔV_α = 0.2 km/sec (a); ΔV_α = 0.6 km/sec (b).

The same dependencies for ΔV_α = 0.6 km/sec for flight with constant lift-drag ratio are shown in Figure 7b. The variation of maximum overloading with lift-drag ratio is also shown in Figure 7.

Conclusions

The results of the calculations presented graphically indicate that the transfer maneuver from a hyperbolic trajectory to a satellite orbit of a planet using aerodynamic braking in the atmosphere imposes rather rigid requirements on the accuracy in determining and correcting the pre-entrance trajectory. The largest entrance corridor is achieved if limitation is set only on the magnitude of the apocenter radius of the orbit obtained after exit from the atmosphere. In this case, the entrance corridor will be wider the greater the velocity at infinity. Thus, for the case of transfer to a satellite orbit of Venus by a craft with k = 0.5 constant along the trajectory under the condition that after exit from the atmosphere $6{,}650 \leq r_\alpha \leq 72{,}500$ km, the width of the entrance corridor is 44, 46, and 54 km for

a pre-entrance trajectory with V_∞ = 3, 5, and 7 km/sec, respectively. The entrance corridor broadens with increased lift-drag ratio; under the same conditions with k = 1, it reaches the values 415, 573, and 800 km.

The overload limitation significantly reduces the width of the entrance corridor because the lower boundary is raised. The lower boundary is lowered with increasing k only up to values of k ≈ 1.6 — 1.8. When the overload is limited, increasing V_∞ decrease the corridor width. However, this occurs only for k greater than the lift-drag ratio at which the minimum r_α and maximum overload limitations determine the same nominal pericenter radius. Thus, for transfer to a satellite orbit of Mars, if the atmosphere corresponds to the maximum density model, the requirement that the maximum overload not exceed 5 reduces the corridor for spacecraft with k > 0.6, and the requirement $n_{max} \leq$ 10 — for spacecraft with k > 1.

Reduction of the corridor width with the introduction of a limitation on the magnitude of the impulse at the apocenter ΔV_α also appears only for spacecraft with a lift-drag ratio greater than some k_1, where the larger k_1, the larger ΔV_α and the smaller V_∞. Thus, for ΔV_α = 0.6 km/sec, k_1 = 0.65, 0.8, and 1.1 for V_∞ = 6.5, 4.5, and 2.5 km/sec, respectively. /22

Application of optimum control permits broadening the entrance corridor in the case of limitation on ΔV_α. The effectiveness of optimum control increases then with lift-drag ratio. However, the application of independent navigation methods for determining and correcting the pre-entrance trajectory is required in all the cases of limitations on which the entrance corridors

depend for spacecraft with $k \leq 0.5$. With overload limitations, spacecraft with larger lift-drag ratio ($k > 1$) also require independent navigation methods, since Earth-bound radio measuring stations cannot ensure the required accuracy in determining trajectories.

The author thanks P. Ye. El'yasberg for useful discussions.

LITERATURE

1. Shy, A. A. and J. A. White. J. Spacecraft and Rockets. Vol. 6, No. 7, 1969, p. 831.

2. Repic, E. M., M. G. Boobar and F. G. Chapel. J. Spacecraft and Rockets, Vol. 5, No. 8, 1968, p. 921.

3. Boobar, M. G., E. M. Repic and A. M. McDermott. J. Spacecraft and Rockets, Vol. 4, No. 5, 1967, p. 682.

4. Repic, E. M. and J. R. Eyman. J. Spacecraft and Rockets. Vol. 6, No. 5, 1969, p. 532.

5. Collection: Gazovaya dinamika kosmicheskikh apparatov (Gas Dynamics of Spacecraft), Moscow, "Mir" Press, 1965.

6. Matting, F. W. J. Spacecraft and Rockets, Vol. 8, No. 1, 1971, p. 35.

7. Stewart, J. D. and D. H. Greenshields. J. Spacecraft and Rockets, Vol. 6, No. 10, 1969, p. 1089.

8. Avduyevskiy, V. S., M. Ya. Marov and M. K. Rozhdestvenskiy. Kosmicheskiye issledovaniya, Vol. 8, No. 6, 1970, p. 871.

9. Lau, R. A. and J. C. Hussong. AIAA Paper No. 1162, 1970 p. 15 (translation: Ekspressinformatsiya, Astronavtika i raketodinamika, No. 14, 1971, ref. 196).

10. Shilov, A. A. and Yu. I. Zhelnin. Kosmicheskiye issledovaniya, Vol. 4, No. 4, 1966.

11. Eysmont, N. A. Kosmicheskiye issledovaniya, Vol. 10, No. 2, 1972, p. 290.

N74-28290

ON CALCULATING THE PARALLAX OF A DISTANT ARTIFICIAL SPACE OBJECT

V. I. Belenko and Z. S. Shilkina

ABSTRACT. The simplest calculation schemes for transforming the spherical coordinates of an object at a significant distance from the Earth with changes in the observation position on its surface are described. The possibility of using them for transmitting the object coordinates from one observation point to another is evaluated.

The parallactic shift of a space object on the celestial sphere with a transition from one observation point on the surface of the Earth ("initial") to another ("final") is easily determined by a direct conversion of the topocentric spherical coordinates α_1, δ_1, r_1 of the object for the initial point to the analogous quantities α_2, δ_2, r_2 for the final. This conversion can be accomplished by an intermediate transformation to the corresponding rectangular coordinate system XYZ according to one of the simplest schemes: /22 /23

$$\begin{aligned} &X_1 = r_1 \cos(\alpha_1 - S)\cos\delta_1, \quad Y_1 = r_1 \sin(\alpha_1 - S)\cos\delta_1, \quad Z_1 = r_1 \sin\delta_1, \\ &X_2 = X_1 - \Delta X, \quad Y_2 = Y_1 - \Delta Y, \quad Z_2 = Z_1 - \Delta Z, \\ &\alpha_2 = S + \operatorname{arctg}\frac{Y_2}{X_2}, \quad \delta_2 = \operatorname{arctg}\frac{Z_2}{\sqrt{X_2^2 + Y_2^2}}, \quad r_2 = \sqrt{X_2^2 + Y_2^2 + Z_2^2}, \end{aligned} \tag{1}$$

or:

$$\begin{aligned} &X_1' = r_1 \cos\alpha_1 \cos\delta_1, \quad Y_1' = r_1 \sin\alpha_1 \cos\delta_1, \quad Z_1' = r_1 \sin\delta_1, \\ &X_2' = X_1' - (\Delta X \cos S - \Delta Y \sin S), \quad Y_2' = Y_1' - (\Delta X \sin S + \Delta Y \cos S), \\ &Z_2' = Z_1' - \Delta Z, \\ &\alpha_2 = \operatorname{arctg}\frac{Y_2'}{X_2'}, \quad \delta_2 = \operatorname{arctg}\frac{Z_2'}{\sqrt{(X_2')^2 + (Y_2')^2}}, \\ &r_2 = \sqrt{(X_2')^2 + (Y_2')^2 + (Z_2')^2}, \end{aligned} \tag{1'}$$

where $\Delta X, \Delta Y, \Delta Z$ are the coordinates of the final point in the rectangular coordinate system XYZ with the origin at the initial point; S is the Greenwich mean time of the observation.

However, this method is not always suitable, since the full number of significant digits is required to perform all the calculations. In the case $r_1 \gg R$, where R is the radius of the Earth, it is simpler to calculate not the coordinates α_2, δ_2 of the object at the final point, but the corrections for parallax $\Delta\alpha, \Delta\delta$ to the corresponding coordinates of this object for the initial point. To derive the necessary formulas, it is sufficient to make successive rotations of the rectangular coordinate system XYZ with the origin at the initial point about the Z axis by an angle $\alpha_1 - S$ measured in the direction of increasing right ascension, and about the intermediate position of the Y_1 axis by an angle δ_1 measured in the direction of increasing declination in the half-plane X'Z' containing the observed object. After performing these operations, the new X" axis coincides with the "initial point - observed object" line, and the other two (Y" and Z") are parallel to the axes of the ideal coordinate system ξ and η with the origin at the point on the celestial sphere with the coordinates α_1, δ_1. It is only necessary to perform the central projection of the final point onto the ideal plane through the point coinciding with the position of the observed object. The rectangular coordinates $\Delta X, \Delta Y, \Delta Z$ of the final point are then transformed in the following manner: /24

$$
\begin{aligned}
\Delta X' &= \Delta X \cos(\alpha_1 - S) + \Delta Y \sin(\alpha_1 - S),\\
\Delta Y' &= -\Delta X \sin(\alpha_1 - S) + \Delta Y \cos(\alpha_1 - S),\\
\Delta Z' &= \Delta Z,\\
\Delta X'' &= \Delta X' \cos\delta_1 + \Delta Z' \sin\delta_1,\\
\Delta Y'' &= \Delta Y',\\
\Delta Z'' &= -\Delta X' \sin\delta_1 + \Delta Z' \cos\delta_1,\\
\xi &= -\frac{\Delta Y''}{r_1 - \Delta X''}, \quad \eta = -\frac{\Delta Z''}{r_1 - \Delta X''}.
\end{aligned}
\tag{2}
$$

The values of the ideal coordinates ξ and η calculated by this scheme coincide with the projections onto the ideal plane of the required corrections for parallax $\Delta\alpha$, and $\Delta\delta$ to the known quantities α_1, δ_1. In some cases, the corrections for parallax can be used directly in the form of the ideal coordinates (for example, for aiming at an object with given α_1, δ_1, ξ, η for observations on an instrument provided with an adjustment for shifting the receiver within the necessary limits in the focal plane of the objective).

The conversion to spherical corrections $\Delta\alpha$, $\Delta\delta$ is carried out with the formulas used in photographic astrometry [1]:

$$\Delta\alpha = \operatorname{arctg}\frac{\xi\cos\Delta d}{\cos(\delta_1+\Delta d)}, \qquad \Delta\delta = \operatorname{arctg}\eta - \varepsilon, \tag{3}$$

where

$$\Delta d = \operatorname{arctg}\eta, \qquad \varepsilon = \operatorname{arctg}\frac{\sin 2(\delta_1+\Delta d)\operatorname{tg}^2\frac{\Delta\alpha}{2}}{1+\cos 2(\delta_1+\Delta d)\operatorname{tg}^2\frac{\Delta\alpha}{2}}.$$

The correction $\Delta\alpha$ can also be determined without preliminary calculation of the ideal coordinates:

$$\Delta\alpha = -\operatorname{arctg}\frac{\Delta Y'}{r_1\cos\delta_1 - \Delta X'}, \tag{3'}$$

in the projection onto the X'Y' plane.

The described method for calculating the parallax [Formulas (2), (3), (3')] can be used, for example, to transmit (to recalculate) the coordinates of a distant artificial space object (when its actual trajectory deviates from the calculated trajectory) from one observation point to another. The comparatively low accuracy required in this case (0'.5 — 1') permits the use of

a graphical method, which significantly reduces the solution time for the problem. As an aid for the graphical solution, it is convenient to use a chart of the relative arrangement of the observation points (in projections onto the XY coordinate plane or /25
onto the Z axis) with a sufficiently large scale; a circle divided into degrees for reading out the rotation angles of the coordinate system, and a grid of rays of equal tangent values (within the working range of the measurement of the quantities $\Delta\alpha$, Δd) with the scale of distances r_1 plotted along the central ray of this grid. A separate graph is constructed to determine the quantity ε (the deflection pointer of the diurnal circle) from the given $\Delta\alpha$ and $d=\delta_1+\Delta d$.

If the ephemeris of the object is known at all observation points and, in addition, the correction to the ephemeris is obtained from observations at one of the points (with the index 1), the corresponding corrections to the ephemeris for the remaining observation points [2] are easily found from the relations:

$$\Delta'\alpha_i = \Delta'\alpha_1 - \left(\frac{\Delta r_i}{r_1}\Delta'\alpha_1 - \Delta\delta_i \operatorname{tg}\delta_1 \Delta'\alpha_1 - \Delta\alpha_i \operatorname{tg}\delta_1 \Delta'\delta_1 + \Delta\alpha_i \frac{\Delta' r_1}{r_1}\right),$$

$$\Delta'\delta_i = \Delta'\delta_1 - \left(\frac{\Delta r_i}{r_1}\Delta'\delta_1 + \Delta\alpha_i \sin\delta_1 \cos\delta_1 \Delta'\alpha_1 + \Delta\delta_i \frac{\Delta' r_1}{r_1}\right), (i=2,3,\ldots), \quad (4)$$

obtained by differentiating Formulas (1) or (1') with subsequent simplification and replacement of the differentials of the coordinates by their finite increments (Δ').

Here $\Delta'\alpha_1, \Delta'\delta_1, \Delta' r_1$ are the corrections to the ephemeris at the first point; $\Delta'\alpha_i, \Delta'\delta_i$ are the corrections to the ephemeris at the other points; $\Delta\alpha_i, \Delta\delta_i, \Delta r_i$ are the differences of the ephemeris values of the quantities α, δ, r, at the time of observation ($\Delta\alpha_i=\bar{\alpha}_i-\bar{\alpha}_1$, etc.).

Transmission accuracy of coordinates ($\Delta'\alpha$, $\Delta'\delta$)	Distance between observation points ($\Delta\rho$, km)	Distance to space object ($r_1 \cdot 10^5$), km				Transmission accuracy of coordinates ($\Delta'\alpha$, $\Delta'\delta$)	Distance between observation points ($\Delta\rho$, km)	Distance to space object ($r_1 \cdot 10^5$), km			
		0.3	0.5	1.0	1.5			0.3	0.5	1.0	1.5
4'	2000	520	1450	5800	13000	1"	2000	2.2	6.0	24	55
	5000	210	580	2300	5200		5000	0.9	2.5	9.7	22
1'	2000	130	360	1450	3300						
	5000	52	145	580	1300						

NOTE: In constructing the table, it is assumed that $\Delta\alpha = \Delta\delta = \Delta\rho/r_1$

The Formulas (4) are convenient for evaluating the effect of errors in each of the variables $(\alpha_1, \delta_1, r_1)$ at the first point on the magnitude of the errors in the coordinates α_i, δ_i for the other points. It is evident, for example, that for a distance to the space object greater than 10^5 km and for a deviation of its coordinates from the ephemeris by an amount up to 1°, it is necessary to calculate all the terms of Formulas (4) in order to transmit corrections to the ephemeris with an accuracy of 2', while for a given accuracy of 5' it is sufficient in a majority of cases to use the simplified formulas:

$$\Delta'\alpha_i \approx \Delta'\alpha_1, \quad \Delta'\delta_i \approx \Delta'\delta_1. \tag{4'}$$

By setting all the terms in Formulas (4), except the last, equal to zero and by giving various values of the left part, one can determine the corresponding values of the possible error $\Delta'r_1$ of the distance measurement (from the first point) to the space object depending on the value r_1 of this distance and the magnitude $\Delta\rho = \sqrt{\Delta X^2 + \Delta Y^2 + \Delta Z^2}$ of the distance between observation points. A table of values of the quantity $\Delta'r_1$ (in km) for various initial data is presented below [see page 36].

/26

REFERENCES

1. Bugoslavskaya, Ye. Ya. Fotograficheskaya astrometriya (Photographic Astrometry). Moscow, State Technical and Theoretical Press, 1947.

2. Isavnina, I. V. In the collection: Matematicheskiye metody modelirovaniya v kosmicheskikh issledovaniyakh (Mathematical Simulation Models in Space Research). Moscow, "Nauka" Press, 1971.

N74 - 28291

AN A POSTERIORI ALGORITHM FOR FILTERING INTERFERING PARAMETERS FOR INDEPENDENT SPACE NAVIGATION

G. A. Mersov

ABSTRACT. Navigation parameters are evaluated in the article from measurements of quantities which depend linearly on the navigation parameters as well as on parameters not directly usable for navigation. In the case when the assumed calculated values of these parameters differ from their true values, the estimates can be shifted. The magnitudes of these deviations are called interfering parameters in the article. Elimination of the estimate shifts can be achieved by combined evaluation of the navigation and interfering parameters. An algorithm is proposed, which permits reducing the dispersion of the estimates of the navigation parameters. In accordance with the algorithm, the interfering parameter is estimated in the case when its absolute value exceeds an assumed threshold value. The results of calculations illustrating the effectiveness in applying the algorithm are presented in the article for the case of a uniform distribution of the interfering parameters whose values do not equal zero.

Various problems in interpreting measured information arise /26
in processing trajectory measurements. Such problems are usually solved by heuristic methods based on the experience and intuition of those making the calculations. Algorithmization of these methods would permit their use for independent navigation to increase its reliability and efficiency. One of the problems of interpretation is the recognition and elimination of shifts caused by parameters whose magnitudes are unknown. These parameters can be called interfering parameters [1]. Unknown or

imprecisely known numerical characteristics of the assumed model of motion can be considered as interfering parameters [2]. Elimination of shifts is achieved by evaluating the interfering parameters. In the general case, there may exist an optimum separation of the interfering parameters into estimable and non-estimable quantities. To determine the optimum separation, one can proceed only from a priori information [3, 4], but one can also use a posteriori information, i.e., the measurements themselves. /27

An algorithm for a posteriori separation of the interfering parameters is considered in the article for the case when the probability that the assumed values of the interfering parameters equal their true values does not equal zero.

1. Problem of Filtering Interfering Parameters

Let $\mathbf{x}$ be an m-dimensional phase vector uniquely determining the trajectory of the motion. For the trajectory equation, let the p-dimensional navigation vector $\mathbf{q}$ be used, which depends linearly on $\mathbf{x}$:

$$q = Qx, \tag{1}$$

Where Q is the matrix of dimension p × m. We consider the problem of evaluating $\mathbf{q}$ from the measurement of an n-dimensional vector depending linearly not only on $\mathbf{x}$ but also on the unknown l-dimensional vector $\mathbf{d}$ of the interfering parameters:

$$\eta = Ax + Bd + \zeta, \tag{2}$$

where the components of ζ are the measurement errors, and A and B are matrices of dimensions n × m and n × l, respectively. All the columns of A are assumed to be mutually linearly independent,

and the columns $\mathbf{b}_k$ of the matrix B are linearly independent of the columns of A:

$$\operatorname{rank}(A) = m, \quad \operatorname{rank}(\|AB\|) = m + \operatorname{rank}(B), \quad 1 \leqslant \operatorname{rank}(B) \leqslant l, \tag{3}$$

where $\|AB\|$ is the partitioned matrix composed of A and B. In accordance with (3), the columns of B can be linearly dependent. For brevity, we will subsequently call the interfering parameters $d_{k_1}, d_{k_2}, \ldots, d_{k_r}$ linearly independent (or linearly dependent), if the columns $b_{k_1}, b_{k_2}, \ldots, b_{k_r}$ of the matrix B corresponding to them are linearly independent (or linearly dependent). The distribution law for ζ will be considered as known

$$M(\zeta) = 0, \quad M(\zeta\zeta^*) = E_n, \tag{4}$$

where E_n is the unit matrix of order n.

We assume that the d_k are independent random quantities equaling zero with the probabilities p_k and having a known distribution $F_k(d_k)$ with the probabilities $q_k = 1 - p_k$.

In calculating the estimate of $\mathbf{x}$, the vector $\mathbf{Bd}$ in (2) can be referred to the measurement errors. Then, by using the method of least squares, one can write for the estimate ξ_0 of the vector $\mathbf{x}$:

$$\xi_0 = F\boldsymbol{x}, \tag{5}$$

where

$$F \equiv (A^*A)^{-1}A^*, \tag{6}$$

and the corresponding estimate of $\mathbf{q}$ will equal /28

$$\boldsymbol{x}_0 = \boldsymbol{q} + QFB\boldsymbol{d} + QF\zeta. \tag{7}$$

Thus, if the columns of A and B are mutually nonorthogonal

$$A^{*}B \neq 0, \tag{8}$$

then the estimate $\hat{x}_0$ will depend on the interfering parameters.

The dependence of the estimate $\mathbf{q}$ on $\mathbf{d}$ can be eliminated, if all the linearly independent d_k are evaluated together with $\mathbf{x}$. Since for an increasing number of evaluated parameters the dispersion of the estimates also increases in the general case, it is desirable to evaluate the d_k not equaling zero. To reveal such d_k, one can attempt to use a posteriori information, i.e., the measurement of η. The estimate of $\mathbf{x}$ must then be calculated together with all $d_k \neq 0$. This calculation process, concluding with the calculation of the estimate of $\mathbf{q}$ using (1), we call the a posteriori algorithm for filtering interfering parameters.

The set of d_k determined as not equaling zero in the analysis we denote by Ω. To construct Ω, we consider all possible separations of $\mathbf{d}$ into $\mathbf{d}_j$ and $\tilde{\mathbf{d}}_j$, excluding those separations for which linearly dependent d_k appear in $\mathbf{d}_j$. In accordance with the separation of $\mathbf{d}$, we produce the separation of B into B_j and $\tilde{B}_j$:

$$B\mathbf{d} \equiv B_j \mathbf{d}_j + \tilde{B}_j \tilde{\mathbf{d}}_j. \tag{9}$$

Since, by construction and as a result of (3), the columns of A and B_j are linearly independent, then the combined estimates $\tilde{\delta}_j$ and $\tilde{\xi}_j$ of the vectors $\mathbf{d}_j$ and $\mathbf{x}$ can be calculated. We denote by ω_j the set consisting of the l_j elements d_{k_r}, $r = 1, 2, \ldots, l_j$, on which the estimate δ_j depends. The set ω_j is formed by all the components of $\mathbf{d}_j$ and some components of $\tilde{\mathbf{d}}_j$ and their union includes

all d_k. From the elements of ω_j, we form the subsets ω_j^i, which are all the possible sets of l_j^i elements taken from the l_j elements of ω_j, also including the empty set.

We consider the hypotheses h_j^i that, if $d_k \in \omega_j$, then

$$d_k \neq 0, \text{ if } d_k \in \omega_j^i,$$

$$d_k = 0, \text{ if } d_k \notin \omega_j^i.$$

Then the unconditional density of the distribution $\varphi(\delta_j)$ of the estimate δ_j can be represented in the form

$$\varphi(\delta_j) = \sum_i p(h_j^i)\varphi(\delta_j/h_j^i), \tag{10}$$

where $p(h_j^i)$ is the a priori probability of h_j^i, and $\varphi(\delta_j/h_j^i)$ is the conditional density of the distribution of δ_j with the hypothesis h_j^i. The probabilities $p(h_j^i)$ and densities $\varphi(\delta_j/h_j^i)$ can be determined from a priori information. We now determine the a posteriori probability $p(h_j^i/\delta_j)$ of the hypothesis h_j^i from the Bayes formula /29

$$p(h_j^i/\delta_j) = p(h_j^i)\varphi(\delta_j/h_j^i)/\varphi(\delta_j). \tag{11}$$

The a posteriori probability (11) will be used as the criterion for the truth of h_j^i, assuming that δ_j defines as true that h_j^i to which the greatest a posteriori probability corresponds. This criterion can be considered as a particular case of the criterion of the ratio of probabilities [5]. It follows from (10) and (11) that the condition

$$T_j^{i_0} \geqslant T_j^i, \; i = 1, 2, \ldots, i_j, \tag{12}$$

where i_j is the number of all possible hypotheses h_j^i and

$$T_j^i \equiv p(h_j^i)\varphi(\delta_j/h_j^i), \tag{13}$$

is equivalent to the maximum $p(h_j^l/\delta_j)$. The hypothesis $h_j^{i_0}$ defines as not equaling zero the d_k which are elements of $\omega_j^{i_0}$ and as equaling zero the d_k which are elements of $\tilde{\omega}_j^{i_0}$, the complement of $\omega_j^{i_0}$ with respect to ω_j. The hypotheses $h_j^{i_0}$ can be shown to be contradictory, when some d_k are included in $\omega_j^{i_0}$ by some hypotheses, and in $\tilde{\omega}_j^{i_0}$ by others. The construction of Ω can be accomplished most simply from the noncontradictory $h_j^{i_0}$, when, if d_k appears even if in only one $\omega_j^{i_0}$, then it does not appear in any $\tilde{\omega}_j^{i_0}$, and conversely. In this case, Ω obviously equals the union of all $\omega_j^{i_0}$:

$$\Omega = \bigcup_j \omega_j^{i_0}, \tag{14}$$

and the union of all $\tilde{\omega}_j^{i_0}$ will be the complement of Ω with respect to the set of all d_k. Such a case can be realized under some condition imposed on the interfering parameters, which we will consider further.

2. Particular Case

Now let ζ be the normal random vector with maintenance of the conditions (4), the probability p_k be the same for all d_k and the densities of the distribution of d_k for $d_k \neq 0$ be normal with zero first moment and dispersion σ_d^2:

$$\begin{aligned} \varphi(\xi) &= N(\xi, E_n), \quad p_k = p, \\ \varphi_k(d_k) &= N(d_k, \sigma_d^2), \quad k = 1, 2, \ldots, l. \end{aligned} \tag{15}$$

In order to formulate the condition for the matrix B, we obtain an expression for the estimates δ_j and ξ_j by using the method of least squares. For this, we present (2), using (9), in /30

the form

$$\eta = \| AB_j \| \begin{Vmatrix} x \\ d_j \end{Vmatrix} + \tilde{B}_j \tilde{d}_j + \zeta. \tag{16}$$

If, for simplicity, the information about d is not used as a priori measurement, then one can write the equation for the estimates δ_i and ξ_j

$$\begin{Vmatrix} A^* \\ B_i^* \end{Vmatrix} \| AB_j \| \begin{Vmatrix} \xi_j \\ \delta_j \end{Vmatrix} = \begin{Vmatrix} A^* \\ B_j^* \end{Vmatrix} \eta. \tag{17}$$

By completing the multiplication of the partitioned matrices, we separate (17) into two equations

$$A^* A\xi_j + A^* B_j \delta_j = A^* \bar{\eta}, \tag{18}$$

$$B_j^* A\xi_j + B_j^* B_j \delta_j = B_j^* \eta. \tag{19}$$

Expressing ξ_j from (18)

$$\xi_j = F\eta - FB_j\bar{\eta} \tag{20}$$

and substituting (20) into (19), we obtain

$$B_j^* S B_j \delta_j = B_j^* S \eta, \tag{21}$$

where

$$S = E_n - A(A^*A)^{-1}A^*. \tag{22}$$

The matrix S is a projecting matrix (6), i.e., $S^2 = S$, $S^* = S$, whose rank equals n - m. The matrix S projects n-dimensional vectors onto a space orthogonal to the space of the columns of A:

$$SA = 0. \tag{23}$$

The possibility of resolving (21) with respect to δ_j follows from (23) and the linear independence of the components of d_j,

$$\delta_j = G_j \eta, \tag{24}$$

where

$$G_j \equiv (B_j^* S B_j)^{-1} B_j^* S. \tag{25}$$

Substituting (17) into (24), we obtain:

$$\delta_j = d_j + G_j \tilde{B}_j \tilde{d}_j + G_j \zeta. \tag{26}$$

From (26), it follows that δ_j depends on all the d_k. In order that δ_j depend only on d_j, it is sufficient that the condition

$$B^* S B = E_l. \tag{27}$$

be satisfied. This condition permits one to obtain a simple solution of the inequality (12), since we can write for (26) /31

$$\delta_j = d_j + B_j^* S \zeta. \tag{28}$$

From (28), it follows that the estimate δ_k of the interfering parameter d_k does not depend on which ω_j d_k appears in, and equals

$$\delta_k = b_k^* S \eta. \tag{29}$$

Since the covariant matrices of the vectors $B_j S \zeta$ equal the unit matrix, then all the δ_k can be represented in the form

$$\delta_k = d_k + \nu_k, \quad k = 1, 2, \ldots, l, \tag{30}$$

ν_k are independent normal standard random quantitites. From (15) and (30), it follws that the conditional density of the estimates of $d_{k_r} \in \omega_j$, $r = 1, 2, \ldots, l_j$, is

$$\varphi(\delta_{k_r}/h_j^i)=\begin{cases}N(\delta_{k_r},\ 1+\sigma_d^2), & \text{if } d_{k_r}\in\omega_j^i,\\ N(\delta_{k_r},\ 1), & \text{if } d_{k_r}\notin\omega_j^i.\end{cases} \tag{31}$$

Since the random quantities δ_{k_r} are independent, then the density $\varphi(\delta_j/h_j^i)$ equals

$$\varphi(\delta_j/h_j^i)=\prod_{r=1}^{l_j}\varphi(\delta_{k_r}/h_j^i). \tag{32}$$

In accordance with (15), (30), and (31), the criterion (12) of the hypothesis h_j^0 of the empty set ω_j^0 equals

$$T_j^0=\prod_{r=1}^{l_j}pN(\delta_{k_r},\ 1). \tag{33}$$

Now let h_j^1 be the hypothesis which includes in ω_j^1 only one element d_{k_s} whose estimate δ_{k_s} is largest in absolute value among the estimates of $d_{k_r}\in\omega_j$. Then

$$T_j^1=T_j^0\beta(\delta_{k_s}), \tag{34}$$

where

$$\beta(\delta)=\frac{qN(\delta,\ 1+\sigma_d^2)}{pN(\delta,\ 1)} \tag{35}$$

The function $\beta(\delta)$ increases monotonically with increasing modulus δ, and T_j^1 is the largest quantity among the T_j^i for all the sets ω_j^i consisting of only one element. If $\beta(\delta_{k_s})\geqslant 1$, then $T_j^1>T_j^0$ and the hypothesis h_j^0 can be rejected. The hypothesis h_j^1 will be rejected in turn, if δ_{k_s} is found among the remaining estimates, /32 which satisfies the condition $\beta(\delta_{k_s})\geqslant 1$.

Thus, the greatest magnitude of the criterion $T_j^{i_0}$ will correspond to the set $\omega_j^{i_0}$, which includes those and only those $d_{k_r}\in\omega_j$, whose estimates satisfy the condition $|\delta_{k_r}|\geqslant t_{\max}$, where

the quantity t_{max}, determined by the equation $\beta(t_{max}) = 1$ equals

$$t_{max} = \left(2\frac{1+\sigma_d^2}{\sigma_d^2}\ln\frac{p}{q}\sqrt{1+\sigma_d^2}\right)^{1/2}. \quad (36)$$

Since the quantity t_{max} does not depend on which set ω_j is being considered, then the set Ω determined in accordance with (14) will include those and only those d_k whose estimates satisfy the condition

$$|\delta_k| \geqslant t_{max}. \quad (37)$$

Thus, under the condition (27), the algorithm reduces to the following operations:

1) the estimates δ_k of all the d_k are calculated in accordance with (29);

2) in accordance with (1) and (20) the estimate of the navigation vestor is calculated:

$$\varkappa = \varkappa_0 - QF\sum_k b_k\delta_k, \quad (38)$$

where the summation extends over all δ_k, satisfying the condition $|\delta_k| \geqslant t$, is calculated.

We call such a calculation process the threshold algorithm for filtering interfering parameters with the threshold t.

3. Optimum Threshold Algorithm

The use of the threshold algorithm will be justified, if the accuracy of the estimate (38) is greater than the accuracy of the estimate $\varkappa_0$, combined with all the d_k. The estimate of $\varkappa_0$

cannot be considered, since for sufficiently large σ_d the accuracy of x_0 will always be less than the accuracy of x_l. In accordance with the algorithm, the statistical characteristics of $\hat{x}$ will depend on the value of the threshold t. For t = 0, it is obvious that $x \equiv x_l$. In order to determine the effect of t on the dispersion of the estimates of the navigation parameters, we introduce the random quantities

$$\lambda_k = \begin{cases} 1, & \text{if } |\delta_k| \geqslant t, \\ 0, & \text{if } |\delta_k| < t, \end{cases} \tag{39}$$

with which we extend the summation in (38) over all δ_k :

/33

$$x = x_0 - QF \sum_{k=1}^{l} \lambda_k b_k \delta_k. \tag{40}$$

Substituting (7) into (40), we obtain

$$x = q + QF\zeta + QF \sum_{k=1}^{l} b_k (d_k - \lambda_k \delta_k). \tag{41}$$

We denote

$$\mu_k \equiv d_k - \lambda_k \delta_k \tag{42}$$

and write (41) in the form

$$x = q + QF\zeta + QFB\mu, \tag{43}$$

where the components of the vector μ are μ_k. The random quantities μ_k are independent with equal dispersions σ_μ^2, depending on the value of t in accordance with (39). One can write for the covariant matrix K of the vector x

$$K = QF(E_n + \sigma_\mu^2 BB^*)F^*Q^*. \tag{44}$$

It follows from (44) that the minimum dispersions of the components of $\varkappa$ are attained for the minimum value of σ_μ^2. For t = 0, $\mu_k = -\nu_k$ and $\sigma_\mu^2 = 1$. Thus, for the optimum algorithm, it is necessary that such t exist in order that $\sigma_\mu^2(t) < 1$. The distribution law for μ in accordance with (15), (30), and (39), is

$$\Phi(\mu) = \int\int_V (p\Delta(d) + qN(d, \sigma_d^2)) N(\nu, 1)\, dV, \tag{45}$$

where $\Delta(d)$ is the delta function, and the region V is defined by the inequality $d - \lambda(d + \nu) \leqslant \mu$. With (45) one can obtain the following expressions for the dispersion σ_μ^2 and its derivative with respect to t:

$$\sigma_\mu^2 = 1 - p\int_{-t}^{t} N(\mu, 1)\mu^2 d\mu + q\int_{-\infty}^{+\infty} \mu^2 \int_{-t+\mu}^{t+\mu} (N(\mu, \sigma_d^2) N(\nu, 1) - N(\nu, \sigma_d^2) N(\mu, 1))\, d\nu\, d\mu, \tag{46}$$

$$\frac{d\sigma_\mu^2}{dt} \equiv 2t^2 \left(q \frac{\sigma_q^2 - 1}{\sigma_q^2 + 1} N(t, 1 + \sigma_d^2) - pN(t, 1) \right). \tag{47}$$

The equation $\frac{d\sigma_\mu^2}{dt} = 0$ has three roots: $t_1 = 0$, $t_2 = 0$, and

$$t_{opt} = \left(2\frac{1 + \sigma_d^2}{\sigma_d^2} \ln \frac{p}{q} \frac{\sigma_d^2 + 1}{\sigma_d^2 - 1} \sqrt{\sigma_d^2 + 1} \right)^{1/2}. \tag{48}$$

One can show that, for $t = t_{opt} \neq 0$, the value of σ_μ^2 reaches its minimum and $\sigma_\mu^2(t_{opt}) < 1$. Thus, the condition for the optimum algorithm can be written in the form /34

$$\frac{p}{q} \frac{\sigma_d^2 + 1}{\sigma_d^2 - 1} \sqrt{\sigma_d^2 + 1} > 1. \tag{49}$$

As is evident from (36) and (48), the value of t_{opt} is always greater than t_{max}. For $\sigma_d \gg 1$

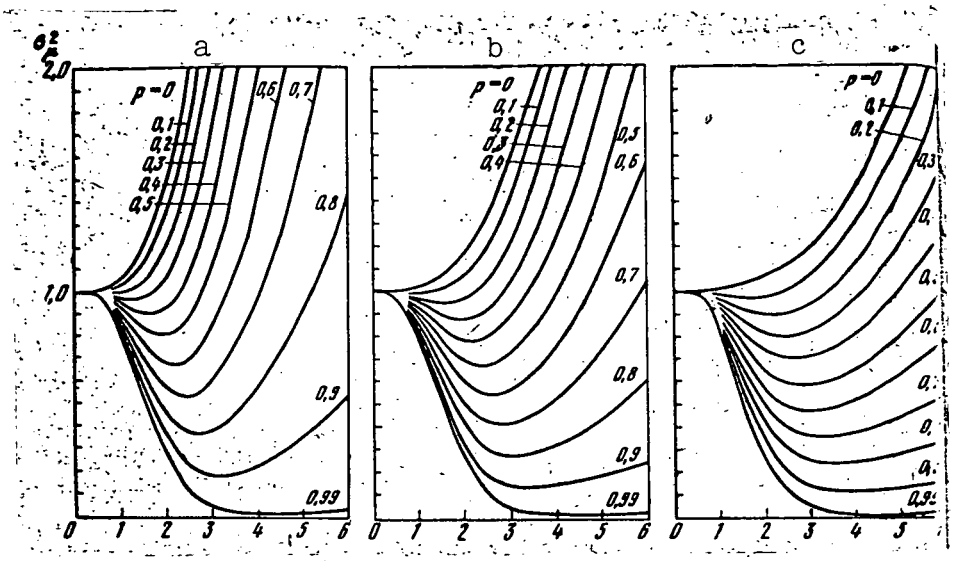

Figure 1. Dependence of σ^2_{μ} on t and p for $\sigma_d=3$ (a); $\sigma_d=9$ (b); $\sigma_d=27$ (c).

$$t_{opt} \approx t_{max} \approx \left(2 \ln \frac{p}{q} \sigma_d\right)^{1/2}. \tag{50}$$

The condition (49) in this case is written in the form /35

$$\sigma_d > \frac{q}{p}. \tag{51}$$

For $p \geq 0.5$, the algorithm is always optimum, since $\sigma_d > 1$. For $p = 0$, the estimate x_t is always worse than x_t.

We consider, for an example, the case when the distribution density of d is uniform on the interval [-D, D]. The dependencies of σ^2_{μ} on t for various values of p are presented in Figure 1. All the curves in one figure correspond to one value of σ_d. Since $\sigma_d^2 = qD^2/3$, then its value $D = (3\sigma_d^2/q)^{1/2}$ corresponds to each curve. As is seen, the optimum values of t appear for smaller p, the larger σ_d. The dependencies of the optimum σ^2_{μ} and t on p are presented in Figure 2. For infinitely large σ_d, $\sigma^2_{\mu opt} = 1 - p$. This follows from the fact that, for infintely large σ_d, the interfering

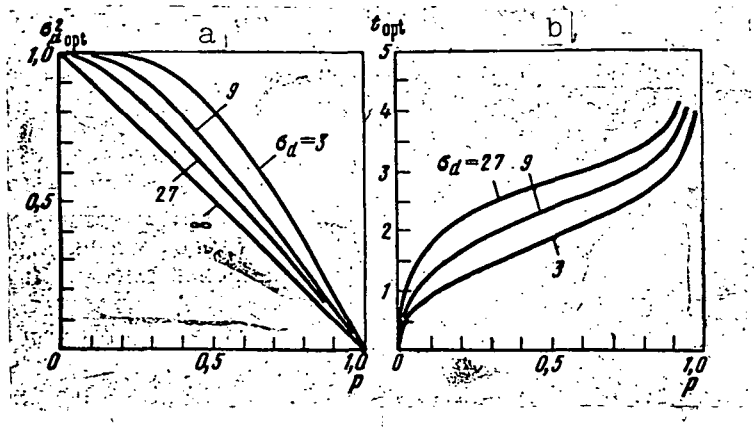

Figure 2. Dependence of the value of $\sigma^2_{\mu_{opt}}$ (a) and t_{opt} (b) on p and t.

parameter d is always estimated, if it does not equal zero, and is not estimated, if it does equal zero. Thus, in $1 - p$ cases $\sigma^2_{\mu} = 1$, and in p cases — zero. Consequently, on the average, $\sigma^2_{\mu_{opt}} = 1 - p$.

Conclusion

The particular solution of the problem of filtering interfering parameters, which is obtained under the condition (27), can be of practical value in several cases. For example, if the columns of the matrix B are orthonormal, then with a large number of measurements, condition (27) will be approximately satisfied.

The cases, when nothing is known about the interfering parameters but their effect matrix B and a priori information about them is constructed arbitrarily, are also possible. Then it is suitable to select such a base in the space of the columns of B such that Condition (27) is satisfied. It is always possible to do this with the linear transformation of the interfering parameters $\bar{d}_s = (B^* S B)^{1/2} \bar{d}$.

The author expresses his appreciation to P. Ye. El'yasberg, M. L. Lidov, and B. Ts. Bakhshiyan for helpful discussion of this work.

REFERENCES

1. Linnik, Yu. V. Statisticheskiye zadichi s meshayushchimi parametrami (Statistical Problems with Interfering Parameters). Moscow, "Nauka" Press, 1966.

2. Akim, E. L. and T. M. Eneyev. Kosmicheskiye issledovaniya, Vol. 1, No. 1, 1963, p. 5.

3. Lidov, M. L. Kosmicheskiye issledovaniya, Vol. 2, No. 5, 1964, p. 713.

4. Bakhshiyan, B. Ts. and P. Ye. El'yasberg. Avtomatika i telemekhanika, No. 3, 1970, p. 16. /36

5. Neyman, J. and E. S. Pearson. Joint Statistical Papers, Berkeley and Los Angeles, University of California Press, 1950.

6. Rao, S. R. Lineynyye statisticheskiye metody i ikh primeneniye (Linear Statistical Methods and Their Application). Moscow, "Nauka" Press, 1968.

N74-28292

METHODS FOR DETERMINING AND PREDICTING ARTIFICIAL EARTH SATELLITE (AES) ORBITS WITH ERRORS PRESENT IN THE MATHEMATICAL DESCRIPTION OF THE MOTION

A. I. Nazarenko and L. G. Markova

ABSTRACT. The problem of determining and predicting AES trajectory parameters from the measurements under the conditions, when the first parts of the integrated equations of motion are calculated approximately is considered. The unconsidered perturbing forces are taken as a gaussian random process of general form. Two methods for determining the estimates of the trajectory parameters are constructed on the basis of using the criterion of maximum a posteriori probability. The first method is based on concurrent analysis of the available measurements. The second method characterized by the successive (recursion) procedure for obtaining estimates is a generalization of the well-known filtration algorithm of Calman-Beussi. A comparison is carried out and the identity of both methods is shown. An approach to the solution of the formulated problem based on the introduction of supplementary refineable parameters and the expansion of the state vector is also investigated.

1. Sources of Errors in Predicting AES Motion

The traditional approach to predicting the motions of celestial objects, which has been developed in classical works with celestial mechanics, is based on formulating and solving the differential equations of motion [1]. This approach is characterized by the assumption that all the forces acting on the space object are known and can be taken into account and that the main source of error is the errors in the initial

conditions. These arise when determining the trajectory parameters (by the method of least squares) because the measurements contain errors.

The traditional approach is also widely used in predicting AES motion. However, it is found that not all the forces acting on the satellite can be considered as known and that not all the known forces can be taken into account on the right sides of the differential equations of motion during their integration. (The errors in the mathematical description of the motion, which arise as a result of this, can in a number of cases appear unfavorably in the results of determining and predicting AES orbits). For example, one of the negative effects of these errors is the limitation of the time interval in which the measurements are used [2].

When studying prediction errors caused by inaccuracies in the known data about the perturbing forces, it is convenient to use the theory of probability. In particular, it is reasonable to consider the perturbing forces, not taken into account in the prediction, as a gaussian random process. The following arguments can be cited to justify such an idea.

1) The theory of probability is applicable not only for cases with a set of recurrent events, but also when there is uncertainty in the conclusions. In our case, there is such uncertainty related, for example, to the expansion coefficients of the gravitational potential, the atmospheric parameters, and the ballistic coefficient of the satellite. /37

2) Application of the characteristics of random processes for describing definite factors does not contradict the possibilities that determinant regularity exists. Thus, for example, the correlation function

$$K_x(t, \tau) = M\{[x(t) - M(t)][x(\tau) - M(\tau)]^T\}$$

characterizes the presence of just such a determinant regularity, and the study of the correlation often serves as a first step in revealing new regularities.

3) The number of perturbing factors not taken into account in the prediction is large, and the conditions of their combined effect are extremely varied, since the location of a given orbit can be distinguished relative to the surface of the Earth, relative to the Moon and the Sun. Thus, for example, the effect of the tesseral (and the sectorial) harmonics in the expansion of the gravitational potential of the Earth depends on the position of the ascending node of the orbit relative to Greenwich ($L = \Omega - S_\Gamma$, where Γ is the sidereal time at Greenwich). The latter quantity varies rapidly, taking the most varied values, and thus for an overwhelming majority of satellites can be considered as a random quantity uniformly distributed on the interval $(0, 2\pi)$. One should also keep in mind here that all the factors not taken into account in the prediction have generally the same order of magnitude, i.e., mutually commensurable, since the main influencing factors are known and are taken into account [3, 4].

These facts permit one to use the central limit theorem and to assume that the value of the perturbations at some moment is a random quantity with normal distribution.

4) The known values of the factors taken into account in prediction are random quantities, since they are determined from a large number of measurements which contain random errors.

5) Braking in the atmosphere, which serves as one of the main perturbing factors, depends significantly on the level of solar activity, which is commonly considered at present as a typical random process [5].

6) The separation of perturbing factors into determinant (taken into account in predicting) and random does not contradict the fact that the nature of an unknown perturbation, which we now refer to as random, will in time be determined as the result of study. Then the conditions for including it among the factors to be taken into account will be created, and the characteristics of the random perturbations will be changed accordingly.

The basic content of this work is an investigation of several ways for increasing the accuracy of determining and predicting AES orbits, which are based on the use of the statistical characteristics of the unconsidered (unknown) perturbing forces. /38

2. Mathematical Formulation of the Problem to Decrease the Systematic Prediction Errors

The true motion of the AES can be represented by the equation

$$\frac{d\mathfrak{s}}{dt} = B(\mathfrak{s}, t)[q_0(\mathfrak{s}, t) + q(\mathfrak{s}, t)]. \qquad (2.1)$$

Here $\mathfrak{s}$, is the vector (column) of the orbital elements; $B(\mathfrak{s}, t)$ is the matrix of coefficients for the forces on the right sides of the equations of the perturbed motion; $q_0(\mathfrak{s}, t)$ is the vector of the known perturbing forces, which are taken into account in predicting; $q(\mathfrak{s}, t)$ is the vector of the perturbing forces not taken into account.

The methods based on the integration of the differential equations of motion with the known external forces

$$\frac{d\tilde{\mathfrak{s}}}{dt} = B(\tilde{\mathfrak{s}}, t)\, q_0(\tilde{\mathfrak{s}}, t). \qquad (2.2)$$

are usually used for prediction. The prediction error is characterized by the difference of the solutions of Equations (2.1) and (2.2)

$$x(t) = \vartheta(t) - \tilde{\vartheta}(t). \tag{2.3}$$

It is not difficult to obtain the differential equation for the prediction error

$$\frac{dx}{dt} = A(t)x + B(t)q(t), \tag{2.4}$$

where

$$A(t) = \frac{\partial [B(\tilde{\vartheta}, t) q_0(\tilde{\vartheta}, t)]}{\partial \tilde{\vartheta}}, \quad B(t) = B(\tilde{\vartheta}, t),$$

on the basis of (2.1) and (2.2) by linearization (under the assumption $|q_0(t)| \gg |q(t)|$).

The perturbations $q(t)$ not taken into account in prediction will be called system noise. It is essential that the noise $q(t)$ differs from white noise, i.e., it is strongly correlated at different moments of time. This fact permits one to plan a way for increasing the prediction accuracy, which is based on estimating and predicting the noise $q(t)$. For example, let an estimate $\hat{q}(t)$ be found. Then, on the basis of the solution of Equation (2.4),

$$x(t) = U(t, t_0)x(t_0) + \int_{t_0}^{t} U(t, \xi)B(\xi)q(\xi)d\xi \tag{2.5}$$

one can find the correction /39

$$\delta x = \int_{t_0}^{t} U(t, \xi)B(\xi)\hat{q}(\xi)d\xi \tag{2.6}$$

to the calculated trajectory (2.2) and determine a refined value for the vector of the elements

$$\tilde{\mathfrak{s}}_{\text{ref}} = \tilde{\mathfrak{s}} + \delta x. \qquad (2.7)$$

It makes sense to seek the estimate $\hat{q}(t)$ for each of the predicted objects and for each of the determinations (refinements) of the trajectory parameters.

From the point of view of determining the corrections x to the calculated trajectory (2.2), the discrepancies between the measured and calculated values of the coordinates can be considered as new measurements, which are a linear function of the unknown corrections.

In fact, let

$$\overline{Y}(t_i) = Y[\mathfrak{s}(t_i)] + v_i$$

be the vector of the values of the coordinates measured at time t_i. These coordinates are a function of the element $\mathfrak{s}$, which contains the measurement error v_i; $\tilde{Y}(t_i) = Y[\tilde{\mathfrak{s}}(t_i)]$ is the calculated value of the measured quantity. Then, considering the smallness of the errors x, we have

$$\overline{Y}(t_i) - \tilde{Y}(t_i) = Y[\tilde{\mathfrak{s}}(t_i) + x(t_i)] + v_i - Y[\tilde{\mathfrak{s}}(t_i)] = \frac{\partial Y[\tilde{\mathfrak{s}}(t_i)]}{\partial \tilde{\mathfrak{s}}(t_i)} x(t_i) + v_i.$$

With the notation

$$z_i = z(t_i) = \overline{Y}(t_i) - \tilde{Y}(t_i), \quad h_i = h(t_i) = \frac{\partial Y[\tilde{\mathfrak{s}}(t_i)]}{\partial \tilde{\mathfrak{s}}(t_i)}, \qquad (2.8)$$

one can write

$$z_i = h_i x(t_i) + v_i. \qquad (2.9)$$

On the basis of this discussion, the problem of decreasing the systematic prediction errors can be formulated in the following manner. The optimum value of the state vector $\mathbf{x}(t)$ at an arbitrary time t is to be found for a system described by Equation (2.4) according to the performed measurements (2.9) $z_i, i=1, \ldots, k$ and the a priori known statistical characteristics

$$M[q(t)]_0 = 0, \quad M[q(t)\,q^T(\tau)]_0 = K_q(t, \tau)_0, \qquad (2.10)$$
$$M(v_i)_0 = 0, \quad M(v_i v_j^T)_0 = R_{ij}$$

The value yielding the maximum of the a posteriori distribution $p(x \mid z_1, \ldots, z_k)$ will be considered as optimum. /40

We note in conclusion that the possibility and relevance of formulating such a problem is due precisely to the fact that the noise $q(t)$ exists and is not white noise. Otherwise, predicting the noise $q(t)$ would be impossible and senseless, since

$$\int_{t_0}^{t} U(t, \xi) B(\xi) \hat{q}(\xi)\, d\xi = 0$$

and in accordance with (2.5)

$$\hat{x}(t) = U(t, t_0)\,\hat{x}(t_0),$$

i.e., in this case, the optimum value of the state vector at an arbitrary time would be uniquely determined by the optimum value of the state vector at a specified time $\hat{x}(t_0)$. The value of this $\hat{x}(t_0)$ can be found on the basis of standard methods of measurement analysis.

3. Prediction with Successive Measurement Analysis

We shall consider the particular case of the problem formulated in Paragraph 2, which is characterized by the condition

$$M(v_i v_j^T) = R_i \delta_{ij}, \tag{3.1}$$

where

$$\delta_{ij} = \begin{cases} 1 & \text{for } j = i, \\ 0 & \text{for } j \neq i, \end{cases}$$

i.e., we assume that the measurement errors at different times are uncorrelated. We note that this assumption is not a necessary one. Successive analysis is also possible with correlated measurement errors. However, since we are considering methods of evaluating the system noise $q(t)$ here, this assumption will simplify the calculation somewhat.

An approach based on successive measurement analysis is used below for solving the formulated problem; the obtained solution has a number of features in common with the well-known filtration algorithm of Calman-Beusi [6]. At the same time, in connection with the peculiarities of the formulated problem with consideration of the "colored" noise $q(t)$ and determination of estimates for the state vector at an arbitrary time, the solution found below differs from the well-known one and can be considered as its generalization.

We assume that, as a result of solving the problem, we obtain at the $(k-1)^{\text{th}}$ step [from the $(k-1)^{\text{th}}$ measurement]

/41

$$\begin{aligned} M[x(t_{k-1})] &= \hat{x}_{k-1|k-1}, \\ M[(x_{k-1} - \hat{x}_{k-1|k-1})(x_{k-1} - \hat{x}_{k-1|k-1})^T] &= P_{k-1|k-1}, \\ M[q(t)] &= \hat{q}(t)_{k-1}, \\ M\{[q(t) - \hat{q}(t)_{k-1}][q(\tau) - \hat{q}(\tau)_{k-1}]^T\} &= K_q(t, \tau)_{k-1}, \\ M\{(x_{k-1} - \hat{x}_{k-1|k-1})[q(t) - \hat{q}(t)_{k-1}]^T\} &= K_{xq}(t_{k-1}, t)_{k-1}. \end{aligned} \tag{3.2}$$

We will take the Bayes approach below. We find and maximize with respect to x_j the a posteriori probability density

$$p(x_j | z_1, z_2, \ldots, z_{k-1}, z_k) = p(x_j | Z_k) = \frac{p(x_j, z_k | Z_{k-1})}{p(z_k | Z_{k-1})}. \qquad (3.3)$$

Since the denominator of the Expression (3.3) does not depend on x_j, then we limit our consideration to the numerator only. We construct the density $p(x_j, z_k | Z_{k-1})$. We shall consider for this the known solution of Equation (2.4) on the basis of which, with (2.9) one can write

$$\begin{aligned} x_j &= U(t_j, t_{k-1}) x_{k-1} + \int_{t_{k-1}}^{t_j} U(t_j, \xi) B(\xi) q(\xi) d\xi, \\ z_k &= h_k U(t_k, t_{k-1}) x_{k-1} + h_k \int_{t_{k-1}}^{t_k} U(t_k, \xi) B(\xi) q(\xi) d\xi + v_k. \end{aligned} \qquad (3.4)$$

The matrix $U(t, t_0)$ is called the fundamental solution matrix for the system of equations $dx/dt = A(t)x$. This matrix itself satisfies the equation, i.e.,

$$\frac{dU(t, t_0)}{dt} = A(t) U(t, t_0).$$

We will use the following notation below for brevity

$$\begin{aligned} U(t_j, t_{k-1}) &= \Phi_j, \quad U(t_k, t_{k-1}) = \Phi_k, \\ \int_{t_{k-1}}^{t_j} U(t_j, \xi) B(\xi) q(\xi) d\xi &= w_{j,k-1}, \quad \int_{t_{k-1}}^{t_j} U(t_j, \xi) B(\xi) \hat{q}(\xi)_{k-1} d\xi = \hat{w}_{j,k-1|k-1}. \end{aligned} \qquad (3.5)$$

Then the Expression (3.4) takes the form

$$x_j = \Phi_j x_{k-1} + w_{j,k-1}, \quad z_k = h_k \Phi_k x_{k-1} + h_k w_{k,k-1} + v_k. \qquad (3.6)$$

It follows from (3.6), with consideration of the initial conditions (3.2) and the a priori statistical characteristics of the

measurement errors (2.10), (3.1), that

$$\hat{x}_{j|k-1} = M(x_j | Z_{k-1}) = \Phi_j \hat{x}_{k-1|k-1} + \hat{w}_{j,k-1|k-1}, \tag{3.7}$$

/42

$$\hat{z}_{k|k-1} = M(z_k | Z_{k-1}) = h_k \hat{x}_{k|k-1}. \tag{3.8}$$

Then, by subtracting

$$\begin{aligned} x_j - \hat{x}_{j|k-1} &= \Phi_j (x_{k-1} - \hat{x}_{k-1|k-1}) + (w_{j,k-1} - \hat{w}_{j,k-1|k-1}), \\ z_k - \hat{z}_{k|k-1} &= h_k (x_k - \hat{x}_{k|k-1}) + v_k, \end{aligned} \tag{3.9}$$

we find, under the same conditions as in (3.7) and (3.8)

$$\begin{aligned} P_{j|k-1} = M[(x_j - \hat{x}_{j|k-1})(x_j - \hat{x}_{j|k-1})^T] &= \Phi_j P_{k-1|k-1} \Phi_j^T + \\ &+ \Phi_j \int_{t_{k-1}}^{t_j} K_{xq}(t_{k-1}, \xi)_{k-1} B^T(\xi)\, U^T(t_j, \xi)\, d\xi + \\ &+ \left[\int_{k-1}^{t_j} U(t_j, \xi) B(\xi) K_{xq}^T(t_{k-1}, \xi)\, d\xi \right] \Phi_j^T + \\ &+ \int_{t_{k-1}}^{t_j} \int_{t_{k-1}}^{t_j} U(t_j, \xi) B(\xi) K_q(\xi, \eta)_{k-1} B^T(\eta) U^T(t_j, \eta)\, d\xi\, d\eta, \end{aligned} \tag{3.10}$$

$$M[(z_k - \hat{z}_{k|k-1})(z_k - \hat{z}_{k|k-1})^T] = h_k P_{k|k-1} h_k^T + R_k, \tag{3.11}$$

$$\begin{aligned} M[(x_j - \hat{x}_{j|k-1})(z_k - \hat{z}_{k|k-1})^T] &= M[(x_j - \hat{x}_{j|k-1})(x_k - \hat{x}_{k|k-1})^T] h_k^T = \\ &= K_x(t_j, t_k)_{k-1} h_k^T = \left[\Phi_j P_{k-1|k-1} \Phi_k^T + \Phi_j \int_{t_{k-1}}^{t_k} K_{xq}(t_{k-1}, \xi)_{k-1} B^T(\xi) \times \right. \\ &\times U^T(t_k, \xi)\, d\xi + \int_{t_{k-1}}^{t_j} U(t_j, \xi) B(\xi) K_{xq}^T(t_{k-1}, \xi)_{k-1}\, d\xi \Phi_k^T + \\ &\left. + \int_{t_{k-1}}^{t_j} \int_{t_{k-1}}^{t_k} U(t_j, \xi) B(\xi) K_q(\xi, \eta)_{k-1} B^T(\eta) U^T(t_k, \eta)\, d\eta\, d\xi \right] h_k^T. \end{aligned} \tag{3.12}$$

The considered density can be expressed in the following manner on the basis of the given (3.7) — (3.12)

$$p(x_j, z_k | Z_{k-1}) = C \exp\left\{-\frac{1}{2}\begin{Vmatrix} x_j - \hat{x}_{j|k-1} \\ z_k - \hat{z}_{k|k-1} \end{Vmatrix}^T \begin{Vmatrix} K & L \\ L^T & M \end{Vmatrix} \begin{Vmatrix} x_j - \hat{x}_{j|k-1} \\ z_k - z_{k|k-1} \end{Vmatrix}\right\}, \quad (3.13)$$

where /43

$$\begin{Vmatrix} K & L \\ L^T & M \end{Vmatrix}^{-1} = \left\| \begin{array}{c|c} P_{j|k-1} & K_x(t_j, t_k)_{k-1} h_k^T \\ \hline h_k K_x^T(t_j, t_k)_{k-1} & h_k P_{k|k-1} h_k^T + R_k \end{array} \right\|. \quad (3.14)$$

Maximizing the density (3.13) is equivalent to minimizing the expression

$$I(x_j) = (x_j - \hat{x}_{j|k-1})^T K (x_j - \hat{x}_{j|k-1}) + (x_j - \hat{x}_{j|k-1})^T L (z_k - \hat{z}_{k|k-1}) + \\ + (z_k - \hat{z}_{k|k-1})^T L^T (x_j - \hat{x}_{j|k-1}) + (z_k - \hat{z}_{k|k-1})^T M (z_k - \hat{z}_{k|k-1}). \quad (3.15)$$

The condition of the minimum from which the unknown estimate $\hat{x}_{j|k}$ is found will be

$$\left[\frac{\partial I(x_j)}{\partial x_j}\right]_{x_j = \hat{x}_{j|k}} = 2(\hat{x}_{j|k} - \hat{x}_{j|k-1})^T K + 2(z_k - \hat{z}_{k|k-1})^T L^T = 0. \quad (3.16)$$

Hence,

$$\hat{x}_{j|k} = \hat{x}_{j|k-1} - K^{-1} L (z_k - \hat{z}_{k|k-1}). \quad (3.17)$$

On the basis of the method for inverting the partitioned matrices [7], we have from (3.14)

$$K_x(t_j, t_k)_{k-1} h_k^T = -K^{-1} L (M - L^T K^{-1} L)^{-1},$$
$$(h_k P_{k|k-1} h_k^T + R_k) = (M - L^T K^{-1} L)^{-1}.$$

By using these relations, we find

$$-K^{-1}L = K_x(t_j, t_k)_{k-1} h_k^T (h_k P_{k|k-1} h_k^T + R_k)^{-1} = K_x(t_j, t_k)_{k-1} h_k^T (R_k^{-1} - \\ - R_k^{-1} h_k P_{k|k} h_k^T R_k^{-1}) = K_x(t_j, t_k)_{k-1} (E - h_k^T R_k^{-1} h_k P_{k|k}) h_k^T R_k^{-1} = \\ = K_x(t_j, t_k)_{k-1} (P_{k|k}^{-1} - h_k^T R_k^{-1} h_k) P_{k|k} h_k^T R_k^{-1} = \\ = K_x(t_j, t_k)_{k-1} P_{k|k-1}^{-1} P_{k|k} h_k^T R_k^{-1}, \quad (3.18)$$

where the notation

$$P_{k|k} = (P_{k|k-1}^{-1} + h_k^T R_k^{-1} h_k)^{-1}. \tag{3.19}$$

Equation (3.17) now takes the form

$$\hat{x}_{j|k} = \hat{x}_{j|k-1} + K_x(t_j, t_k)_{k-1} P_{k|k-1}^{-1} P_{k|k} h_k^T R_k^{-1} (z_k - \hat{z}_{k|k-1}). \tag{3.20}$$

This expression can be used both for solving the filtration problem ($t_j = t_k$) and for interpolation (fitting) and extrapolation (predicting). It is not difficult to note that, in the particular case when $t_j = t_k$, the mutual correlation matrix $K_x(t_j, t_k)_{k-1}$ /44 degenerates into the matrix $P_{k|k-1}$ and Expression (3.20) simplifies to

$$\hat{x}_{k|k} = \hat{x}_{k|k-1} + P_{k|k} h_k^T R_k^{-1} (z_k - \hat{z}_{k|k-1}), \tag{3.21}$$

acquiring the form of the well-known discrete filter equation of Calman-Beusi. It is known [6] that the correlation matrix of the extimate $\hat{x}_{k|k}$ is expressed in the following manner

$$\begin{aligned} M[(x_k - \hat{x}_{k|k})(x_k - \hat{x}_{k|k})^T] &= (P_{k|k-1}^{-1} + h_k^T R_k^{-1} h_k)^{-1} = \\ &= P_{k|k-1} - P_{k|k-1} h_k^T (h_k P_{k|k-1} h_k^T + R_k)^{-1} h_k P_{k|k-1}, \end{aligned} \tag{3.22}$$

which is used with the introduction of the notation (3.19).

The distinguishing characteristic in using Expressions (3.19) and (3.21) for solving the filtration problem in this case is that, to predict the correlation matrix of the state vector at point t_k, an expression of more general form (3.10) than usual [6, 8] is used, which takes into account the presence of correlation between the state vector estimate and the noise (the matrix $K_{xq}(t_{k-1}, t)_{k-1}$). We note that Equations (3.19) and (3.21) do not exhaust the solution of the filtration problem in this case. The a posteriori values of $\hat{q}(t)_k$, $K_{xq}(t_k, t)_k$, $K_q(t, \tau)_k$, still remain to be obtained.

We set up the differential equation for the estimate $\hat{x}_{j|k}$. For this, we differentiate the terms on the right side of Expression (3.20) with respect to t_j. The derivative of the first term in accordance with (3.7), (3.5) is

$$\frac{d\hat{x}_{j|k-1}}{dt_j}=\frac{d\Phi_j}{dt_j}\hat{x}_{k-1|k-1}+\frac{d\hat{w}_{j,k-1|k-1}}{dt_j}=A(t_j)\Phi_j\hat{x}_{k-1|k-1}+$$
$$+A(t_j)\hat{w}_{j,k-1|k-1}+B(t_j)\hat{q}(t_j)_{k-1}=A(t_j)\hat{x}_{j|k-1}+B(t_j)\hat{q}(t_j)_{k-1}. \quad (3.23)$$

In order to find the derivative of the second term, we first differentiate all the terms appearing in the Expression (3.12) for the matrix function $K_x(t_j, t_k)_{k-1}$. We have

$$\frac{d\Phi_j}{dt_j}=A(t_j)\Phi_j,$$
$$\frac{d}{dt_j}\int_{t_{k-1}}^{t_j}U(t_j,\xi)B(\xi)K_{xq}^T(t_{k-1},\xi)_{k-1}\,d\xi=$$
$$=A(t_j)\int_{t_{k-1}}^{t_j}U(t_j,\xi)B(\xi)K_{xq}^T(t_{k-1},\xi)_{k-1}\,d\xi+B(t_j)K_{xq}^T(t_{k-1},t_j)_{k-1},$$
$$\frac{d}{dt_j}\int_{t_{k-1}}^{t_j}\int_{t_{k-1}}^{t_k}U(t_j,\xi)B(\xi)K_q(\xi,\eta)_{k-1}B^T(\eta)U^T(t_k,\eta)\,d\eta\,d\xi=$$
$$=A(t_j)\int_{t_{k-1}}^{t_j}\int_{t_{k-1}}^{t_k}U(t_j,\xi)B(\xi)K_q(\xi,\eta)_{k-1}B^T(\eta)U^T(t_k,\eta)\,d\eta\,d\xi+$$
$$+B(t_j)\int_{t_{k-1}}^{t_k}K_q(t_j,\eta)_{k-1}B^T(\eta)U^T(t_k,\eta)\,d\eta. \quad (3.24)$$

/45

Using (3.24) and (3.12), we obtain

$$\frac{dK_x(t_j,t_k)_{k-1}}{dt_j}=A(t_j)K_x(t_j,t_k)_{k-1}+$$
$$+B(t_j)\left[K_{xq}^T(t_{k-1},t_j)_{k-1}\Phi_k^T+\int_{t_{k-1}}^{t_k}K_q(t_j,\eta)_{k-1}B^T(\eta)U^T(t_k,\eta)\,d\eta\right]. \quad (3.25)$$

Now on the basis of (3.25), (3.23) and (3.20) with the notation

$$K_{wq}(t_j)_{k-1} = \int_{t_{k-1}}^{t_k} U(t_k, \eta) B(\eta) K_q(\eta, t_j)_{k-1} d\eta \tag{3.26}$$

one can write

$$\begin{aligned}
&\frac{d\hat{x}_{j|k}}{dt_j} = A(t_j)\hat{x}_{j|k-1} + B(t_j)\hat{q}(t_j)_{k-1} + \frac{dK_x(t_j, t_k)_{k-1}}{dt_j} P_{k|k-1}^{-1} P_{k|k} h_k^T R_k^{-1} \times \\
&\times (z_k - \hat{z}_{k|k-1}) = A(t_j)[\hat{x}_{j|k-1} + K_x(t_j, t_k)_{k-1} P_{k|k-1}^{-1} P_{k|k} h_k^T R_k^{-1} \times \\
&\times (z_k - \hat{z}_{k|k-1})] + B(t_j)\left\{\hat{q}(t_j)_{k-1} + \left[K_{xq}^T(t_{k-1}, t_j)_{k-1}\Phi_k^T + \right.\right. \\
&\left.\left. + \int_{t_{k-1}}^{t_k} K_q(t_j, \eta)_{k-1} B^T(\eta) U^T(t_k, \eta)\, d\eta\right] P_{k|k-1}^{-1} P_{k|k} h_k^T R_k^{-1} (z_k - \hat{z}_{k|k-1})\right\} = \\
&= A(t_j)\hat{x}_{j|k} + B(t_j)\{\hat{q}(t_j)_{k-1} + [\Phi_k K_{xq}(t_{k-1}, t_j)_{k-1} + \\
&+ K_{wq}(t_j)_{k-1}]^T P_{k|k-1}^{-1} P_{k|k} h_k^T R_k^{-1} (z_k - \hat{z}_{k|k-1})\}.
\end{aligned} \tag{3.27}$$

From a comparison of (3.27) and (3.23), it is obvious that the a posteriori estimate for the mathematical expectation of the random process is

$$\begin{aligned}
\hat{q}(t)_k = \hat{q}(t)_{k-1} + [\Phi_k K_{xq}(t_{k-1}, t)_{k-1} + K_{wq}(t)_{k-1}]^T \times \\
\times P_{k|k-1}^{-1} P_{k|k} h_k^T R_k^{-1} (z_k - \hat{z}_{k|k-1}).
\end{aligned} \tag{3.28}$$

Before proceeding to the immediate construction of the a posteriori values of the functions $K_{xq}(t_k, t)_k$ and $K_q(t, \tau)_k$, we derive some supplementary relations. It follows from the formulas (3.9), (3.5), (3.21) and the initial conditions (3.2) and notation (3.26) that /46

$$\hat{x}_k - x_{k|k} = (x_k - \hat{x}_{k|k-1}) - P_{k|k} h_k^T R_k^{-1} (z_k - \hat{z}_{k|k-1}), \tag{3.29}$$

$$M\{(x_k-\hat{x}_{k|k-1})[q(t)-\hat{q}(t)_{k-1}]^T\}=K_{xq}(t_k,\ t)_{k-1}=$$
$$=\Phi_k M\{(x_{k-1}-\hat{x}_{k-1|k-1})[q(t)-\hat{q}(t)_{k-1}]^T\}+$$
$$+\int_{t_{k-1}}^{t_k}U(t_k,\ \xi)B(\xi)M\{[q(\xi)-\hat{q}(\xi)_{k-1}][q(t)-\hat{q}(t)_{k-1}]^T\}d\xi= \qquad (3.30)$$
$$=\Phi_k K_{xq}(t_{k-1},\ t)_{k-1}+K_{wq}(t)_{k-1},$$

$$M\{(z_k-\hat{z}_{k|k-1})[q(t)-\hat{q}(t)_{k-1}]^T\}=h_k M\{(x_k-\hat{x}_{k|k-1})\times$$
$$\times[q(t)-\hat{q}(t)_{k-1}]^T\}=h_k K_{xq}(t_k,\ t)_{k-1}. \qquad (3.31)$$

In accordance with (3.30), Expression (3.28) takes the form

$$\hat{q}(t)_k=\hat{q}(t)_{k-1}+K_{xq}^T(t_k,\ t)_{k-1}P_{k|k-1}^{-1}P_{k|k}h_k^TR_k^{-1}(z_k-\hat{z}_{k|k-1}). \qquad (3.32)$$

In addition, the following identities are valid

$$M[(x_k-\hat{x}_{k|k})(z_k-\hat{z}_{k|k-1})^T]=0, \qquad (3.33)$$

$$M\{(z_k-\hat{z}_{k|k-1})[q(t)-\hat{q}(t_k)]^T\}=0. \qquad (3.34)$$

Actually, by replacing the differences $x_k-\hat{x}_{k|k}$ and $q(t)-\hat{q}(t)_k$ with the help of (3.29) and (3.32) respectively, and also in view of (3.10), (3.11) and the relation $h_k^TR_k^{-1}h_k=P_{k|k}^{-1}-P_{k|k-1}^{-1}$, resulting from (3.19), we have

$$M[(x_k-\hat{x}_{k|k})(z_k-\hat{z}_{k|k-1})^T]=M[(x_k-\hat{x}_{k|k-1})(z_k-\hat{z}_{k|k-1})^T]-$$
$$-P_{k|k}h_k^TR_k^{-1}M[(z_k-\hat{z}_{k|k-1})(z_k-\hat{z}_{k|k-1})^T]=$$
$$=P_{k|k-1}h_k^T-P_{k|k}h_k^TR_k^{-1}(h_kP_{k|k-1}h_k^T+R_k)=$$
$$=(P_{k|k-1}-P_{k|k}h_k^TR_k^{-1}h_kP_{k|k-1}-P_{k|k})h_k^T=$$
$$=(P_{k|k-1}-P_{k|k}P_{k|k}^{-1}P_{k|k-1}+P_{k|k}P_{k|k-1}^{-1}P_{k|k-1}-P_{k|k})h_k^T=0,$$
$$M\{(z_k-\hat{z}_{k|k-1})[q(t)-\hat{q}(t)_k]^T\}=M\{(z_k-\hat{z}_{k|k-1})[q(t)-\hat{q}(t)_{k-1}]^T\}-$$
$$-M[(z_k-\hat{z}_{k|k-1})(z_k-\hat{z}_{k|k-1})^T]R_k^{-1}h_kP_{k|k}P_{k|k-1}^{-1}K_{xq}(t_k,\ t)_{k-1}=$$
$$=h_kK_{xq}(t_k,\ t)_{k-1}-(h_kP_{k|k-1}h_k^T+R_k)R_k^{-1}h_kP_{k|k}P_{k|k-1}^{-1}K_{xq}(t_k,\ t)_{k-1}=$$
$$=h_k(E-P_{k|k-1}h_k^TR_k^{-1}h_kP_{k|k}P_{k|k-1}^{-1}-P_{k|k}P_{k|k-1}^{-1})K_{xq}(t_k,\ t)_{k-1}=$$
$$=h_k(E-P_{k|k-1}P_{k|k}^{-1}P_{k|k}P_{k|k-1}^{-1}+P_{k|k-1}P_{k|k-1}^{-1}P_{k|k}P_{k|k-1}^{-1}-P_{k|k}P_{k|k-1}^{-1})\times$$
$$\times K_{xq}(t_k,\ t)_{k-1}=0.$$

/47

Now, on the basis of the relations (3.32), (3.33), (3.29), (3.10), (3.11), and (3.34), it is easy to determine the unknown correlation functions

$$\begin{aligned} K_{xq}(t_k, t)_k &= M\{(x_k - \hat{x}_{k|k})[q(t) - \hat{q}(t)_k]^T\} = \\ &= M\{(x_k - \hat{x}_{k|k})[q(t) - \hat{q}(t)_{k-1}]^T\} - \\ &- M[x_k - \hat{x}_{k|k})(z_k - \hat{z}_{k|k-1})^T] R_k^{-1} h_k P_{k|k} P_{k|k-1}^{-1} K_{xq}(t_k, t)_{k-1} = \\ &= M\{(x_k - \hat{x}_{k|k})[q(t) - \hat{q}(t)_{k-1}]^T\} = K_{xq}(t_k, t)_{k-1} - \\ &- P_{k|k} h_k^T R_k^{-1} h_k K_{xq}(t_k, t)_{k-1} = (E - P_{k|k} P_{k|k}^{-1} + P_{k|k} P_{k|k-1}^{-1}) \times \\ &\times K_{xq}(t_k, t)_{k-1} = P_{k|k} P_{k|k-1}^{-1} K_{xq}(t_k, t)_{k-1}, \end{aligned} \tag{3.35}$$

$$\begin{aligned} K_q(t, \tau)_k &= M\{[q(t) - \hat{q}(t)_k][q(\tau) - \hat{q}(\tau)_k]^T\} = \\ &= M\{[q(t) - \hat{q}(t)_{k-1}][q(\tau) - \hat{q}(\tau)_k]^T\} - \\ &- K_{xq}^T(t_k, t)_{k-1} P_{k|k-1}^{-1} P_{k|k} h_k^T R_k^{-1} M\{(z_k - \hat{z}_{k|k-1})[q(\tau) - \hat{q}(\tau)_k]^T\} = \\ &= M\{[q(t) - \hat{q}(t)_{k-1}][q(\tau) - \hat{q}(\tau)_k]^T\} = K_q(t, \tau)_{k-1} - \\ &- K_{xq}^T(t_k, t)_{k-1} h_k^T R_k^{-1} h_k P_{k|k} P_{k|k-1}^{-1} K_{xq}(t_k, \tau)_{k-1} = K_q(t, \tau)_{k-1} - \\ &- K_{xq}^T(t_k, t)_{k-1} (h_k^T R_k^{-1} h_k - h_k^T R_k^{-1} h_k P_{k|k} h_k^T R_k^{-1} h_k) K_{xq}(t_k, \tau)_{k-1}. \end{aligned} \tag{3.36}$$

Thus, the construction of the filgration algorithm is completed. The obtained Expressions (3.21), (3.19), (3.32), (3.35), (3.36), together with the supplementary dependencies (3.5), (3.7), (3.8), (3.10), (3.26), (3.30) containing the introduced notations exhaust the solution of the filtration problem. In addition, the independencies (3.20) and (3.12) permit one to find the estimate for the state vector at any time, i.e., they are the solution of the fitting and predicting problems.

We consider the relation of the obtained expression (3.20) with the approximate expression

$$\tilde{x}_{j|k} = U(t_j, t_k)\hat{x}_{k|k}, \tag{3.37}$$

which is usually used for prediction when there is no data on the system noise $q(t)$. It follows from (3.27), (3.28) that

$$\hat{x}_{j|k} = U(t_j, t_k)\hat{x}_{k|k} + \int_{t_k}^{t_j} U(t_j, \xi)B(\xi)\hat{q}(\xi)_k d\xi, \qquad (3.38)$$

and, consequently, the dependencies (3.37), (3.38) give different results. Since the solution (3.38) ensures the maximum a posteriori probability $p(x_j|Z_k)$, it should be considered more accurate, and the error in Expression (3.37) in comparison with (3.38) will equal /48

$$\hat{w}_{j,k|k} = \int_{t_k}^{t_j} U(t_j, \xi)B(\xi)\hat{q}(\xi)_k d\xi. \qquad (3.39)$$

The following properties of this error are obvious:

a) $\lim_{t_j \to t_k} \hat{w}_{j,k|k} = 0$, i.e., the greater effectiveness of the solution (3.38) begins to appear for significant prediction intervals;

b) for $\hat{q}(\xi)_k = 0$, the dependencies (3.37), (3.38) coincide and, conversely, the quantity $w_{j,k|k}$ is larger, the larger the noise $\hat{q}(\xi)_k$.

On this basis, one can characterize in general outline the region where the obtained prediction algorithm is more effective compared with approximate algorithms, which are not connected with obtaining an estimate of the noise $q(t)$. There appear in this region systems for which the noise $q(t)$, firstly, is appreciable correlated in time and, secondly, causes a significant variation of the state vector over the prediction interval (t_k, t_j).

In conclusion, we investigate the accuracy of the obtained estimate (3.20) of the state vector at time t_j. We transform the functional expression (3.15) by using the relation of the vectors $(z_k - \hat{z}_{k|k-1})$, $(\hat{x}_{j|k} - \hat{x}_{j|k-1})$, resulting from (3.20) and the identity

$$M = (h_k P_{k|k-1} h_k^T + R_k)^{-1} + L^T K^{-1} L.$$

We obtain

$$I(x_j) = (x_j - \hat{x}_{j|k})^T K (x_j - \hat{x}_{j|k}) + (z_k - \hat{z}_{k|k-1})^T (h_k P_{k|k-1} h_k^T + R_k)^{-1} (z_k - \hat{z}_{k|k-1}), \quad (3.40)$$

where

$$K^{-1} = P_{j|k-1} - K_x(t_j, t_k)_{k-1} h_k^T (h_k P_{k|k-1} h_k^T + R_k)^{-1} h_k K_x^T (t_j, t_k)_{k-1}. \quad (3.41)$$

It is easy, on the basis of (3.40), (3.3) and (3.13), to write an expression for the a posteriori distribution

$$p(x_j | Z_k) = C \exp\left\{-\frac{1}{2}(x_j - \hat{x}_{j|k})^T K (x_j - \hat{x}_{j|k})\right\}. \quad (3.42)$$

Thus, the estimate (3.20) is the a posteriori mathematical expectation of the vector x_j, i.e.,

$$M(x_j | Z_k) = \hat{x}_{j|k}, \quad (3.43)$$

and K^{-1} (3.41) is its correlation matrix

$$M[(x_j - \hat{x}_{j|k})(x_j - \hat{x}_{j|k})^T] = K^{-1}. \quad (3.44)$$

We note that the maximum value of the functional (3.40) achieved /49 for $x_j = \hat{x}_{j|k}$, equals

$$I(\hat{x}_{j|k}) = (z_k - \hat{z}_{k|k-1})^T (h_k P_{k|k-1} h_k^T + R_k)^{-1} (z_k - \hat{z}_{k|k-1}) \quad (3.45)$$

and is a random quantity with a χ^2 distribution with m degrees of freedom (m is the dimension of the vector z).

It is obvious that any estimate of the state vector differing from (3.20) will have a greater dispersion. Actually, for $x_j^* \neq \hat{x}_{j|k}$ it follows from the relation

$$(K^*)^{-1} = M[(x_j - x_j^*)(x_j - x_j^*)^T] = K^{-1} + (\hat{x}_{j|k} - x_j^*)(\hat{x}_{j|k} - x_j^*)^T$$

that the diagonal elements of the matrix $(K^*)^{-1}$ are strictly larger than the corresponding diagonal terms of the matrix K^{-1}. This indicates that the estimate (3.20) also minimizes the dispersion of the state vector and, in addition, that any linear transformation of the vector $\hat{x}_{j|k}$ will have the minimum dispersion.

4. Prediction with Concurrent Measurement Analysis

The problem formulated in Paragraph 2 can be solved by different methods. One method connected with the use of successive methods of measurement analysis [6] is considered in Paragraph 3. It is possible to solve the problem using the methods of least squares and maximum probability [9, 10], which provide for concurrent measurement analysis. We know of no investigations in which the random process $q(t)$ is taken into account with the use of these methods. Thus, to obtain such a solution is very tempting, since it will generalize the known solution [9] to the case when the random process $q(t)$ appears in the description of the motion.

It is well known that, without a priori data about the vector x_j, the estimates obtained by the methods of maximum probability and maximum a posteriori probability density coincide. We will maximize with respect to x_j the probability function $L(z_1, \ldots, z_k | x_j) = L(Z_k | x_j)$.

It follows from the solution of the Equation (3.4) and the relations (2.9) that

$$x_i = U(t_i, t_j)\, x_j + \int_{t_j}^{t_i} U(t_i, \xi) B(\xi) q(\xi) d\xi, \tag{4.1}$$

$$z_i = h_i U(t_i, t_j)\, x_j + h_i \int_{t_j}^{t_i} U(t_i, \xi) B(\xi) q(\xi) d\xi + v_i. \tag{4.2}$$

It is easy, on the basis of Expression (4.2) and the a priori data on the statistical characteristics of the noise $q(t)$ and v_i (2.10), to construct the probability function. For this, we introduce the notation /50

$$Z_k = \begin{Vmatrix} z_1 \\ z_2 \\ \cdot \\ \cdot \\ z_k \end{Vmatrix}, \quad H = \begin{Vmatrix} h_1 & & & \\ & h_2 & & \\ & & \cdot & \\ & & & h_k \end{Vmatrix}, \quad R_\Sigma = \begin{Vmatrix} R_{11} & \dots & R_{1k} \\ \cdot & \cdot & \cdot \\ \cdot & \cdot & \cdot \\ R_{k1} & \dots & R_{kk} \end{Vmatrix},$$

$$w_{ij} = \int_{t_j}^{t_i} U(t_i, \xi) B(\xi) q(\xi) d\xi,$$

$$U_j = \begin{Vmatrix} U(t_1, t_j) \\ \cdot \\ \cdot \\ \cdot \\ U(t_k, t_j) \end{Vmatrix}, \quad HU_j = X_j, \tag{4.3}$$

$$Q_{il} = M(w_{ij} w_{ij}^T) = \int_{t_j}^{t_i} \int_{t_j}^{t_l} U(t_i, \xi) B(\xi) K_q(\xi, \eta) B^T(\eta) U^T(t_l, \eta) d\eta\, d\xi,$$

$$K_{wj} = \{Q_{il}\}, \quad i, l = 1, \dots, k.$$

We finally obtain

$$M(Z_k | x_j) = \begin{Vmatrix} h_1 U(t_1, t_j) \\ \cdot \\ \cdot \\ \cdot \\ h_k U(t_k, t_j) \end{Vmatrix} x_j = HU_j x_j = X_j x_j, \tag{4.4}$$

$$\operatorname{cov}(Z_k | x_j) = M\{[Z_k - M(Z_k | x_j)][Z_k - M(Z_k | x_j)]^T\} = HK_{wj}H^T + R_\Sigma, \tag{4.5}$$

$$L(Z_k|x_j) = C\exp\left\{-\frac{1}{2}(Z_k - X_j x_j)^T (HK_{wj}H^T + R_\Sigma)^{-1}(Z_k - X_j x_j)\right\}. \quad (4.6)$$

The maximum of the probability function is provided by the estimate [9]

$$\hat{x}_j = (X_j^T N_j X_j)^{-1} X_j^T N_j Z_k, \quad (4.7)$$

with the notation

$$N_j = (HK_{wj}H^T + R_\Sigma)^{-1}. \quad (4.8)$$

It is easy to show that

$$K_x(t_j, t_j) = M[(x_j - \hat{x}_j)(x_j - \hat{x}_j)^T] = (X_j^T N_j X_j)^{-1}. \quad (4.9)$$

The solution (4.7) does not differ in form from that obtained in [9]. The difference is in the formation of the matrix N_j, which takes into account the effect not only of the measurement errors (the matrix R_Σ), but also the system noise (the matrix K_{wj}). In the particular case without noise $q(t)$, i.e., for $K_q(t, \tau) = 0$, the term $HK_{wj}H^T$ vanishes and the solution (4.7), (4.8) coincides with the known solution. The term $HK_{wj}H^T$ also equals zero in another particular case, when the times t_j and t_i, $i = 1, \ldots, k$ coincide, i.e., when the state vector is estimated at the time of measurement. The matrices X_j and N_j appearing in the solution (4.7) are functions of the time t_j. Thus, the given solution can be used for determining estimates of the state vector at arbitrary times, i.e., for predicting the motion of the system. /51

However, the use of the solution (4.7) for prediction is not always convenient. When it is necessary to determine the state vector at different times, repeated matrix inversions have to be carried out. Another disadvantage of the solution (4.7)

is that it does not contain a clear link between this prediction method and the integration of the equations of motion (2.4), the solution of the Cauchy problem, which is ordinarily used. It is of interest in connection with this to find on the basis of (4.7) the system of differential equations of the form

$$\frac{d\hat{x}_j}{dt_j} = A(t_j)\hat{x}_j + B(t_j)\hat{q}(t_j)$$

and, thus, to construct a prediction algorithm equivalent to (4.7), which is based on the integration of this system of equations.

To begin this problem, we differentiate the expression for the estimate $\hat{x}_j$ (4.7), introducing the notation

$$(X_j^T N_j X_j)^{-1} = C_j. \tag{4.10}$$

We have

$$\frac{d\hat{x}_j}{dt_j} = \frac{d(C_j X_j^T N_j)}{dt_j} Z_k = \left[\frac{dC_j}{dt_j} X_j^T N_j + C_j \frac{dX_j^T}{dt_j} N_j + C_j X_j^T \frac{dN_j}{dt_j}\right] Z_k. \tag{4.11}$$

We obtain expressions for a number of derivatives, which, while having supplementary value now, will be necessary in a later discussion. We differentiate the corresponding expressions from (4.3), (4.8), and (4.10)

$$\frac{dX_j}{dt_j} = -X_j A(t_j),$$

$$\frac{dK_{wj}}{dt_j} = \frac{d}{dt_j}\left\{\int_{t_j}^{t_i}\int_{t_j}^{t_l} U(t_i, \xi) B(\xi) K_q(\xi, \eta) B^T(\eta) U(t_l, \eta)\, d\eta\, d\xi\right\}_{i,l=1,\ldots,k} =$$

$$= \left\{-\left[\int_{t_j}^{t_l} U(t_i, \xi) B(\xi) K_q(\xi, t_j)\, d\xi\right] B^T(t_j) U^T(t_l, t_j) - \right.$$

$$\left. - U(t_i, t_j) B(t_j)\left[\int_{t_j}^{t_l} K_q(t_j, \eta) B^T(\eta) U^T(t_l, \eta)\, d\eta\right]\right\}_{i,l=1,\ldots,k} =$$

$$= -W_j(t_j) B^T(t_j) U_j^T - U_j B(t_j) W_j^T(t_j),$$

where

$$W_j(t_j) = \begin{Vmatrix} K_{wq}(t_1, t_j) \\ \cdots\cdots \\ \cdots\cdots \\ K_{wq}(t_k, t_j) \end{Vmatrix}, \tag{4.12}$$

$$K_{wq}(t_i, t_j) = \int_{t_j}^{t_i} U(t_i, \xi) B(\xi) K_q(\xi, t_j)\, d\xi, \tag{4.13}$$

$$\frac{dN_j}{dt_j} = -N_j \frac{dN_j^{-1}}{dt_j} N_j = -N_j H \frac{dK_{wj}}{dt_j} H^T N_j = N_j H W_j(t_j) B^T(t_j) \times$$
$$\times X_j^T N_j + N_j X_j B(t_j) W_j^T(t_j) H^T N_j, \tag{4.14}$$

$$\frac{dC_j}{dt_j} = -C_j \frac{dC_j^{-1}}{dt_j} C_j = -C_j \left[\frac{dX_j^T}{dt_j} N_j X_j + X_j^T \frac{dN_j}{dt_j} X_j + \right.$$
$$\left. + X_j^T N_j \frac{dX_j}{dt_j} \right] C_j = C_j A^T(t_j) + A(t_j) C_j - \tag{4.15}$$

$$\frac{d(C_j X_j^T N_j)}{dt_j} = -C_j X_j^T N_j H W_j(t_j) B^T(t_j) - B(t_j) W_j^T(t_j) H^T N_j X_j C_j,$$
$$= [C_j A^T(t_j) + A(t_j) C_j - C_j X_j^T N_j H W_j(t_j) B^T(t_j) -$$
$$- B(t_j) W_j^T(t_j) H^T N_j X_j C_j] X_j^T N_j - C_j A^T(t_j) X_j^T N_j +$$
$$+ C_j X_j^T N_j H W_j(t_j) B^T(t_j) X_j^T N_j + C_j X_j^T N_j X_j B(t_j) W_j^T(t_j) H^T N_j = \tag{4.16}$$
$$= A(t_j) C_j X_j^T N_j + B(t_j) W_j^T(t_j) H^T N_j (E - X_j C_j X_j^T N_j).$$

Finally, we write , with consideration of (4.16), (4.7), (4.11),

$$\frac{d\hat{x}_j}{dt_j} = A(t_j)\hat{x}_j + B(t_j) W_j^T(t_j) H^T N_j (Z_k - X_j \hat{x}_j). \tag{4.17}$$

Thus, the posed problem is solved. The differential equation for the estimate of the maximum probability is constructed. It /53 is evident from a comparison of (2.4) and (4.17) ,that the function

$$\hat{q}(t_j) = W_j^T(t_j) H^T N_j (Z_k - X_j \hat{x}_j) \tag{4.18}$$

is the estimate of the system noise at time t_j. Integration of Equation (4.18) with initial conditions found with the solution (4.7) for a fixed $t_j = t_0$ permits one to determine the estimate of the state vector at an arbitrary time, i.e., it provides the solution of the prediction problem.

It is obvious from Equation (4.17) that the integration of the equation

$$\frac{d\hat{x}}{dt_l} = A(t_l)\hat{x}_l$$

ordinarily used for prediction or the solution equivalent to it

$$\hat{x}_l = U(t_l, t_0)\hat{x}_0$$

do not ensure obtaining effective estimates, since the possibilities of determining and using the estimate of the system noise (4.18) is not taken into account.

We present the prediction algorithm based on the solution of the Equation (4.17)

$$\hat{x}_l = U(t_l, t_0)\hat{x}_0 + \int_{t_0}^{t_l} U(t_l, \xi) B(\xi) \hat{q}(\xi) d\xi.$$

We introduce several supplementary identities for this and make a number of simplifications. By dividing the integration interval at the arbitrary point t_0 and using the property of the transfer matrices $U(t_i, \xi) = U(t_i, t_j)$, $U(t_j, \xi)$, we transform the expression (4.13) and hence, (4.12)

$$K_{wq}(t_i, t_j) = U(t_i, t_j) \int_{t_j}^{t_0} U(t_j, \xi) B(\xi) K_q(\xi, t_j) d\xi + \int_{t_0}^{t_i} U(t_i, \xi) B(\xi) K_q(\xi, t_j) d\xi, \quad (4.19)$$

$$W_l(t_j) = U_l \Delta K_{wq} + W_0(t_j),$$

with the notation

$$\Delta K_{wq} = \int_{t_j}^{t_0} U(t_j, \xi) B(\xi) K_q(\xi, t_j) d\xi.$$

We substitute (4.19) and (4.7) into the expression for estimating the system noise (4.18)

$$\hat{q}(t_j) = [\Delta K_{wq}^T U_j^T + W_0^T(t_j)] H^T (N_j - N_j X_j C_j X_j^T N_j) Z_k. \qquad (4.20)$$

We denote /54

$$G_j = N_j - N_j X_j C_j X_j^T N_j. \qquad (4.21)$$

The matrix G_j has the following properties, which will be used to simplify Expression (4.20)

$$X_j^T G_j = 0, \quad G_j X_j = 0, \quad \frac{dG_j}{dt_j} = 0. \qquad (4.22)$$

In fact, with consideration of (4.11), (4.14), (4.16)

$$X_j^T G_j = X_j^T N_j - X_j^T N_j X_j C_j X_j^T N_j = X_j^T N_j - C_j^{-1} C_j X_j^T N_j = 0,$$
$$G_j X_j = N_j X_j - N_j X_j C_j X_j^T N_j X_j = N_j X_j - N_j X_j C_j C_j^{-1} = 0,$$
$$\frac{dG_j}{dt_j} = \frac{dN_j}{dt_j} - \frac{dN_j}{dt_j} X_j C_j X_j^T N_j - N_j \frac{dX_j}{dt_j} C_j X_j^T N_j - N_j X_j \frac{d(C_j X_j^T N_j)}{dt_j} =$$
$$= N_j H W_j(t_j) B^T(t_j) X_j^T N_j (E - X_j C_j X_j^T N_j) +$$
$$+ N_j X_j B(t_j) W_j^T(t_j) H^T N_j (E - X_j C_j X_j^T N_j) +$$
$$+ N_j X_j A(t_j) C_j X_j^T N_j - N_j X_j A(t_j) C_j X_j^T N_j -$$
$$- N_j X_j B(t_j) W_j^T(t_j) H^T N_j (E - X_j C_j X_j^T N_j) =$$
$$= N_j H W_j(t_j) B^T(t_j) X_j^T N_j - N_j H W_j(t_j) B^T(t_j) (X_j^T N_j X_j) C_j X_j^T N_j = 0.$$

It follows from the last property that, in particular, $G_j = G_k$.

Then, we have on the basis of (4.21) and these properties of the matrix G_j

$$\hat{q}(t_j) = W_0^T(t_j) H^T G_k Z_k$$

for an arbitrary initial time t_0 or

$$\hat{\boldsymbol{q}}(t_j) = W_k^T(t_j) H^T G_k Z_k = W_k^T(t_j) H^T \check{N}_k (Z_k - X_k \hat{\boldsymbol{x}}_k) \,, \tag{4.23}$$

for the initial time t_0 coinciding with the time of the k^{th} measurement.

By writing the solution of Equation (2.4) with the initial data at time t_k and substituting the estimate of the system noise (4.23), we have finally

$$\begin{aligned}
\hat{\boldsymbol{x}}_j &= U(j, t_k)\hat{\boldsymbol{x}}_k + \left[\int_{t_k}^{t_j} U(t_j, \xi) B(\xi) W_k^T(\xi)\, d\xi\right] H^T G_k Z_k = \\
&= U(t_j, t_k)\hat{\boldsymbol{x}}_k + \left\{\int_{t_k}^{t_j} U(t_j, \xi) B(\xi) \left[\int_{t_k}^{t_i} U(t_i, \eta) B(\eta) K_q(\eta, \xi) \times\right.\right. \\
&\left.\left. \times d\eta\right]_{i=1,\ldots,k}^T d\xi\right\} H^T G_k Z_k = U(t_j, t_k)\hat{\boldsymbol{x}}_k + \\
&+ \left[\int_{t_k}^{t_j}\int_{t_k}^{t_i} U(t_j, \xi) B(\xi) K_q(\xi, \eta) B^T(\eta) U^T(t_i, \eta)\, d\eta\, d\xi\right]_{i=1,\ldots,k} \times \\
&\times H^T G_k Z_k = U(t_j, t_k)\hat{\boldsymbol{x}}_k + \{Q_{ji}\}_{i=1,\ldots,k} H^T G_k Z_k .
\end{aligned} \tag{4.24}$$

/55

The dependence (4.24) ensures obtaining more precise values of the state vector for prediction. It contains the term $\delta \boldsymbol{x} = \{Q_{ji}\}_{i=1,\ldots,k} H^T G_k Z_k$, which can be considered as a correction decreasing the effect of the perturbing forces not taken into account in the prediction.

The correlation matrix of the prediction errors can be determined by various methods. One of them is based on the use of the dependence (4.9), another — on the solution of the differential equations for the correlation matrix. The latter uses as initial conditions the matrices

$$\begin{aligned}
M[(\boldsymbol{x}_j - \hat{\boldsymbol{x}}_{j|k})(\boldsymbol{x}_j - \hat{\boldsymbol{x}}_{j|k})^T] &= P_{j|k}, \\
M\{(\boldsymbol{x}_j - \hat{\boldsymbol{x}}_{j|k})[\boldsymbol{q}(\tau) - \hat{\boldsymbol{q}}(\tau)_k]^T\} &= K_{xq}(t_j, \tau)_k, \\
M\{[\boldsymbol{q}(t) - \hat{\boldsymbol{q}}(t)_k][\boldsymbol{q}(\tau) - \hat{\boldsymbol{q}}(\tau)_k]^T\} &= K_q(t, \tau)_k.
\end{aligned}$$

In conclusion, we construct, in connection with this the a posterior correlation functions $K_{xq}(t_j, \tau)_k$, $K_q(t, \tau)_k$.

It follows from (4.7), (4.2), (4.3), that

$$x_j - \hat{x}_{j|k} = x_j - (X_j^T N_j X_j)^{-1} X_j^T N_j [X_j x_j + H(w_{ij})_{i=1,\ldots,k} + V_k] = \\ = -(X_j^T N_j X_j)^{-1} X_j^T N_j [H(w_{ij})_{i=1,\ldots,k} + V_k], \tag{4.25}$$

where

$$V_k = \begin{Vmatrix} v_1 \\ \cdot \\ \cdot \\ \cdot \\ v_k \end{Vmatrix}.$$

On the basis of (4.23) for $G_k = G_j$ and $t_0 = t_j$ and also by using the expression for Z_k appearing in (4.25) and the property (4.22), we obtain

$$q(\tau) - \hat{q}(\tau)_k = q(\tau) - W_j^T(\tau) H^T G_j [X_j x_j + H(w_{ij})_{i=1,\ldots,k} + V_k] = \\ = q(\tau) - W_j^T(\tau) H^T G_j [H(w_{ij})_{i=1,\ldots,k} + V_k]. \tag{4.26}$$

Then, with consideration of (4.25) and (4.26)

$$K_{xq}(t_j, \tau)_k = -(X_j^T N_j X_j)^{-1} X_j^T N_j M \{[H(w_{ij})_{i=1,\ldots,k} + V_k] q^T(\tau)\} + \\ + (X_j^T N_j X_j)^{-1} X_j^T N_j M \{[H(w_{ij})_{i=1,\ldots,k} + \\ + V_k] [H(w_{ij})_{i=1,\ldots,k} + V_k]^T\} G_j H W_j(\tau).$$

The mathematical expectation appearing in the first term equals $[HW_j(\tau)]$, in view of the notations (4.12), (4.13), and also the noncorrelation of the measurement errors and system noise. The mathematical expectation present in the second term equals N_j^{-1} in accordance with (4.3), (4.8). Thus, we have with consideration of the notation (4.10) /56

$$K_{xq}(t_j, \tau)_k = -C_j X_j^T N_j H W_j(\tau) + C_j X_j^T N_j N_j^{-1} G_j H W_j(\tau) = \\ = -C_j X_j^T N_j H W_j(\tau). \tag{4.27}$$

The second term in (4.27) vanishes in view of property (4.22).

Analogous to the preceding, we obtain, on the basis of (4.26)

$$K_q(t_j, \tau)_k = M[q(t_j)\, q^T(\tau)] - M\{q(t_j)[(w_{ij})^T_{i=1,\ldots,k} H^T + V_k^T]\}\, G_j H W_j(\tau) -$$
$$- W_j^T(t_j)\, H^T G_j M\{[H(w_{ij})_{i=1,\ldots,k} + V_k]\, q^T(\tau)\} +$$
$$+ W_j^T(t_j)\, H^T G_j M\{[H(w_{ij})_{i=1,\ldots,k} + V_k]\, [H(w_{ij})_{i=1,\ldots,k} + V_k]^T\} \times$$
$$\times G_j H W_j(\tau) = K_q(t_j, \tau)_0 - W_j^T(t_j)\, H^T G_j H W_j(\tau) -$$
$$- W_j^T(t_j)\, H^T G_j H W_j(\tau) + W_j^T(t_j)\, H^T G_j N_j^{-1} G_j H W_j(\tau) =$$
$$= K_q(t_j, \tau)_0 - W_j^T(t_j)\, H^T [G_j + G_j - G_j N_j^{-1} G_j] H W_j(\tau).$$

We show that the square bracket in the last expression equals G_j

$$G_j + G_j - G_j N_j^{-1} G_j = 2G_j - N_j (E - X_j C_j X_j^T N_j) N_j^{-1} N_j (E - X_j C_j X_j^T N_j) =$$
$$= 2G_j - N_j (E - X_j C_j X_j^T N_j) = 2G_j - G_j = G_j.$$

Finally

$$K_q(t_j, \tau)_k = K_q(t_j, \tau)_0 - W_j^T(t_j)\, H^T G_j H W_j(\tau). \qquad (4.28)$$

5. Prediction with the Use of Correcting Functions

One of the possible methods for solving the problem formulated in Paragraph 2 is a method based on the introduction of correcting functions of the form

$$\delta a = \sum_{m=1}^{n} c_m f_m(t). \qquad (5.1)$$

into the prediction algorithm of the type (2.2). In this case, not only are the trajectory parameters (orbital elements) at some time refined (determined), but also the coefficients c_m of the /57
polynomials (5.1). The prediction algorithm can be written in the following form:

$$\tilde{\tilde{\vartheta}}(t) = \tilde{\vartheta}(\tilde{\tilde{\vartheta}}_0, t) + F(t)C. \qquad (5.2)$$

Here the vector function $\tilde{\vartheta}(\tilde{\tilde{\vartheta}}_0, t)$ is the solution of the system of Equations (2.2); $F(t) = \|f_1(t) \ldots f_n(t)\|$ is a known function selected on the basis of the a priori data and satisfying the condition $F(t_0) = 0$;

$$C = \begin{Vmatrix} C_1 \\ \vdots \\ C_n \end{Vmatrix}$$

is the vector of coefficients to be refined by the measurements.

The prediction error is denoted, as previously

$$x = \vartheta - \tilde{\tilde{\vartheta}}. \qquad (5.3)$$

On the basis of (2.1), (2.2), (5.2), we construct the linear differential equation for the prediction error. By differentiating (5.3), we obtain

$$\begin{aligned} \frac{dx}{dt} &= \frac{d\vartheta}{dt} - \frac{d\tilde{\vartheta}}{dt} - F'(t)C = B(\tilde{\tilde{\vartheta}} + x, t)[q_0(\tilde{\tilde{\vartheta}} + x, t) + q(\tilde{\tilde{\vartheta}} + x, t)] - \\ &- B[\tilde{\tilde{\vartheta}} - F(t)C, t]\, q_0[\tilde{\tilde{\vartheta}} - F(t)C, t] - F'(t)C = \\ &= A(t)x + [A(t)F(t) - F'(t)]C + B(t)q(t), \end{aligned} \qquad (5.4)$$

where

$$A(t) = \frac{\partial [B(\tilde{\tilde{\vartheta}}, t)\, q_0(\tilde{\tilde{\vartheta}}, t)]}{\partial \tilde{\tilde{\vartheta}}}, \qquad B(t) = B(\tilde{\tilde{\vartheta}}, t).$$

By introducing the expanded state vector

$$y = \begin{Vmatrix} x \\ C \end{Vmatrix} \qquad (5.5)$$

and with consideration of the constancy of the vector C in the analysis and prediction interval, we write the equation of motion in the form of (2.4) for the new (expanded) state vector

$$\frac{dy}{dt} = \tilde{A}(t)\,y + \tilde{B}(t)\,q(t), \tag{5.6}$$

where

$$\tilde{A}(t) = \begin{Vmatrix} A(t) & A(t)F(t) - F'(t) \\ 0 & 0 \end{Vmatrix}, \quad \tilde{B}(t) = \begin{Vmatrix} B(t) \\ 0 \end{Vmatrix}.$$

The discrepancies between the measured and calculated values (analogous to that done in Paragraph 2) can be considered as measurements /58

$$z_i = h_i x_i + v_i = \tilde{h}_i y_i + v_i, \tag{5.7}$$

where $\tilde{h}_i = \|h_i 0\|$.

Thus, the problem reduces to the formulation considered in Paragraph 2.

Consequently, the methods proposed in Paragraphs 3 and 4 can be applied for its solution.

We consider the properties of this problem connected with the expansion of the state vector in more detail. We write out separately the derivative of the calculated trajectory parameters

$$\begin{aligned} \frac{d\tilde{\tilde{\vartheta}}}{dt} = \frac{d\tilde{\vartheta}}{dt} + F'(t)C = B[\tilde{\tilde{\vartheta}} - F(t)C, t]\,q_0[\tilde{\tilde{\vartheta}} - F(t)C, t] + F'(t)C = \\ = B(\tilde{\tilde{\vartheta}}, t)\,q_0(\tilde{\tilde{\vartheta}}, t) + [F'(t) - A(t)F(t)]C. \end{aligned} \tag{5.8}$$

It is evident from the comparison of (5.8) and (2.2) that the second term of Expression (5.8) has the meaning of a correction to the right sides of Equations (2.1), which takes into account the estimate of the system noise, i.e.,

$$[F'(t) - A(t)F(t)]C = B(t)\hat{q}(t). \tag{5.9}$$

We write (5.9) in the following form

$$\frac{d[F(t)C]}{dt} = A(t)[F(t)C] + B(t)\hat{q}(t).$$

Hence, under the condition $F(t_0) = 0$, we obtain

$$F(t)C = \int_{t_0}^{t} U(t, \xi)B(\xi)\hat{q}(\xi)d\xi. \qquad (5.10)$$

The relation between the correcting function and the estimate of the system noise can also be established in another way. We will seek an estimate of the system noise (2.4) in the form of a polynomal

$$\hat{q}(t) = \Phi(t)C,$$

where $\Phi(t) = \|\varphi_1(t) \ldots \varphi_n(t)\|$.

The solution of the Equation (2.4) takes the form

$$x(t) = U(t, t_0)x(t_0) + \left[\int_{t_0}^{t} U(t, \xi)B(\xi)\Phi(\xi)d\xi\right]C. \qquad (5.11)$$

The term of (5.11) containing the integral can be considered as a correction to the prediction algorithm which reflects the effect of the unconsidered factors (system noise). By using the notation (5.1), (5.2), we can write /59

$$\delta э = F(t)C = \left[\int_{t_0}^{t} U(t, \xi)B(\xi)\Phi(\xi)d\xi\right]C.$$

Hence,

$$F(t) = \int_{t_0}^{t} U(t, \xi)B(\xi)\Phi(\xi)d\xi. \qquad (5.12)$$

The dependence (5.12) links the function approximating the system noise and the correcting function. From the relations:

$$[F'(t) - A(t)F(t)]C = B(t)\hat{q}(t) = B(t)\Phi(t)C$$

it follows that the more fortunate the selection of the approximating functions, the better the quantity $[F'(t)-A(t)F(t)]C$ reflects the actual noise variation law $q(t)$.

We find the fundamental solution matrix for the system of Equations (5.6). We assume $(t)=0$ and write the solution for each of the components of the vector y

$$\begin{aligned} x &= U(t, t_0)x_0 + \left\{\int_{t_0}^{t} U(t, \xi)[A(\xi)F(\xi) - F'(\xi)]\, d\xi\right\}C, \\ C &= C_0. \end{aligned} \tag{5.13}$$

Hence, it follows that the fundamental solution matrix for the system (5.6) is expressed in the following form

$$\tilde{U}(t, t_0) = \left\| \begin{array}{c|c} U(t, t_0) & D(t, t_0) \\ \hline 0 & E \end{array} \right\|, \tag{5.14}$$

where

$$D(t, t_0) = \int_{t_0}^{t} U(t, \xi)[A(\xi)F(\xi) - F'(\xi)]\, d\xi \tag{5.15}$$

for the case of the correction functions;

$$D(t, t_0) = -\int_{t_0}^{t} U(t, \xi)B(\xi)\Phi(\xi)\, d\xi \tag{5.16}$$

for the case for the system noise approximation.

We note, in conclusion, that the solution of the problem formulated in this section and connected with predicting the system (5.6) from the measurements (5.7) with the known statistical characteristics of the noise (2.10) can also be accomplished by other methods. We will carry out an investigation of the obtained solutions below.

6. Investigation of the Obtained Solutions

Various prediction methods characterized by obtaining and using estimates of the system noise (a priori unknown perturbations) have been discussed in Sections 3, 4, and 5. Here we carry out a comparison of the effectiveness of the state vector estimates for prediction, which have been found by various methods. /60

First, we show that the prediction methods based on the concurrent and successive measurement analysis provide estimates of the same effectiveness. We assume that the effectiveness of the state vector estimates for predicting by the considered methods is the same, if the following conditions are satisfied:

$$\begin{aligned} K_x(t_k, t_k)_k \text{ (concurrent)} &= K_x(t_k, t_k)_k \text{ (successive)}, \\ K_{xq}(t_k, \tau)_k \text{ (concurrent)} &= K_{xq}(t_k, \tau)_k \text{ (successive)}, \\ K_q(t_j, \tau)_k \text{ (concurrent)} &= K_q(t_j, \tau)_k \text{ (successive)}. \end{aligned}$$

We justify the proposed criteria for evaluating the solutions obtained in Paragraphs 3 and 4 by deriving the differential equations, which the evolution of the correlation matrices for prediction satisfy. Generally speaking, this can be done by different methods. We use here the results of Paragraph 4. By using the relations found previously (4.9), (4.10), (4.15), we have

$$\frac{dK_x(t_j, t_j)_k}{dt_j} = \frac{dC_j}{dt_j} = C_j A^T(t_j) + A(t_j) C_j - B(t_j) W_j^T(t_j) H^T N_j X_j C_j - C_j X_j^T N_j H W_j(t_j) B^T(t_j),$$

and with consideration of (4.27), we obtain the desired equation

$$\frac{dK_x(t_j, t_j)_k}{dt_j} = K_x(t_j, t_j)_k A^T(t_j) + A(t_j) K_x(t_j, t_j)_k + B(t_j) K_{xq}^T(t_j, t_j)_k + K_{xq}(t_j, t_j)_k B^T(t_j). \quad (6.1)$$

The value of $K_x(t_j, t_j)$ at any time is uniquely determined by the initial conditions $K_x(t_0, t_0)_k$ and the function $K_{xq}(t_j, t_j)_k$.

We construct the differential equation for the matrix function $K_{xq}(t_j, \tau)_k$. By differentiating (4.27) with respect to t_j and in view of (4.16), (4.12), (4.21), we have

$$\frac{\partial K_{xq}(t_j, \tau)_k}{\partial t_j} = -\frac{d(C_j X_j^T N_j)}{dt_j} H W_j(\tau) - (C_j X_j^T N_j) H \frac{\partial W_j(\tau)}{\partial t_j} =$$
$$= -[A(t_j) C_j X_j^T N_j + B(t_j) W_j^T(t_j) H^T G_j] H W_j(\tau) -$$
$$- (C_j X_j^T N_j) H \left\{\frac{d}{dt_j}\int_{t_j}^{t_i} U(t_i, \xi) B(\xi) K_q(\xi, \tau)_0 d\xi\right\}_{i=1,\ldots,k} = \quad /61$$
$$= A(t_j) K_{xq}(t_j, \tau)_k - B(t_j) W_j^T(t_j) H^T G_j H W_j(\tau) +$$
$$+ C_j (X_j^T N_j H U_j) B(t_j) K_q(t_j, \tau)_0 = A(t_j) K_{xq}(t_j, \tau)_k +$$
$$+ B(t_j)[K_q(t_j, \tau)_0 - W_j^T(t_j) H^T G_j H W_j(\tau)].$$

Noting that, from (4.28), the square bracket in the last expression is $K_q(t_j, \tau)_k$, we finally write

$$\frac{\partial K_{xq}(t_j, \tau)_k}{\partial t_j} = A(t_j) K_{xq}(t_j, \tau)_k + B(t_j) K_q(t_j, \tau)_k. \quad (6.2)$$

The solution of Equation (6.2) is uniquely determined by the initial conditions and the perturbing function $K_q(t_j, \tau)_k$. We point out that the obtained equations (6.1) and (6.2) have a structure analogous to the structure of the equations of motion (2.4) for the investigated system. The fact that their solution is uniquely determined by the initial conditions $K_x(t_k, t_k)_k$, $K_{xq}(t_k, \tau)_k$ and the perturbing function $K_q(t_j, \tau)_k$ justifies the correctness and sufficiency of the proposed conditions for comparison.

Thus, in accordance with this, we will compare the precision characteristics of the state vector for prediction by the two methods. For convenience in the discussion, we tabulate the necessary formulas from Paragraphs 3 and 4.

It should be noted that the corresponding formulas of Paragraph 3 were obtained under the assumption of the noncorrelation of the measurement errors $M(v_i v_j^T) = 0,\ i \neq j$. The formulas of the prediction algorithm with concurrent measurement analysis have a more general nature in this sense. However, for the correctness of the comparison to be carried out, we will consider both prediction algorithms under the same conditions, i.e., under this assumption.

We try to reduce the formulas of concurrent analysis to the form of the formulas of successive analysis by using the technique of partitioning matrices into squares. We introduce supplementary indices into the matrices X_k, N_k, H_k, K_{wk}, R_Σ, G_k, which indicate the number of measurements to which they correspond. We have

$$X_{k(k)} = \left\| \begin{array}{l} h_1 U(t_1, t_k) \\ \cdots\cdots\cdots \\ \cdots\cdots\cdots \\ \cdots\cdots\cdots \\ h_{k-1} U(t_{k-1}, t_k) \\ h_k U(t_k, t_k) \end{array} \right\| = \left\| \begin{array}{c} X_{k(k-1)} \\ \hline h_k \end{array} \right\|,$$

$$H_k = \left\| \begin{array}{ccc} h_1 & & \\ & \ddots & \\ & & h_{k-1} \\ & & h_k \end{array} \right\| = \left\| \begin{array}{c|c} H_{k-1} & 0 \\ \hline 0 & h_k \end{array} \right\|, \qquad (6.3)$$

$$R_{\Sigma(k)} = \left\| \begin{array}{ccc} R_1 & & \\ & \ddots & \\ & & R_{k-1} \\ & & R_k \end{array} \right\| = \left\| \begin{array}{c|c} R_{\Sigma(k-1)} & 0 \\ \hline 0 & R_k \end{array} \right\|,$$

$$K_{wk(k)} = \left\| \begin{array}{ccc} Q_{11} & \cdots & Q_{1k-1} \quad Q_{1k} \\ \cdots\cdots & \cdots & \cdots\cdots \\ \cdots\cdots & \cdots & \cdots\cdots \\ \cdots\cdots & \cdots & \cdots\cdots \\ Q_{k-1,1} & \cdots & Q_{k-1,k-1} \quad Q_{k-1,k} \\ Q_{k1} & \cdots & Q_{k,k-1} \quad Q_{kk} \end{array} \right\| = \left\| \begin{array}{c|c} K_{wq(k-1)} & 0 \\ \hline 0 & 0 \end{array} \right\|.$$

TABLE

FORMULAS FOR COMPARING THE PRECISION CHARACTERISTICS OF THE STATE VECTOR FOR PREDICTION BY THE TWO METHODS

Concurrent analysis	Successive analysis
$K_x(t_k, t_k)_k = (X_k^T N_k X_k)^{-1} = C_k,$ (4.9)	$K_x(t_k, t_k)_k = P_{k\mid k} = (P_{k\mid k-1}^{-1} + h_k^T R_k^{-1} h_k)^{-1} =$ (3.19)
where	$= P_{k\mid k-1} - P_{k\mid k-1} h_k^T (h_k P_{k\mid k-1} h_k^T + R_k)^{-1} h_k P_{k\mid k-1},$ (3.22)
$X_k = HU_k,$ (4.3)	where
$N_k = (HK_{wk}H^T + R_\Sigma)^{-1},$ (4.8)	$P_{k\mid k-1} = K_x(t_k, t_k)_{k-1}.$
$K_{wk} = \left\{ \int_{t_k}^{t_l} \int_{t_k}^{t_l} U(t_l, \xi) B(\xi) K_q(\xi, \eta)_0 B^T(\eta) \times \right.$	
$\left. \times U^T(t_l, \eta) d\eta d\xi \right\}_{l,\, l=1,\ldots,k} = \{Q_{il}\}_{i,\, l=1,\ldots,k}.$ (4.3)	
$K_{xq}(t_k, \tau)_k = -C_k X_k^T N_k H W_k(\tau),$ (4.27)	$K_{xq}(t_k, \tau)_k = P_{k\mid k} P_{k\mid k-1}^{-1} K_{xq}(t_k, \tau)_{k-1},$ (3.35)
where	where
$W_k(\tau) = \left\{ \int_{t_k}^{t_l} U(t_l, \xi) B(\xi) K_q(\xi, \tau)_0 d\xi \right\}_{l=1,\ldots,k}$ (4.12)	$K_{xq}(t_k, \tau)_{k-1} = U(t_k, t_{k-1}) K_{xq}(t_{k-1}, \tau)_{k-1} + K_{wq}(\tau)_{k-1},$ (3.30)
	$K_{wq}(\tau)_{k-1} = \int_{t_{k-1}}^{t_k} U(t_k, \eta) B(\eta) K_q(\eta, \tau)_{k-1} d\eta.$ (3.26)
$K_q(t_j, \tau)_k = K_q(t_j, \tau)_0 - W_k^T(t_j) H^T G_k H W_k(\tau),$ (4.28)	$K_q(t_j, \tau)_k = K_q(t_j, \tau)_{k-1} - K_{xq}^T(t_k, t_j)_{k-1} h_k^T (R_k^{-1} - R_k^{-1} h_k P_{k\mid k} h_k^T R_k^{-1}) \times$
where	$\times h_k K_{xq}(t_k, \tau)_{k-1},$ (3.36)
$G_k = N_\kappa - N_k X_k C_k X_k^T N_k.$ (4.21)	where
	$R_k^{-1} - R_k^{-1} h_k P_{k\mid k} h_k^T R_k^{-1} = (R_k + h_k P_{k\mid k-1} h_k^T)^{-1}$

We express the matrix $N_{k(k)}$ with the help of (6.3)

$$N_{k(k)} = \left(\begin{Vmatrix} H_{k-1} & 0 \\ 0 & h_k \end{Vmatrix} \begin{Vmatrix} K_{wk(k-1)} & 0 \\ 0 & 0 \end{Vmatrix} \begin{Vmatrix} H_{k-1}^T & 0 \\ 0 & h_k^T \end{Vmatrix} + \begin{Vmatrix} R_{\Sigma(k-1)} & 0 \\ 0 & R_k \end{Vmatrix} \right)^{-1} =$$
$$= \begin{Vmatrix} H_{k-1} K_{wk(k-1)} H_{k-1}^T + R_{\Sigma(k-1)} & 0 \\ 0 & R_k \end{Vmatrix}^{-1} = \begin{Vmatrix} N_{k(k-1)} & 0 \\ 0 & R_k^{-1} \end{Vmatrix}. \qquad (6.4)$$

By analogy to (6.4), we also express

$$K_x(t_k, t_k)_k = \left(\left\| X^T_{k(k-1)} \middle| h^T_k \right\| \left\| \begin{array}{c|c} N_{k(k-1)} & 0 \\ \hline 0 & R_k^{-1} \end{array} \right\| \left\| \begin{array}{c} X_{k(k-1)} \\ h_k \end{array} \right\| \right)^{-1} =$$
$$= (X^T_{k(k-1)} N_{k(k-1)} X_{k(k-1)} + h^T_k R_k^{-1} h_k)^{-1}.$$

In accordance with (4.9), (3.10), the first term is $[K_x(t_k, t_k)_{k-1}]^{-1}$, i.e.,

$$X^T_{k(k-1)} N_{k(k-1)} X_{k(k-1)} = [K_x(t_k, t_k)_{k-1}]^{-1} = P^{-1}_{k|k-1}. \tag{6.5}$$

The formula takes the form

$$K_x(t_k, t_k)_k = (P^{-1}_{k|k-1} + h^T_k R_k^{-1} h_k)^{-1} \tag{6.6}$$

or

$$C_k = P_{k|k}, \tag{6.7}$$

coinciding with the corresponding formula (3.19) of the algorithm of successive analysis. Thus, the first condition is satisfied.

We proceed to the second condition. By using (4.12), (4.13), (4.27), (6.3) and (6.7), we have

$$W_{k(k)}(\tau) = \left\{ \int_{t_k}^{t_i} U(t_i, \xi) B(\xi) K_q(\xi, \tau)_0 \, d\xi \right\}_{i=1,\ldots,k} = \tag{6.8}$$
$$= \left\| \begin{array}{c} \left\{ \int_{t_k}^{t_i} U(t_i, \xi) B(\xi) K_q(\xi, \tau)_0 \, d\xi \right\}_{i=1,\ldots,k-1} \\ \hline 0 \end{array} \right\| = \left\| \begin{array}{c} W_{k(k-1)}(\tau) \\ \hline 0 \end{array} \right\|, \qquad /64$$

$$K_{xq}(t_k, \tau)_k = -P_{k|k} \left\| X^T_{k(k-1)} \middle| h^T_k \right\| \left\| \begin{array}{cc} N_{k(k-1)} & 0 \\ 0 & R_k^{-1} \end{array} \right\| \left\| \begin{array}{cc} H_{k-1} & 0 \\ 0 & h_k \end{array} \right\| \left\| \begin{array}{c} W_{k(k-1)}(\tau) \\ 0 \end{array} \right\| = \tag{6.9}$$
$$= -P_{k|k} X^T_{k(k-1)} N_{k(k-1)} H_{k-1} W_{k(k-1)}(\tau).$$

It follows from the dependence (4.27) that

$$K_{xq}(t_k, \tau)_{k-1} = -P_{k|k-1} X^T_{k(k-1)} N_{k(k-1)} H_{k-1} W_{k(k-1)}(\tau). \tag{6.10}$$

Hence,

$$X^T_{k(k-1)} N_{k(k-1)} H_{k-1} W_{k(k-1)}(\tau) = -P^{-1}_{k|k-1} K_{xq}(t_k, \tau)_{k-1}.$$

By substituting this relation into the Expression (6.9), we obtain

$$K_{xq}(t_k, \tau)_k = P_{k|k} P^{-1}_{k|k-1} K_{xq}(t_k, \tau)_{k-1}. \tag{6.11}$$

It is evident by comparing with (3.35) that both expressions are identical, and thus, the second condition is satisfied.

Proceeding to the third condition, we write on the basis of (4.21), (6.3)

$$G_{k(k)} = \begin{Vmatrix} N_{k(k-1)} & 0 \\ 0 & R_k^{-1} \end{Vmatrix} - \begin{Vmatrix} N_{k(k-1)} & 0 \\ 0 & R_k^{-1} \end{Vmatrix} \begin{Vmatrix} X_{k(k-1)} \\ h_k \end{Vmatrix} P_{k|k} \| X^T_{k(k-1)} \vdots h^T_k \| \begin{Vmatrix} N_{k(k-1)} & 0 \\ 0 & R_k^{-1} \end{Vmatrix} =$$
$$= \begin{Vmatrix} N_{k(k-1)} - N_{k(k-1)} X_{k(k-1)} P_{k|k} X^T_{k(k-1)} N_{k(k-1)} & \vdots & -N_{k(k-1)} X_{k(k-1)} P_{k|k} h^T_k R_k^{-1} \\ \cdots\cdots\cdots & \cdots & \cdots\cdots \\ R_k^{-1} h_k P_{k|k} X^T_{k(k-1)} N_{k(k-1)} & \vdots & R_k^{-1} - R_k^{-1} h_k P_{k|k} h^T_k R_k^{-1} \end{Vmatrix}, \tag{6.12}$$

$$H_k W_{k(k)}(\tau) = \| 0 \vdots h_k \| \begin{Vmatrix} W_{k(k-1)}(\tau) \\ 0 \end{Vmatrix} = \| H_{k-1} W_{k(k-1)}(\tau) \|. \tag{6.13}$$

Then, we transform Expression (4.28) with consideration of (6.12), (6.13)

$$K_q(t_j, \tau)_k = K_q(t_j, \tau)_0 - \| W^T_{k(k-1)}(t_j) H^T_{k-1} \vdots 0 \| G_{k(k)} \cdot \| H_{k-1} W_{k(k-1)}(\tau) \| =$$
$$= K_q(t_j, \tau)_0 - W^T_{k(k-1)}(t_j) H^T_{k-1} (N_{k(k-1)} -$$
$$- N_{k(k-1)} X_{k(k-1)} P_{k|k} X^T_{k(k-1)} N_{k(k-1)}) H_{k-1} W_{k(k-1)}(\tau).$$

By substituting the previously presented Expression (3.22) in place of $P_{k|k}$ here, we obtain

$$K_q(t_j, \tau)_k = K_q(t_j, \tau)_0 - W^T_{k(k-1)}(t_j) H^T_{k-1} (N_{k(k-1)} -$$
$$- N_{k(k-1)} X_{k(k-1)} P_{k|k-1} X^T_{k|k-1} N_{k(k-1)}) H_{k-1} W_{k(k-1)}(\tau) -$$
$$- W^T_{k(k-1)}(t_j) H^T_{k-1} N_{k(k-1)} X_{k(k-1)} P_{k|k-1} h^T_k (h_k P_{k|k-1} h^T_k +$$
$$+ R_k)^{-1} h_k P_{k|k-1} X^T_{k(k-1)} N_{k(k-1)} H_{k-1} W_{k(k-1)}(\tau).$$

In accordance with the solution (4.28), the first two terms /65
equal $K_q(t_j, \tau)_{k-1}$, i.e.,

$$K_q(t_j, \tau)_{k-1} = K_q(t_j, \tau)_0 - W^T_{k(k-1)}(t_j) H^T_{k-1} G_{k(k-1)} H_{k-1} W_{k(k-1)}(\tau).$$

The third term, considering (6.10), can be written more compactly. We finally obtain

$$K_q(t_j, \tau)_k = K_q(t_j, \tau)_{k-1} - K^T_{xq}(t_k, t_j)_{k-1} h^T_k (h_k P_{k|k-1} h^T_k + R_k)^{-1} h_k K_{xq}(t_k, \tau)_{k-1}.$$

This expression coincides with the corresponding Expression (3.36) of the algorithm of successive analysis.

Thus, the correctness of all three conditions has been shown, which indicates the same effectiveness of the estimates of the solutions obtained from the prediction algorithms with concurrent and successive measurement analysis. We will call these algorithms the optimum analysis algorithms.

There remains now a comparison of the effectiveness of the estimates with the different methods of evaluating the system noise:

a) optimum;

b) introduction of correcting functions;

c) approximation of the system noise.

It was shown in Paragraph 5 that the last two methods characterized by expanding the state vector can be reduced to the formulation of the problem given in Paragraph 2 and, consequently, solved by the methods discussed above. On this basis, we use the optimum analysis algorithm to obtain the estimate of the expanded state vector

$$\tilde{x} = \begin{Vmatrix} y \\ C \end{Vmatrix}.$$

For convenience in the discussion, we present once again the original system (5.6) in the form

$$\frac{d\tilde{x}}{dt} = \tilde{A}(t)\,\tilde{x} + \tilde{B}(t)\,q(t), \qquad \tilde{z}_i = \tilde{h}_i \tilde{x}_i + v_i, \qquad i = 1, \ldots, k.$$

Writing its solution on the basis of (4.7), we have

$$\hat{x}_j = (\tilde{X}_j^T \tilde{N}_j \tilde{X}_j)^{-1} \tilde{X}_j^T \tilde{N}_j \tilde{Z}_k,$$

where $\tilde{P}_{j|k} = (\tilde{X}_j^T \tilde{N}_j \tilde{X}_j)^{-1}$ is the correlation matrix of the expanded state vector.

We isolate in the state vector $\tilde{\mathbf{x}}$ the components (the vector **y**) corresponding to the old state vector **x**. In accordance with this, we also partition into squares the correlation matrix $\tilde{P}_{j|k}$ by introducing the notations $K_y(t_j, t_j)$, $K_c(t_j, t_j)$ and $K_{yc}(t_j, t_j)$ for the correlation matrices of the vector **y** and the noise parameters **C** and their mutual correlation matrix, respectively /66

$$\tilde{P}_{j|k} = \begin{Vmatrix} K_y(t_j, t_j) & K_{yc}(t_j, t_j) \\ K_{cy}(t_j, t_j) & K_c(t_j, t_j) \end{Vmatrix}. \tag{6.14}$$

Our goal is to find the relation between the correlation matrices $P_{j|k}$ and $K_y(t_j, t_j)$. For this, we try to express all the matrices appearing in the correlation matrix of the expanded state vector in terms of the corresponding matrices of the old state vector x.

We have, from (4.3), (5.14) — (5.16)

$$\widetilde{X}_j = \widetilde{H}\,\widetilde{U}_j, \qquad \widetilde{H} = \begin{Vmatrix} \widetilde{h}_1 & & \\ & \ddots & \\ & & \widetilde{h}_k \end{Vmatrix} = \begin{Vmatrix} h_1 & 0 & 0 & 0 & \dots & 0 & 0 \\ 0 & 0 & h_2 & 0 & \dots & 0 & 0 \\ \dots & \dots & \dots & \dots & \dots & \dots & \dots \\ 0 & 0 & 0 & 0 & \dots & h_k & 0 \end{Vmatrix},$$

$$\widetilde{U}_j = \begin{Vmatrix} \widetilde{U}(t_1, t_j) \\ \dots \\ \widetilde{U}(t_k, t_j) \end{Vmatrix} = \begin{Vmatrix} U(t_1, t_j) & \dots & D(t_1, t_j) \\ 0 & \dots & E \\ \dots & \dots & \dots \\ U(t_k, t_j) & \dots & D(t_k, t_j) \\ 0 & \dots & E \end{Vmatrix}.$$

Then

$$\widetilde{X}_j = \widetilde{H}\,\widetilde{U}_j = \left\| \begin{array}{c|c} h_1 U(t_1, t_j) & h_1 D(t_1, t_j) \\ h_2 U(t_2, t_j) & h_2 D(t_2, t_j) \\ \dots & \dots \\ h_k U(t_k, t_j) & h_k D(t_k, t_j) \end{array} \right\| = H \| U_j | D_j \| = \| X_j | S_j \|,$$

with the notation

$$D_j = \begin{Vmatrix} D(t_1, t_j) \\ \dots \\ D(t_k, t_j) \end{Vmatrix}, \qquad S_j = HD_j.$$

By analogy, we express $\widetilde{N}_j$ with the help of (4.8), (4.3)

$$\widetilde{N}_j = (\widetilde{H}\,\widetilde{K}_{wj}\widetilde{H}^T + R_\Sigma)^{-1}, \qquad \widetilde{K}_{wj} = \{\widetilde{Q}_{il}\}_{i,l=1,\dots,k},$$

$$\widetilde{Q}_{il} = \int_{t_j}^{t_i}\int_{t_j}^{t_l} \widetilde{U}(t_i, \xi)\widetilde{B}(\xi) K_q(\xi, \eta)\widetilde{B}^T(\eta) U^T(t_l, \eta)\, d\eta\, d\xi,$$

/67

$$\widetilde{U}(t_i, \xi)\widetilde{B}(\xi) = \left\| \begin{array}{c|c} U(t_i, \xi) & D(t_i, \xi) \\ \hline 0 & E \end{array} \right\| \left\| \begin{array}{c} B(\xi) \\ \hline 0 \end{array} \right\| = \left\| \begin{array}{c} U(t_i, \xi) B(\xi) \\ \hline 0 \end{array} \right\|,$$

$$\widetilde{U}(t_i, \xi)\widetilde{B}(\xi) K_q(\xi, \eta)\widetilde{B}^T(\eta)\widetilde{U}^T(t_l, \eta) =$$

$$= \left\| \begin{array}{c} U(t_i, \xi) B(\xi) \\ \hline 0 \end{array} \right\| K_q(\xi, \eta) \| B^T(\eta) U^T(t_l, \eta) | 0 \| =$$

$$= \left\| \begin{array}{c|c} U(t_i, \xi) B(\xi) K_q(\xi, \eta) B^T(\eta) U^T(t_l, \eta) & 0 \\ \hline 0 & 0 \end{array} \right\|.$$

Hence,

$$\widetilde{Q}_{il}=\begin{Vmatrix} Q_{il} & 0 \\ 0 & 0 \end{Vmatrix}, \qquad \widetilde{K}_{wj}=\begin{Vmatrix} Q_{11} & 0 & \dots & Q_{1k} & 0 \\ 0 & 0 & & 0 & 0 \\ \dots & \dots & \dots & \dots & \dots \\ Q_{k1} & 0 & \dots & Q_{kk} & 0 \\ 0 & 0 & \dots & 0 & 0 \end{Vmatrix},$$

$$\widetilde{H}\widetilde{K}_{wj}=\begin{Vmatrix} h_1Q_{11} & 0 & \dots & h_1Q_{1k} \\ \dots & \dots & \dots & \dots \\ h_kQ_{k1} & 0 & \dots & h_kQ_{kk} \end{Vmatrix},$$

$$\widetilde{H}\widetilde{K}_{wj}\widetilde{H}^T=\begin{Vmatrix} h_1Q_{11}h_1^T & \dots & h_1Q_{1k}h_k^T \\ \dots & \dots & \dots \\ h_kQ_{k1}h_1^T & \dots & h_kQ_{kk}h_k^T \end{Vmatrix}=HK_{wj}H^T.$$

Consequently,

$$\widetilde{N}=(HK_{wj}H^T+R_\Sigma)^{-1}=N_j.$$

Thus, we have

$$\widetilde{P}_{jk}=(\widetilde{X}_j^TN_j\widetilde{X}_j)^{-1}=\left(\begin{Vmatrix} X_j^T \\ S_j^T \end{Vmatrix}N_j\|X_j\,|\,S_j\|\right)^{-1}=\left\|\begin{array}{c|c} X_j^TN_jX_j & X_j^TN_jS_j \\ \hline S_j^TN_jX_j & S_j^TN_jS_j \end{array}\right\|^{-1}=\begin{Vmatrix} A & B \\ B^T & C \end{Vmatrix}^{-1}.$$

By using the technique of partitioned matrix inversion and considering (6.14), one can write

$$\widetilde{P}_{jk}=\left\|\begin{array}{c|c} A^{-1}+A^{-1}B(C-B^TA^{-1}B)^{-1}B^TA^{-1} & -A^{-1}B(C-B^TA^{-1}B)^{-1} \\ \hline -(C-B^TA^{-1}B)^{-1}B^TA^{-1} & (C-B^TA^{-1}B)^{-1} \end{array}\right\|=$$
$$=\begin{Vmatrix} K_y(t_j,t_j) & K_{yc}(t_j,t_j) \\ K_{cy}(t_j,t_j) & K_c(t_j,t_j) \end{Vmatrix}.$$

Hence, we have the relations /68

$$K_y(t_j,t_j)=A^{-1}+A^{-1}B(C-B^TA^{-1}B)^{-1}B^TA^{-1}, \quad K_c(t_j,t_j)=(C-B^T\ {}^{-1}B)^{-1},$$
$$K_{yc}(t_j,t_j)=-A^{-1}B(C-B^TA^{-1}B)^{-1}, \quad K_{cy}(t_j,t_j)=-(C-B^TA^{-1}B)^{-1}B^TA^{-1}.$$

By transforming the first of them with consideration of the remaining relations and the equality $A^{-1}=(X_j^T N_j X_j)^{-1}=P_{j|k}$, we obtain

$$K_y(t_j, t_j)=P_{j|k}+K_{yc}(t_j, t_j)K_c^{-1}(t_j, t_j)K_{cy}(t_j, t_j).$$

It follows from the last expression, since $\det K_c^{-1}(t_j, t_j)>0$, that the diagonal elements of the matrix $K_y(t_j, t_j)$ are no smaller than the corresponding diagonal elements of the matrix $P_{j|k}$. This means that expanding the state vector even with the optimum analysis algorithm does not improve the prediction accuracy. The effectiveness of the estimates will be the same only in the particular case when there is no correlation of the vector **y** and the noise parameters **c**.

REFERENCES

1. Dyboshin, G. N. Nebesnaya mekhanika. Osnovnyye zadichi i metody (Celestial Mechanics. Basic Problems and Methods). Moscow, State Physics and Mathematics Press, 1963.

2. Yastrebov, V. D. Kosmicheskiye issledovaniya, Vol. 4, No. 4, 1966.

3. Kaula, W. M. J. Geophys. Res., Vol. 64, 1959, p. 2401.

4. Gersten, R. Kh., R. K. Gor and N. S. Kholl. Raketnaya tekhnika i kosmonavtika, Vol. 5, No. 10, 1967.

5. Chertoprud, V. Ye. Nauchnyye informatsii astrosoveta AN SSSR, No. 9, 1968.

6. Lu, R. Optimal'nyye otsenki, opredeleniye kharakteristik i upravleniye (Optimum Estimates, Characteristics, Determination, and Control). Moscow, "Nauka" Press, 1966.

7. Gantmakher, F. R. Teoriya matrits (Theory of Matrices). Moscow, "Nauka" Press, 1967.

8. Parayev, Yu. I. Tekhnicheskaya kibernetika, No. 1, 1966.

9. Linnik, Yu. V. Metod naimen'skikh kvadratov i osnovy matematiko-statisticheskoy teorii obrabotki nablyudeniy (Method of Least Squares and the Principles of the Mathematical and Statistical Theory of Observation Analysis). Moscow, State Physics and Mathematics Press, 1962.

10. Akim, E. L. and T. M. Eneyev. Kosmicheskiye issledovaniya, Vol. 1, No. 1, 1963.

N74-28293

STATISTICAL ANALYSIS OF THE DAILY MEAN FLUCTUATIONS OF THE PARAMETERS FOR THE UPPER ATMOSPHERE OF THE EARTH

V. Ye. Chertoprud

ABSTRACT. The statistical properties of the response of the parabolic equation to small daily mean temperature fluctuations in the neutral atmosphere are discussed. A technique is described for obtaining the correlation functions of the response of this equation to white noise, and, in the final analysis, to steady-state disturbances with a given autocorrelation function. The distribution of fluctuation dispersion with altitude and a determination of satellite slowing fluctuations caused by variations of soft solar x-rays of wavelength 40 — 100 A are presented as examples. Formulation of the inverse problem is discussed: to obtain the characteristics of the fluctuation source (i.e., information about the width, effective altitude and vertical profile of the variable radiation absorption, etc.) from the statistical properties of satellite slowing fluctuations and variations of activity indices.

The presence of temperature fluctuations in the upper /68
atmosphere of the Earth, which are particularly apparent in the slowing of satellites, requires answers to at least three questions:

1) How are such fluctuations to be taken into account (predicted) for refining the theory and predicting satellite motion?

2) How are the fluctuations to be used as a source of additional information about the dynamic state of the atmosphere?* /69

3) What is the physical nature of the fluctuations?

The fluctuations are divided into two groups according to their nature: strong, but very infrequent and short-term bursts related to very strong flare activity, and small, almost steady-state random variations. In accordance with this, two alternative but complementary approaches to the study of the fluctuations are possible: 1) analysis of the sharp variations of the parameters of the upper atmosphere during strong flare activity; 2) study of the statistical (correlation) properties of small steady-state fluctuations over long time intervals. As in [2, 3], we will discuss the second approach here.

The first attempt to extract information from the statistical properties of small fluctuations in the slowing of satellites was made in [4] (evaluations of this work were later reviewed in [2, 3]). A systematic development of a method for studying the fluctuations on the basis of the parabolic heat conductivity equation is contained in [2, 3].

We will apply the method when:

1) the neutral atmosphere is considered;

2) global effects (averaged over latitude and longitude) are studied;

*For the formulation of an analogous problem on the coupling of the fluctuation properties with the dynamic parameters for the brightness variability of the quasar 3C273, cf. in [1].

3) the time resolution of the fluctuations $t_0 \geq 1^d$;

4) the fluctuations are small on the average.

Since the basic technical difficulties in realizing the method of [2, 3] have been overcome, its complication is possible below: 1) transition from linear equations to nonlinear and 2) transition to a three-dimensional model, i.e., in the final analysis a rejection of these limitations.

The purpose of this work is to reduce the method of [2, 3] to numerical evaluations carried out by computer and to study on the basis of these evaluations the statistical properties of the fluctuations of the parameters of the upper atmosphere.

1. Equation for the Temperature Fluctuations

The initial equation for the analysis is the heat transfer equation of Harries-Priester [5]:

$$\frac{1}{\rho c_p}\frac{\partial}{\partial z}\left(\varkappa(T, z)\frac{\partial T}{\partial z}\right) - T\frac{\partial T}{\partial z}\int_{z_0}^{z}\frac{1}{T^2}\frac{\partial T}{\partial t}dz + \frac{P(z) - L(z)}{c_p\rho} = \frac{\partial T}{\partial t}. \quad (1)$$

The first term on the left side of the equation is related to the thermal conductivity of the atmosphere, the second — to the expansion of the atmosphere with heating, the third — to the presence of heat inflow and outflow due to the absorption of solar /70 radiation in infrared losses.

As was shown in [2, 3], by using the gasdynamic equations, one can transform in the linear approximation from Equation (1) to the equation

$$\frac{\partial \tilde{T}}{\partial t} + a_0 T_p(z) \int_{z_0}^{z} \frac{1}{T_p(z_1)} \frac{\partial \tilde{T}}{\partial t}(z_1)\, dz_1 = a_1 \frac{\partial^2 \tilde{T}}{\partial z^2} + a_2 \frac{\partial \tilde{T}}{\partial z} + a_3 \tilde{T} + a_4 \int_{z_0}^{z} \frac{\tilde{T}(z_1)}{H_p(z_1)}\, dz_1 + \frac{P_p(z)}{c_p \rho_p T_p} \tilde{P}(t), \tag{2}$$

where

$$a_0(z) = \frac{\partial}{\partial z}(\ln T_p),\ a_1(z) = \frac{\varkappa_p}{\rho_p c_p} = \chi_p(z),$$

$$a_2(z) = 3a_0 a_1 + T_p \int_{z_0}^{z} \frac{\partial}{\partial t}\left(\frac{1}{T_p(t, z_1)}\right) dz_1,$$

$$a_3(z) = a_0 T_p \int_{z_0}^{z} \frac{\partial}{\partial t}\left(\frac{1}{T_p(t, z_1)}\right) dz_1 + a_1 \left[\left(\frac{3}{2} a_0\right)^2 + \frac{3}{2} \frac{da_0}{dz}\right], \tag{3}$$

$$a_4(z) = a_0 T_p \int_{z_0}^{z} \frac{\partial}{\partial t}\left(\frac{1}{T_p(t, z_1)}\right) dz_1 - \frac{\partial}{\partial t} \ln T_p \cdot [1 + H_p a_0].$$

Here, as usual, T, ρ, χ are the temperature, density, and thermal diffusivity; $P_p(z)$ is the vertical absorption profile of a variable heat source in the upper atmosphere, which is responsible for the fluctuations; P(t) describes the time (statistical) properties of the source.

For any parameter Y, Y_p is the normal (unperturbed) value of the parameter; $\tilde{Y} = (Y - Y_p)/Y_p$.

We note that Equations (2) and (3) describe the transient (unsmoothed) fluctuations of temperature at a fixed local time, and the source of the perturbations is not specified. In particular, we have, for the diurnal maximum of the atmosphere:

$$a_0(z) = \frac{\partial}{\partial z}(\ln T_p), \quad a_1(z) = \chi_p(z), \quad a_2(z) = 3a_0(z)a_1(z),$$

$$a_3(z) = a_1(z)\left[\left(\frac{3}{2} a_0(z)\right)^2 + \frac{3}{2} \frac{da_0}{dz}\right], \quad a_4 = 0. \tag{4}$$

If data on satellite slowing at intervals of one day are used for analyzing temperature fluctuations, then one should take the fact into account that the fluctuations thus obtained are averaged over latitude, longitude, and time (at one-day intervals). Equation (2) with coefficients averaged over a day: /71

$$a_0(z) = \overline{\frac{\partial}{\partial z}(\ln T_p)}, \quad a_1(z) = \overline{\chi_p(z)}, \quad a_2(z) = 3a_0(z)a_1(z),$$
$$a_3(z) = a_1(z)\left[\left(\frac{3}{2}a_0(z)\right)^2 + \frac{3}{2}\frac{da_0}{dz}\right], \quad a_4 = 0, \tag{5}$$

is suitable for describing such fluctuations. Of course, this method can describe only the fluctuations with a characteristic variation time of not less than a day, and all the limitations cited above remain valid. The statistical properties of such fluctuations do not, in practice, have to depend on the local time of satellite perigee; incidentally, the numerical difference between the coefficients (4) and (5) is insignificant.

The explicit relationship of the functions $P_p(z)$, $\tilde{P}(t)$, and $\tilde{T}(t)$ in Equation (2) produces a logical formulation of the problem of deriving the absorption profile $P_p(z)$ from the statistical estimates of the variability of $\tilde{T}(t)$, $\tilde{P}(t)$ and from the known parameters a_i (another approach for studying small perturbations consists of analyzing the response of linearized gasdynamic equations to periodic perturbations or of Fourier analysis [6, 7], cf. also [3, 8]). In order to find the relation between the correlation functions for $\tilde{P}(t)$ and $\tilde{T}$, one must find first of all the correlation function for the response of $\tilde{T}$ in Equation (2) to white noise. Having found such a function, it is not difficult to find the autocorrelation function for the response of $\tilde{T}(t)$ to any steady-state effect $\tilde{P}(t)$ with a given autocorrelation function (for details, cf. in [3]). Finding the response of $\tilde{T}$ reduces to numerical integration of Equation (2), the peculiarities of the

problem being considered, as noted in [9], being: 1) the presence of a random function in the equation and finding, in the final analysis, not a solution, but correlation functions; 2) the almost exponential growth of the coefficients a_1, a_2, a_3 with altitude z. These peculiarities do not change the choice of the difference method proposed in [10], but the parameters of such a method (the increment in time t and altitude z, the value of the weighting coefficient, etc.) become a priori unknowns, and preliminary "numerical experiments" are required to answer the question of the most rational choice of calculation method.

2. Difference Method. Choice of Parameters /72

If the second term in the Harries-Priester Equation (1) is discarded, then

$$\frac{\partial \tilde{T}}{\partial t} = a_1 \frac{\partial^2 \tilde{T}}{\partial z^2} + a_2 \frac{\partial \tilde{T}}{\partial z} + a_3 \tilde{T} + \frac{P_p(z)}{c_p \rho_p T_p} \tilde{P}(t). \tag{6a}$$

is obtained in place of Equation (2).

The difference method for this equation was considered in [9]. The presence of the integral term in the equation for the temperature fluctuations creates difficulties for direct numerical solution by computer, since a significant operating memory is required. By taking into account the specifics of our problem (the smallness of the integral term), it is suitable to use the successive approximation method:

$$\frac{\partial \tilde{T}}{\partial t} = a_1 \frac{\partial^2 \tilde{T}}{\partial z^2} + a_2 \frac{\partial \tilde{T}}{\partial z} + a_3 \tilde{T} + \frac{P_p(z)}{c_p \rho_p T_p} \tilde{P}(t) - a_0 \int_{z_0}^{z} \frac{T_p(z)}{T_p(\xi)} \frac{\partial \tilde{T}}{\partial t}(\xi, (t - t_1))\, d\xi, \tag{6b}$$

where t_1 is so small that $\tilde{T}(t) \approx \tilde{T}(t - t_1)$, i.e.,

$$t_1 \ll \sqrt{\langle \gamma_1^2 \rangle / \langle \gamma_2^2 \rangle},$$

where

$$\gamma_1 = \int_{z_0}^{z} \frac{T_p(z)}{T_p(\xi)} \frac{\partial \tilde{T}}{\partial t}(\xi, t)\, d\xi, \qquad \gamma_2 = \int_{z_0}^{z} \frac{T_p(z)}{T_p(\xi)} \frac{\partial^2 \tilde{T}}{\partial t^2}(\xi, t)\, d\xi.$$

One can use a sequence of calculations for different values of t_1 to control the accuracy of the approximation (6b). Since the temperature fluctuation equation is inconvenient for numerical integration (the equation is given not on an interval, but on the half-line $0 \leq z < \infty$, and its coefficients change rapidly with z), a transformation to the dimensionless variables θ and x was proposed in [3]:

$$\theta = a^2 t, \qquad a = a_1^{1/3}(z_*)/2H_p(z_*), \qquad x = a \int_{z_*}^{z} a_1^{-1/3}(z_1)\, dz_1, \qquad z_* = z_0,$$

which reduces Equations (6a), (6b) to (7a), (7b):

$$\tilde{T}_\theta = \tilde{T}_{xx} + 2k_1(x)\tilde{T}_x + k_2(x)\tilde{T} + \varphi(x)\psi(0),$$
$$\tilde{T}_\theta = \tilde{T}_{xx} + 2k_1(x)\tilde{T}_x + k_2(x)\tilde{T} + \varphi(x)\psi(0) - \tag{7a}$$

$$- l(x) \int_0^x k_3(\xi) \frac{\partial \tilde{T}}{\partial 0}(\xi, (0 - 0_1))\, d\xi, \tag{7b}$$

where /73

$$k_1(x) \equiv k_1[z(x)], \qquad k_1(z) = 1{,}5 \frac{a_0(z)}{a} a_1^{1/2}(z) \left[1 - \frac{\frac{d}{dz} \ln a_1(z)}{6a_0(z)} \right],$$

$$k_2(x) \equiv k_2[z(x)], \qquad k_2(z) = \frac{a_1(z)}{a^2} \left[\frac{9}{4} a_0^2(z) + \frac{3}{2} \frac{d}{dz} a_0(z) \right],$$

$$k_3(x) = \frac{\sqrt{a_1[z(x)]}}{T_p[z(x)]}, \qquad l(x) = \frac{a_0[z(x)]}{a} T_p[z(x)],$$

$$\varphi(x) = \frac{\sigma P_x[z(x)]}{c_p a^2 T_p[z(x)] \rho_p[z(x)]}, \qquad \psi(\theta) = \tilde{P}[l(0)]/\sigma\tilde{P}, \ \sigma\psi = 1.$$

TABLE 1*

x	0,22	0,26	0,32	0,48	0,50	0,62	0,74	0,76
$k_1(\kappa)$	0,03	0,03	0,05	0,29	0,30	0,34	0,39	0,40
$k_2(x)$	0,00	0,00	0,00	0,75	0,80	—0,30	— 0,60	— 0,60
x	0,88	0,94	0,96	1,00	1,04	1,08	1,10	1,12
$k_1(x)$	0,32	0,18	0,11	0,00	—0,20	—0,30	— 0,3	— 0,4
$k_2(x)$	—0,95	—1,3	—1,4	—1,6	—2,0	—8,0	—13	—17
x	1,15	1,17	1,19	1,22	1,24	1,26	1,28	1,30
$k_1(x)$	—0,8	—1,6	—2,0	—3,3	—4,3	—6,3	—11,8	—21,5
$k_2(x)$	—21	—23	—26	—38	—54	—68	—80	—110

* Translator's Note: Commas in numbers indicate decimals.

For calculating the parameters below, $z_* = 105$ km is taken for the origin $x = 0$, while $a = 0.221\ d^{-1/2}$ and the unit of θ corresponds roughly to 20 days; the variable x varies in the range from 0 to 1 — 2, and the coefficients k_1, k_2, k_3 vary within significantly smaller limits than a_1, a_2, a_3. Equation (7a) with the coefficients k_i presented in Table 1 was used for the selection of parameters of the difference method in the "numerical experiments" [9].

It should be noted that small changes in the coefficients k_i and scale x for transformation to other models and consideration of the following approximation (7b) have practically no effect on the choice of the increment in the difference method and of the weighting coefficient, since all the results about the most rational choice of parameters in the calculation method are also preserved for these models. The relation between x and z is illustrated in Table 2.

The difference method and the algorithm of all the calculations was presented in [3], and the results of the choice of parameters — in [9].

TABLE 2*

z	x	z	x	z	x
105	0	130	0,76	260	1,12
110	0,29	140	0,85	300	1,14
115	0,46	160	0,96	lim	1,15—1,16
120	0,61	200	1,06		

*Translator's Note: Commas in numbers indicate decimals.

We will reproduce this difference method in a modified form, which takes into account the transformation from Equation (7a) to (7b), while maintaining the notations of [9]. For the solution of /74 the initial equation

$$\frac{\partial u}{\partial \theta}=\frac{\partial^2 u}{\partial x^2}+2q(x)\frac{\partial u}{\partial x}+\mathscr{E}(x)u+e(x)J(\theta)-l(x)\int_0^x L(\xi)\frac{\partial u}{\partial \theta}(\xi,(\theta-\tau))\,d\xi,$$

$$0\leqslant x<x_N,\quad \tau\to 0,\quad u(\theta=0,x)=0,\quad u(\theta,x=0)=0, \tag{7c}$$

$$u_x(\theta),\ x=x_N)=-\frac{\mathscr{E}(x_N)u(0,x_N)}{2q(x_N)},$$

where

$$u\equiv\tilde{T},\quad q(x)\equiv k_1(x),\quad \mathscr{E}(x)\equiv k_2(x),\quad L(x)\equiv k_3(x),$$
$$e(x)\equiv\varphi(x),\quad J(\theta)\equiv\psi(\theta),$$

the two-layer six-point method (method with weights) [10] with a nonuniform lattice was selected. Following the notation of [9, 10], the variable increment in the argument x is denoted by h_i ($i = 1, 2, \ldots, N$; N is the number of lattice nodes), the constant increment in the time θ — by τ_0, the discrete analog of $u(\theta, x)$ — by y_k^j (everywhere $\theta_j = j\tau_0$, $x_0 = 0$, $x_k = \sum_{i=1}^{k} h_i$), the discrete analog of $f(\theta, x)$ — by f_k^j, the lattice functions of the coefficients of Equation (7c) — by q_k, $\mathscr{E}_k$, l_k, L_k, etc.

We take as the difference equation for (7c) in the modified six-point method

$$\frac{y_i^{j+1}-y_i^j}{\tau_0}=\Lambda[ay_i^{j+1}+(1-a)y_i^j]+f_i^{j+1},\quad y_N^j=\varkappa y_{N-1}^j,$$
$$\varkappa\equiv 1-\mathscr{E}_N h_N/2q_N,\quad j=1,2,\ldots,M;\quad i=1,2,\ldots,N,$$

where 0 < a < 1 is the weight of the upper layer;

$$\Lambda y_i^j\equiv\frac{2q_i}{h_i+h_{i+1}}\left[\frac{h_i}{h_{i+1}}(y_{i+1}^j-y_i^j)+\frac{h_{i+1}}{h_i}(y_i^j-y_{i-1}^j)\right]+$$
$$+\mathscr{E}_i y_i^j+\frac{2}{h_i+h_{i+1}}\left(\frac{y_{i+1}^j-y_i^j}{h_{i+1}}-\frac{y_i^j-y_{i-1}^j}{h_i}\right);$$

/75

$$f_i^j=e_iJ_i^j;$$
$$f_{*i}^j=\begin{cases}f_i^j \text{ for } j<3,\\ f_i^j+l_i\sum\limits_{m=1}^{i}\frac{h_m}{4\tau_0}[L_{m-1}(y_{m-1}^{j-2}-y_{m-1}^{j-1})+\\ \quad+L_m(y_m^{j-2}-y_m^{j-1})] \text{ for } j\geq 2.\end{cases}$$

The modification of the method, which is due to the presence of the Harries-Priester integral in Equation (7c), consists of replacing f_i^j by f_{*i}^i. Solution is by the die method [10, 11]. Sequences of values of y_I^j, f^j (x_I is the altitude at which the fluctuations are measured) and then the correlation functions for the temperature perturbations $\tilde{T}$ are found as a result. In addition, by using the following relations for the small relative perturbations of temperature $\tilde{T}$, density $\tilde{\rho}$, pressure $\tilde{p}$, and rate of change of the anomalous period $\dot{\tilde{P}}_A$ [3]:

$$\tilde{p}(z)=\int_{z_0}^{z}\frac{\tilde{T}(z_1)}{H_p(z_1)}dz_1,\quad \tilde{\rho}(z)=\tilde{p}(z)-\tilde{T}(z),\quad \tilde{P}_A(z)=\tilde{p}(z)-\frac{1}{2}\tilde{T}(z),$$

the correlation functions of the processes $\tilde{\rho}$, $\tilde{p}$, $\dot{\tilde{P}}_A$ are calculated. The increment of the sequences $\tilde{T}^i$, $\tilde{\rho}^i$, $\tilde{p}^i$, and $\dot{\tilde{P}}_A{}^i$ for calculating the correlation functions is $\tau^0 = 1^d$ (or 0.05 in units of θ), and the time increment in calculating τ_0 is significantly smaller:

$$\tau_0 = \tau^0/Q = 0{,}05/Q.$$

The successful performance of the calculation depends in many respects on the proper choice of τ_0. A value of τ_0 which is too small leads to an unjustifiably large consumption of computer time, and one too large — to a loss of the accuracy permitted by the selected increment h. The classical relations for τ and h are not applicable here, since in the final analysis it is necessary to obtain not the solution of the equation, but only the correlation function in which there is significantly less information than in the solution. Thus, one has to make use of the "numerical experiments" [9]. The following parameters were finally selected:

$$N = 24,\ h_{min} = 0.02,\ \tau_0 = 0.005\ (Q = 10),\ a = 0.5 — 0.6 \tag{8}$$

For the selected parameters and $M < 10^6$, the main errors in evaluating the correlation function are caused by the smallness of the sample volume. The time for obtaining the correlation functions of the processes $\tilde{T}(t)$, $\tilde{\rho}(t)$, $\tilde{p}(t)$, $\tilde{\dot{P}}_A(t)$ with a sample volume of 501 (i.e., M ~ 5500) is 25 minutes on the BESM-3.

The following problems can be solved by the method under consideration: /76

1) to determine the fluctuations in satellite slowing caused by the variability of known radiation with known or given effective absorption altitude (for example, to explain to which fluctuations of satellite slowing the variability of the soft solar x-rays $\lambda\lambda$ = 40 — 60 Å leads);

2) to find the autocorrelation function of the response $\tilde{T}$ (or $\tilde{P}_A$) in Equation (4) to white noise for different altitudes of the absorption zone, which will permit, in the final analysis, determining the autocorrelation function of the response of $\tilde{T}$ to any steady-state effect $\tilde{P}(t)$.

3. White Noise Generator. Accuracy of the Estimates of the Correlation Function

The sequence of random numbers ξ_k

$$\langle \xi_k \rangle = 0, \quad \langle \xi_k \xi_l \rangle = \langle \xi^2 \rangle \delta_{kl}, \tag{9}$$

where δ_{kl} is the Kronecker delta, corresponds to white noise, i.e., to a random process with a δ-correlated autocorrelation function in the difference method.

It is clear that nonobservance of the condition (9) leads to distortion of the correlation function for the response of $\tilde{T}$ and, in the final analysis, to errors in solving the second problem. To control the operation of the random number generator, the following random sequences were calculated:

$$\xi_{k,q} = J'_{(q)}, \tag{10}$$

where $j = (k + M_1)Q$; $k = 1, 2, \ldots, M_0$, $q = 1, 2, \ldots, q_0$; $Q = 10$; $M_1 \approx 20 — 40$; $M_0 = 501$; q is the count version number; the remaining notations are as before, and the sampling autocorrelation functions were determined:

$$r_q(\tau) = \frac{1}{501 - \tau} \sum_{i=1}^{501-\tau} (\xi_{i,q} - \bar{\xi}_q)(\xi_{i+\tau,q} - \bar{\xi}_q)/s_q^2, \tag{11}$$

where

$$\bar{\xi}_q = \frac{1}{501}\sum_{i=1}^{501}\xi_{i,q}, \quad s_q^2 = \frac{1}{500}\sum_{i=1}^{501}(\xi_{i,q}-\bar{\xi}_q)^2, \quad i = 1, 2, \ldots, 10.$$

If the values of $r_q(\tau)$ do not differ significantly from zero,* then condition (9) is considered satisfied. As for the univariate distribution of the quantity ξ_k, its selection can be rather arbitrary [the choice of one distribution or another, generally speaking, is reflected in the accuracy of the estimate of the sampling correlation function $r_q(\tau)$, but for a large sample volume (M_0 = 501), these differences are insignificant]. The discrete distribution: ξ = 1 with probability 1/2, ξ = -1 with probability 1/2, is taken, and the following is taken as the algorithm for calculating the sequence of random numbers: /77

1) three arbitrary numbers A_0, B_0, and C, different for each q are selected;

2) for i = 1, 2, ..., $q(M_1 + M_0)$:

$$B_i = l_i = 7531 \sin^2(iB_{i-1} + A_{i-1} + C), \tag{12}$$

$$j^i = \begin{cases} 1, & \text{if } \{l_i\} < 0{,}5, \\ -1, & \text{if } \{l_i\} \geqslant 0{,}5, \end{cases}$$

{x} fractional part of the number x;

are calculated sequentially;

3) for k = 1, 2, ..., M_0

*In mathematical statistics, a deviation exceeding an α-percent critical value is called a *significant* deviation [with a confidence coefficient (1 — 100α)]. One speaks analogously about a significant rejection of a null hypothesis, etc.

$$\xi_k = J^{j_*}, \quad j_* = (k + M_1)Q.$$

are determined.

It should be noted that the more efficient RAND procedure used at the Computer Center of the AN SSSR does not give a random sequence of the quality we need; besides, the time for calculating a random sequence is a negligible part of the calculation time for the whole program and is not of great value in machine time economy.

To verify the satisfaction of condition (9) for the sequences of random numbers $\xi_{k,\ q}$ obtained with the algorithm (12), the sampling autocorrelation functions (11) were calculated, and then the correlation function averaged over the ensemble q (q = 1, 2, ..., q_0; q_0 = 100):

$$\bar{r}(\tau) = \frac{1}{q_0} \sum_{q=1}^{q_0} r_q(\tau), \quad \tau = 1, 2, \ldots, 10,$$

the sampling standard deviations

$$s(\bar{r}(\tau)) = \sqrt{\frac{\sum_{q=1}^{q_0} (r_q(\tau) - \bar{r}(\tau))^2}{q_0(q_0 - 1)}} \tag{13}$$

and the normalized quantities

$$\zeta(\tau) = \frac{\bar{r}(\tau)}{s(\bar{r}(\tau))}, \quad \zeta_0(\tau) = \frac{\bar{r}(\tau)}{\sigma[\bar{r}(\tau)]},$$

where σ is the true standard deviation:*

$$\sigma \approx (M_0 q_0)^{-1/2},$$

*The relative error in this formula $\leq \tau_{max}/2M_0 = 5/M_0$ cannot be taken into account.

TABLE 3*

SAMPLING CORRELATION ESTIMATES FOR THE WHITE NOISE GENERATOR

τ	$10^3 \cdot \bar{r}(\tau)$	$10^3 \cdot s[\bar{r}(\tau)]$	$\zeta(\tau)$	$\zeta_0(\tau)$	τ	$10^3 \cdot \bar{r}(\tau)$	$10^3 \cdot s[\bar{r}(\tau)]$	$\zeta(\tau)$	$\zeta_0(\tau)$
1	3,0	4,0	0,75	0,67	6	6,3	4,1	1,53	1,40
2	3,8	3,3	1,18	0,87	7	—4,2	4,7	—0,89	—0,93
3	—8,1	4,5	—1,80	—1,80	8	0,2	3,8	0,05	0,04
4	—4,3	4,5	—0,96	—0,96	9	1,9	4,3	0,44	0,42
5	—7,8	4,7	—1,66	—1,73	10	—4,2	4,3	—0,98	—0,93

* Translator's Note: Commas in numbers indicate decimals.

were determined. The results of the calculations for $\bar{r}(\tau)$, $s[\bar{r}(\tau)]$, $\zeta(\tau)$ and $\zeta_0(\tau)$ from 100 sampling autocorrelation functions $r_q(\tau)$ are presented in Table 3. /78

As is seen from this table, the deviations of $\bar{r}(\tau)$ from zero nowhere exceed 1.8 sampling or true standard deviations, $|\zeta_0| \leq 1.8$, $|\zeta| \leq 1.8$, and, consequently, are insignificant. Verification of the hypothesis $\langle r \rangle = 0$ with the help of the statistics:

$$\zeta_1 = \sum_{i=1}^{10} \zeta_0^2(\tau),$$

which in the case of null hypothesis truth is distributed asymptotically ($M_0 \to \infty$) as χ^2 with ten degrees of freedom, that the null hypothesis is not rejected with a 20% significance level ($\zeta_1 = 12.23 < \zeta_{20\%} = 13.44$).* Thus, the choice of the method (12) is quite sound.

*We note that the Anderson criterion [12, 13] can also be used to verify the deviation of a normal process from white noise.

The final goal of the machine calculation is to obtain with a given accuracy the correlation functions for the response of the heat transfer equation (2) [or (6a), (7a), (7b), (7c)]. In order to estimate the volume of calculations (or the number of calculation series q_0) necessary for the given accuracy, it is necessary to estimate the standard deviation of the sampling correlation functions as a function of sample volume.

Two methods of estimation are possible. The first of these is to calculate the q_0 sequences of correlation functions for the response of Equations (7) and to determine $s[\bar{r}(\tau)]$ from Formula (13). For this, q_0 cannot be too large, and the estimate

$$\sigma(\bar{r}(\tau))_{q_1} \approx s(\bar{r}(\tau))_{q_0} \sqrt{\frac{q_0}{q_1}}. \qquad (14)$$

is used as an estimate of the standard deviations $\sigma[\bar{r}(\tau)]_{q_1}$ of the average correlation function obtained from q_1 ($q_1 \gg q_0$) sequences. The second method is a theoretical estimate of $\sigma(\tau)$ /79 with a known form of the true correlation function (since it is unknown, the sampling correlation function $\bar{r}(\tau)$ is used) and some limits placed on the distribution of ξ_i. In the general case, such an analysis is rather cumbersome [14]. But as an approximate estimate, taking the fact into account that, in our case, the correlation function usually has a single maximum (for $\tau = 0$) and decreases rapidly with increasing τ, the following can be recommended:*

$$\sigma[\bar{r}(\tau)] = \frac{1-\rho^2(\tau)}{\sqrt{N_{eff}}},$$

$$N_{eff} = \begin{cases} M_0 q_0 & \text{for} \quad \tau_1 < 0{,}5, \\ M_0 q_0 / 2\tau_1 & \text{for} \quad 0{,}5 \leqslant \tau_1 < 3, \end{cases} \qquad (15)$$

*The slowing of the decline of the correlation function for $\bar{r} < e^{-1}$ is also taken into account. Other simplified estimates are presented in [13, 15].

$$\tau_1 = \int_0^\infty \rho(\tau)\, d\tau, \qquad (15a)$$

where $\rho(\tau)$ is the true correlation function for the response; $M_0 q_0$ is the sample volume; N_{eff} is the effective sample volume; τ_1 is the correlation interval.

Replacement of the true correlation function by the sampling in (15), (15a) produces practically no change in the results.

The consistancy of the estimates (14) and (15) can serve as some control of the stability of the calculation method. By taking the fact into account that for large q_0 the standard deviation of the quantity s/σ is:

$$\sqrt{2/(4q_0+3)} \approx (2q_0)^{-1/2},$$

and for large M_0, the relative error of (15) does not exceed 20 — 30%, one can consider the divergence of the estimates as significant, if

$$\left| \sigma_{\text{from (14)}} - \sigma_{\text{from (15)}} \right| > \left(0{,}3 + \frac{3}{\sqrt{2q_0}}\right)\sigma. \qquad (16)$$

Examples of the correlation function calculations are presented in Table 4.

The divergence of the estimates (14) and (15) was found to be insignificant [i.e., Condition (16) was not satisfied], and the method for calculating the correlation functions for the response of the equation is satisfactory. Thus, an algorithm is obtained for the problem of finding the correlation function for the response of $\tilde{T}$ (or $\tilde{\dot{P}}_A$) in Equation (2) to white noise for different altitudes of the absorption zone.

TABLE 4*

τ	r (τ)	$\sigma^{(1)}(\tau)$	$\sigma^{(2)}(\tau)$	η (τ)
1. M_0=501, q_0=37, τ_1=2,14, $\sqrt{N_{eff}}$ =67, η_0=0,65				
1	0,673	0,008	0,008	0,00
2	0,430	0,011	0,010	0,10
3	0,292	0,013	0,014	0,08
4	0,204	0,015	0,015	0,00
5	0,154	0,016	0,015	0,07
6	0,106	0,016	0,015	0,07
7	0,076	0,016	0,015	0,07
8	0,053	0,015	0,015	0,00
9	0,034	0,014	0,015	0,07
10	0,028	0,013	0,015	0,14
11	0,027	0,012	0,015	0,21
12	0,022	0,011	0,015	0,30
13	0,014	0,011	0,015	0,30
14	0,011	0,011	0,015	0,30
15	0,017	0,009	0,015	0,50

τ	r (τ)	$\sigma^{(1)}(\tau)$	$\sigma^{(2)}(\tau)$	η (τ)
2. M_0=200, q_0=31, τ=2,53, $\sqrt{N_{eff}}$=49, η_0=0,68				
1	0,845	0,004	0,006	0,20
2	0,609	0,009	0,013	0,36
3	0,431	0,015	0,016	0,06
4	0,284	0,020	0,018	0,10
5	0,184	0,023	0,019	0,19
6	0,116	0,025	0,020	0,22
7	0,065	0,026	0,020	0,26
8	0,025	0,027	0,020	0,30
9	—0,002	0,027	0,020	0,30
10	—0,024	0,026	0,020	0,26

* Translator's Note: Commas in numbers indicate decimals.

NOTE: $\sigma^{(1)}$ was calculated from Formula (14), and $\sigma^{(2)}$ — from Formula (15). The divergence between $\sigma^{(1)}$ and $\sigma^{(2)}$ $\eta = 2|\sigma^{(1)} - \sigma^{(2)}|/(\sigma^{(1)} + \sigma^{(2)})$ is significant, if $\eta > \eta_0 = 0.3 + 3/\sqrt{2q_0}$.

4. Response of the Parabolic Equation to White Noise. Statistical Properties of the Fluctuations

We present preliminary calculation results to illustrate the possibilities of this technique. Data of the standard atmosphere CIRA-1965 [16] for the minimum of the 11-year cycle (model I) were used as the normal parameters, and the vertical profile $\varphi(x)$ of the variable source appearing in the initial equations (7a), (7b) was selected as rectangular with a width equal to the height of the homogeneous atmosphere H_p:

$$\varphi(x(z)) = \begin{cases} 1 \text{ for } z_{eff} - \frac{H_p(z_{eff})}{2} \leq z \leq z_{eff} + \frac{H_p(z_{eff})}{2}, \\ 0 \text{ for } z < z_{eff} - \frac{H_p(z_{eff})}{2} \text{ or } z > z_{eff} + \frac{H_p(z_{eff})}{2} \end{cases} \quad (17)$$

The following effective source altitudes were considered: z_{eff} = 120, 132, 150, and 175 km. The parameters of the difference method were selected according to (8), and the lattice functions were calculated from the Formulas (7). As was already stated, by knowing the statistical properties of the response of the linear equation (7a), or (7b) to white noise, it is not difficult /81 to obtain the statistical properties of the response of this equation to any steady-state noise with given correlation properties (for details, cf. in [3]). Thus, the main consideration was given to the response of the parabolic equation to white noise, whose generator is described in the preceding section.

By analyzing the properties of the fluctuations in the upper atmosphere, one wants, first of all, to explain how the fluctuations are propagated from the source of the perturbations and, in particular, how the fluctuation amplitude varies with altitude. The simultaneous observations of seven satellites with different perigees (from 205 to 1121 km) during the strong geomagnetic disturbance in November, 1960 [17], was an excellent solution of this question. These observations clearly indicated the tendency for growth of the relative perturbations with altitude. The peculiarities of this example involved the following:

1) a very strong disturbance was observed (the density increased by more than two times);

2) the disturbance was the only one;

3) the phase of the 11-year-cycle was close to the activity maximum;

4) there were secondary effects distorting the picture of the perturbation amplitude distribution with altitude (in particular, the geocentric angle between the perigee and the Sun for the different satellites varied in the range 3 to 149°).

Of course, with the transition to small fluctuations, it is impossible to separate the individual strong flares in the rate of satellite slowing and to compare their values at different altitudes. Instead, the standard deviations of the relative fluctuations are calculated and compared at different altitudes. Judging from the estimates of the dispersions of the relative fluctuations in the slowing of six satellites with perigees from 250 to 750 km during the minimum of the 11-year-cycle [18], the standard deviation of the small fluctuations increases with altitude.

Unfortunately, in both [17] and [18], the secondary effects could not be disengaged from the distortion of the distribution, and the results are more qualitative than quantitative. The theoretical variation of the standard deviation of the small fluctuations calculated on the basis of the method described above (Equation 7b) is presented in Figure 1. The source of the perturbations is located at an altitude t_{eff} = 120 km. As should be expected, the temperature fluctuations $\tilde{T}$ decrease with altitude, and the relative fluctuations of the density $\tilde{\rho}$ and the satellite slowing rate $\tilde{P}_A$ increase with altitude. The approximate relation presented in [3]:

$$\tilde{P}_A(z) \approx h\tilde{T}(z),$$

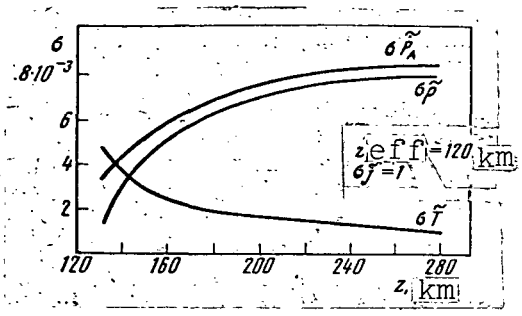

Figure 1. Dependencies of the standard deviations of the small fluctuations on altitude.

where h is the number of "homogeneous heights" between the zone of the variable radiation absorption and the satellite perigee z, is sufficiently well satisfied.

We note that the functions $\sigma\tilde{P}_A(z)$, $\sigma\tilde{\rho}(z)$, $\sigma\tilde{T}(z)$ were determined with an accuracy to a single constant multipler depending on the characteristics of the variable radiation source. An example of estimates of the absolute values of the standard deviations for a specified variable radiation source will be given below. /82

Thus, the amplitude of the relative fluctuations in the density of the upper atmosphere and in satellite slowing increases with increasing altitude.

What is the time of fluctuation propagation or of perturbation lag in the atmosphere? Numerous determinations of the average time between geomagnetic disturbance peaks and perturbations in satellite slowing have been conducted. It is 5 — 9^h according to various estimates. The lag time of the so-called "27-day variations" of 0.5 — 2^d, 1 has been obtained by the same method [16, 17, 19 — 25], which agrees with the statistical estimate of McDonald [26], who observed a 56-hour shift between the variations of the 20 cm radio emission of the Sun and the response of the atmosphere. This lag is related to the heat transfer time in the atmosphere [16]. However, with examination of the thermal inertia of the atmosphere, a more correct characteristic is not the lag time of the atmospheric response to a disturbance, but the nature of disturbance distortion in the

atmosphere. We will explain this with the example of the simplest relaxation system:

$$\frac{dx}{dt} + \frac{x}{\Delta} = F(t), \tag{18}$$

where Δ is the relaxation time (or, in other terms, the thermal inertia time). The response x(t) of the system (18) to a rectangular pulse disturbance:

$$F(t) = \begin{cases} 0 & \text{for } t \leqslant 0, \text{ or } t > D, \\ a & \text{for } 0 < t \leqslant D \end{cases}$$

will be: /83

$$x(t) = \begin{cases} 0 & \text{for } t \leqslant 0, \\ a\Delta(1 - e^{-t/\Delta}) & \text{for } 0 \leqslant t \leqslant D, \\ a\Delta(e^{-\frac{D}{\Delta}} - 1)e^{-t/\Delta} & \text{for } t \geqslant D. \end{cases}$$

The form of the response x(t) does not repeat the form of the disturbance F(t), the distortions can be significant, and the concept of the lag of x(t) relative to F(t) is ambiguous. For example, if one defines the lag time as the time between the maxima of F(t) and x(t), then it will not depend on the parameters of (18), but equals D/2.

Another method for defining the lag involves comparing the medians of the pulses F and x. The lag time τ_3 defined by such a method is related to the relaxation time Δ by the simple relation:*

$$\tau_3 = \begin{cases} \Delta \ln 2, & \text{if } D \ll \Delta, \\ \Delta k, \text{ where } k \approx 1, & \text{if } D \sim \Delta, \\ \Delta, & \text{if } D \gg \Delta, \end{cases} \tag{19}$$

and can serve as its estimate.

*The relation (19) is also preserved with a transition to pulses of other forms.

However, a statistical examination is more natural. It is not difficult to see that the autocorrelation function for the response to white noise

$$\langle F(t)\rangle = 0, \quad \langle F(t)F(t+\tau)\rangle = C\delta(\tau),$$

is an exponential

$$\rho_x(\tau) \equiv \frac{\langle x(t)\,x(t+\tau)\rangle}{\langle x^2\rangle} = \exp(-|\tau|/\Delta), \tag{20}$$

and the smaller the relaxation time Δ, the closer the correlation function for the response is to the correlation function for the disturbance F. By knowing the correlation function for the system response to white noise, we obtain the relaxation time Δ at once. Clearly, it is not the true correlation function $\rho(\tau)$ which is determined from the observations, but the sampling $r(\tau)$, which will always differ from the exponential; Δ is evaluated statistically and the following can be proposed as its estimate.*

$$\tau_1 = \int_0^\infty r(\xi)\,d\xi, \qquad r(\tau_2) = e^{-1} = 0{,}37. \tag{21}$$

For a sufficiently large sample volume, $\tau_1 \approx \tau_2 \approx \Delta$.

Thus far, the simplest system (18) defined by one parameter — the relaxation time Δ — has been considered. The fluctuation equations (7a) and (7b) are not defined by one parameter; however, even in this case, the quantities τ_1 and τ_2 (21) are the essential /84 characteristics of the system. The closeness of τ_2 to τ_1 would signify the closeness of Equation (7a) or (7b) to (18); on the

*Of course, only a sequence of sample values $r(\tau_i)$ is obtained from the observations, then an interpolation is carried out. The value $\xi = (2 - 4)\Delta$ is taken as the upper limit in the integral.

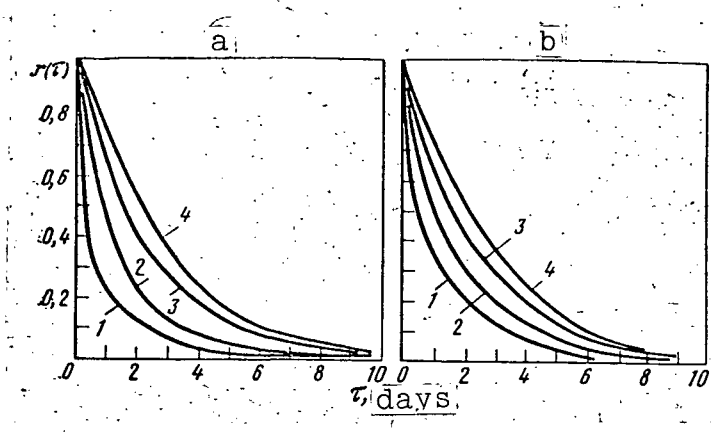

Figure 2. Autocorrelation functions of the fluctuations $\tilde{T}$ (a) and $\tilde{\dot{P}}_A$ (b) for source with different effective altitudes z_{eff}. 1- 175 km; 2- 150 km; 3- 132 km; 4- 120 km.

other hand, to estimate the relaxation time of the system, one can use the relation

$$\Delta \approx \frac{\tau_1 + \tau_2}{2}. \tag{22}$$

We return to the numerical results obtained for Equation (7b). The autocorrelation functions for the fluctuations $\tilde{T}$ and $\tilde{\dot{P}}_A$ for different effective altitudes z are presented in Figure 2, and the variation of the quantities $\tau_1(z_{eff})$, $\tau_2(z_{eff})$ for $\tilde{\dot{P}}_A$ is given in Figure 3. As is seen from these graphs, for an effective absorption altitude of 120 km,

$$\Delta \approx 3^d. \tag{23}$$

If the lag of fluctuations is estimated from the measurement of the sharpest (short-term) impulses in satellite slowing, which was evidently done in [22 — 24], then the theoretical lag time /85 according to [23] and (19) is

$$\tau_3 \approx \Delta \ln 2 \approx 2^d. \tag{24}$$

Thus, the concept of the effective altitude of the absorption zone $z_{eff} \approx 120$ km does not contradict the observations. The

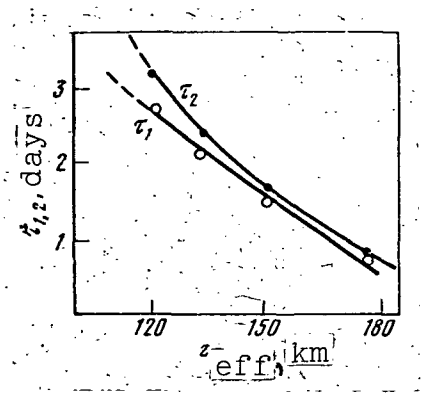

Figure 3. Functions $\tau_1(z_{eff})$, $\tau_2(z_{eff})$ for the fluctuations $\tilde{\dot{P}}_A$.

autocorrelation functions shown in Figure 2 differ from exponentials. However, as the calculations show, for a sample volume $n \leq 150 - 200$, the differences of the autocorrelation functions for the responses of Equations (7b) and (18) are not statistically significant. Because of this, interpreting the results of correlation analysis for not very long series of observations can be carried out on the basis of Equation (18), which was actually done in [8, 27, 28]. The form of the autocorrelation function for the response (18) x to the disturbance F different from white noise was considered in [2], in particular, for the triangle-correlated disturbances F

$$\langle F\rangle = 0, \quad \langle F(t)F(t+\tau)\rangle = \begin{cases} \langle F^2\rangle\left(1-\frac{|\tau|}{\tau_0}\right) & \text{for } |\tau|\leqslant\tau_0, \\ 0 & \text{for } |\tau|\geqslant\tau_0; \end{cases} \tag{25}$$

the response x has the autocorrelation functions

$$r_x(\tau) = \begin{cases} l\left(1-\frac{|\tau|}{\tau_0}+\frac{\Delta}{\tau_0}e^{-\frac{\tau_0}{\Delta}}\operatorname{ch}\frac{|\tau|}{\Delta}\frac{\Delta}{\tau_0}e^{-\left|\frac{\tau}{\Delta}\right|}\right) & \text{for } |\tau|\leqslant\tau_0, \\ \frac{2\Delta l}{\tau_0}\operatorname{sh}^2\left(\frac{\tau_0}{2\Delta}\right)e^{-\frac{|\tau|}{\Delta}} & \text{for } |\tau|\geqslant\tau_0 \end{cases} \tag{25a}$$

and dispersion

$$\sigma^2(x) = \Delta^2\langle F^2\rangle/l, \quad \text{where } l = \left(1+\frac{e^{-\tau_0/\Delta}-1}{\tau_0/\Delta}\right)^{-1}.$$

Clearly, if the disturbances F_1 and F_2 have the same dispersion but different characteristic times τ_{01} and τ_{02}, then the standard deviations of the responses x_1 and x_2 will differ:

$$\frac{\sigma x_2}{\sigma x_1} = k(\tau_{01}, \tau_{02}) = \sqrt{\frac{\tau_{02}/\Delta + \exp(-\tau_{02}/\Delta) - 1}{\tau_{01}/\Delta + \exp(-\tau_{01}/\Delta) - 1}}. \quad (26)$$

The variation of the standard deviation of small fluctuations $\sigma\tilde{P}_A(z)$ for a variable source with a unique dispersion and characteristic time $\tau_{01} = 0^d.1$ is presented in Figure 1. For the transition to a specific source with a characteristic time τ_{02}, it is necessary to introduce the normalizing multiplier

$$I = \frac{\sigma P_x k(\tau_{01}, \tau_{02})}{c_p a^2 T_p \rho_p} = \frac{\sigma E_x k(\tau_{01}, \tau_{02})}{H_p c_p a^2 T_p \rho_p} = \frac{K_0 \sigma F_{1x} k(\tau_{01}, \tau_{02})}{H_p c_p a^3 T_p \rho_p}. \quad (27)$$

We will estimate the contribution in the fluctuation $\tilde{P}_A$ from the variable solar emission $\lambda\lambda$ 40 — 100 Å. The emission $\lambda\lambda$ 44 — 60 Å (E_{1x}) is measured directly. The autocorrelation functions of the relative fluctuations $\tilde{E}_{1x}$ are approximated by (25) with $\tau_0 = 7^d$, hence, $\tau_{01} = 7^d$, and $\tilde{k}(\tau_{01}, \tau_{02}) \approx 20$. According to [29 — 31], the coefficient $k_0 \approx 2.5 — 5$, and according to [28], at the minimum of the 11-year activity $\sigma E \approx (0.01 — 0.03)$ erg/(cm^2/sec). At an altitude z = 120 km, we have $(c_p a^2 T_p \rho_p H_p)^{-1} = 20$ for model I [16]; thus, I ~ 4 — 12, and at altitudes of 230 — 260 km, the variable emission $\lambda\lambda$ 40 — 100 Å absorbed at an effective altitude z_{eff} = 120 km should cause fluctuations in satellite slowing with a standard deviation

/86

$$\sigma\tilde{P}_A = 0{,}03 \div 0{,}1. \quad (28)$$

This theoretical estimate agrees well with the direct determination of the standard deviation of the fluctuations for the satellite "Injun-3" with a perigee of 230 km [18]:

$$\sigma\tilde{P}_A \approx 0{,}1. \tag{29}$$

5. Consideration of the X-Ray Background (λλ 40 — 100 Å)

The estimates (28) and (29) presented above show the necessity of considering the variations of soft x-rays λλ 40 — 100 Å for analysis of the fluctuations in satellite slowing. These variations are also the principal cause of thermal fluctuations in the upper atmosphere with the characteristic time of 10 to 20 days [8, 26, 27].* Of course, variations of the soft x-rays are not the unique source of the daily mean fluctuations: besides the two-week fluctuations, fluctuations are not related to the variations of λλ 40 — 100 Å have been traced with characteristic times $\tau_* \leq 3$ days and dispersion on the order of the dispersion of the two-week fluctuations [28]. Of course, one must eliminate the effect of the variations of λλ 40 — 100 Å to reveal and study

*As was already noted in [3], the term "27-day variations" established in the literature does not quite fit for designating such fluctuations. Firstly, because the whole range of variations from 1 to 30 days is used in the correlation analysis of satellite slowing. Secondly, the term "27-day variations" for indices of solar activity is very idealized. For example, for the middle phase of solar activity, the emission λλ 40 — 100 Å had an autocorrelation function $\exp[-0.1|\tau|]\cos 0.22\tau$ [27], and for the activity minimum, this function was triangular (25) with $\tau_0 = 7^d$ [28]. A Fourier analysis of the indices of solar radio emission and satellite slowing, which was carried out by Lespes [32], also reveals the presence of several frequencies not multiples of each other.

such fluctuations. Predicting the fluctuations in satellite slowing caused by variations of the emission λλ 44 — 60 Å (E_1) also is of independent value, since at the minimum of the 11-year cycle, the correlation coefficient between $\tilde{E}_1$ and $\tilde{P}$ is rather large: $r = 0.58 \pm 0.13$. Numerous data on the variations of soft x-rays can be found, for example, in [29 — 31, 33 — 37], and /87
some statistical estimates are presented in [8, 27, 28]. The temperature fluctuations of the upper atmosphere caused by these variations have a characteristic time of 10 — 20 days, are global in nature, and Equations (2) or (7b) are suitable for their examination. Thus, there is a possibility, given the vertical absorption profile and effective absorption altitude, of finding the two-week fluctuations in satellite slowing with the help of Equation (7b) or (in the simplified version) with the help of Equation (18) from data on the variable emission λλ 40 — 100 Å (or λλ 44 — 60 Å, or somewhat worse, from the solar decimeter radio emission). Since the techniques for such calculations were discussed in detail above, we will limit ourselves to one example. The relative variations of the emission λλ 44 — 60 Å ($\tilde{E}_1$) and the corresponding fluctuations in the slowing of the object 1964-5A (February — March, 1964) $\tilde{\dot{P}}_{theo}$ are presented in Figure 4. The effective altitude of the absorption zone was taken as 120 km, and the rectangular vertical absorption profile with width H_p (height of the homogeneous atmosphere) was selected. The calculations of the relative fluctuations were carried out with the formula

$$\tilde{x} = \frac{x - \bar{x}^{t_0}}{\bar{x}^{t_0}}$$

with the averaging time $t_0 = 40^d$. For convenience of comparison, all the functions are normalized to their standard deviations.

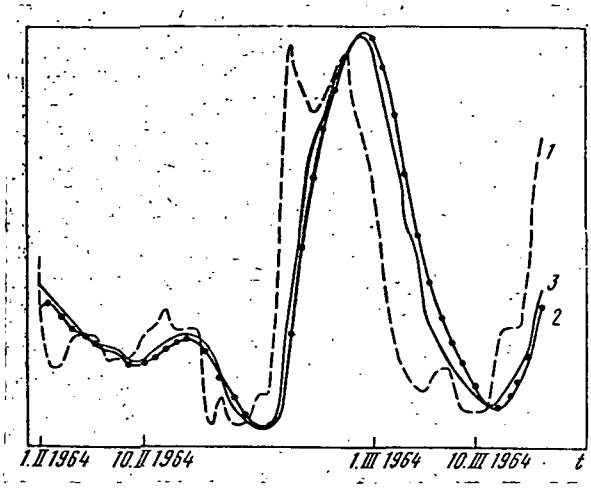

Figure 4. Relative variations of the λλ 44 — 60 Å radiation (curve 1) and the corresponding theoretical fluctuations in satellite slowing (curves 2, 3).

The function $\tilde{\tilde{E}}_1(t)/\sigma E_1$ is presented in Figure 4 by curve 1, /88 the function $\dot{\tilde{P}}_{theo}/\sigma\dot{\tilde{P}}_{theo}$ obtained without consideration of the Harries-Priester integral term in Equation (2) [i.e., for the initial Equation (7a)] — by curve 3, and the same function with consideration of the Harries-Priester term — by curve 2. The fluctuation curves 1, 2 averaged by sliding summation with an interval of 10 days is shown in Figure 5; curve 3 reproduces the observed fluctuations $\dot{\tilde{P}}_A(t)/\sigma\dot{\tilde{P}}_A$ in the slowing of object 1964-5A ("Saturn-5" rocket stage) also smoothed by sliding summation with an averaging interval of 10 days. As is seen in Figure 4, the presence or absence of the Harries-Priester integral term in the heat conductivity Equation [(6a) or (6b)] has a weak effect on the form of the fluctuations, and long series of observations are required to evaluate this term. Figure 4 also illustrates well the comment made above that the form of the system response can differ significantly from the form of the original disturbance (there is no shift along the abscissa which will superimpose curve 1 on curve 2, and it is not clear what to call the lag time). With a transition to smoothed fluctuations with a smoothing time $t_0 \gg \Delta$ (Δ is the system relaxation time as before), the differences of the disturbance and response gradually disappear, and the concept of the fluctuation lag becomes well defined. This is illustrated by the curves 1, 2 in Figure 5, which almost repeat each other with a time shift of 3^d. As was already mentioned, at the activity minimum of the 11-year cycle,

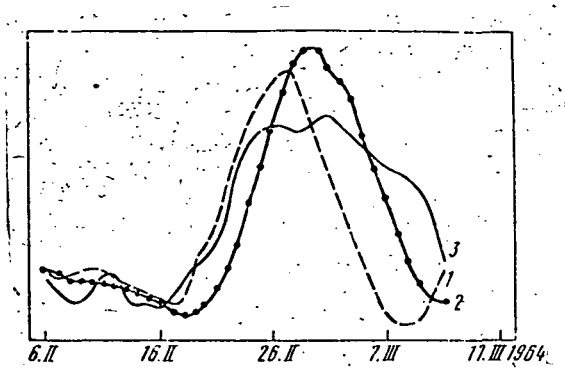

Figure 5. Smoothed (10^d interval) variations of the λλ 44 — 60 Å radiation (curve 1), theoretical (curve 2), and observed (curve 3) fluctuations in satellite slowing.

besides the two-week fluctuations, fluctuations are observed with a dispersion of the same order and a characteristic time of $t_* \leq 3^d$. Smoothing the data $\tilde{P}_A$ with the time $t_0 = 10^d$ decreases the dispersion of such fluctuations by $K = t_*/t_0 > 3.3$ times, but there is practically no change of the two-week fluctuation dispersion. Thus, the averaged theoretical fluctuations should not differ too /89 much from the observed ones, which is confirmed in Figure 5 (curves 2, 3). Unfortunately, this series of observations is not sufficiently large to make any sort of reliable statistical estimates (some statistical estimates of the fluctuations in the slowing of object 1965-5A and soft x-rays were presented in [8]).

One should also note another long-practiced method for considering variations with a characteristic time of 10 — 20^d (often called the "27-day variations" in the literature) [16, 38, 39]. Such fluctuations of temperature are connected by a linear dependence with the fluctuations of the solar decimeter radio emission ($F_{10,7}$)

$$\Delta T = \alpha (F_{10,7} - \overline{F}^{t_0}_{10,7}), \tag{30}$$

where $t_0 = 3 \cdot 27^d$ or $t_0 = 5 \cdot 27^d$ is the averaging time, F is taken in 10^{-22} W/(m^2/Hz).

The value $\alpha = 1^{\circ}.9$ (according to [16, 38]) and $\alpha = 1^{\circ}.3$ (according to [39]) was determined from the observations, and a disturbance lag time $\tau_{lag} = 0.5 - 2^{d}1$ [16, 38] and $\tau_{lag} = 1.0 \pm 0.1$ [39] was indicated.

There is no need to note once again that such a description is quite suitable for data on the fluctuations averaged with a characteristic time $t_0 \geq 10^{d}$ (cf. Figure 5), but for the 1- to 3-day variations in satellite slowing caused by soft x-ray variations, it is not justified.*

However, one can change Formula (30) somewhat in order to describe the thermal inertia of the upper atmosphere:

$$\Delta T = \sum_{i=0}^{I} \alpha_i [F_{10.7}(t-i) - \bar{F}_{10.7}], \quad I = 2 \div 5. \tag{31}$$

As in the case of (30), the coefficients α_i are found by the method of least squares [40].

Another approach involves returning to Equation (18). In the framework of this approximation, the contribution to the fluctuations of satellite slowing due to soft x-ray variations is:

$$\dot{\tilde{P}}_{theo}(t) = \alpha_0 \int_{-\infty}^{t} e^{-\xi/\Delta} \tilde{E}_1(\xi)\, d\xi \approx \alpha_0 \int_{t-3\Delta}^{t} e^{-\xi/\Delta} \tilde{E}_1(\xi)\, d\xi \approx$$
$$\approx \frac{\alpha_0}{2} [\tilde{E}_1(t) + e^{-k_0/\Delta} \tilde{E}_1(t-k_0)] + \alpha_0 \sum_{l=1}^{k_0-1} e^{-l/\Delta} \tilde{E}_1(t-l), \tag{32}$$

where k_0 is the integer part of the number 3Δ.

*We also note that the variations of the solar decimeter radio emission index are not completely adequate for the soft x-ray variations. For example, the correlation coefficient between E_1(λλ 44 — 60 Å) and $\tilde{F}_{10,7}$ in 1965 — 1966 was only 0.66, and the forms of their autocorrelation functions were significantly different.

The two unknown parameters α_0 and Δ_0 in relation (32) are /90
either estimated from the model the same way as was done above, or found by the method of least squares [40] from the observations. In place of the index $\tilde{E}_1$, one can use the index $\tilde{F}_{10,7}$, or any other related to the soft x-ray variations. Of course, the coefficients α_0 and Δ will then be different. It is proposed to carry out estimates of α_0 and Δ (for $\tilde{E}_1$ and $\tilde{F}_{10,7}$) for all phases of the 11-year cycle on the basis of the model CIRA-1971.

6. Inverse Problem

The question about the inverse problem considered in [2, 3] has been practically untouched in this article: to obtain the characteristics of the fluctuation source (i.e., information about the effective altitude, width and vertical profile of the variable radiation absorption zone, the absorbed energy, etc.) from the statistical properties of the fluctuations in satellite slowing and the variations of activity indices. The first attempt to carry out such an analysis [4, 8] led to the conclusion that the main cause of the two-week temperature fluctuations of the upper atmosphere is the variation of soft solar x-rays in the range 40 — 100 Å absorbed at an effective altitude of about 120 km.

Since the small fluctuations are described by the parabolic Equation (7a) or (7b), when the conditions cited at the beginning of the article are satisfied, one can discuss the narrower problem, the inverse heat conduction problem. If Equation (7a) had constant coefficients, and not random, but ordinary functions of time stood on the right side, then even in the two-dimensional (and, in general, in the n-dimensional!) case, the problem would reduce to the inverse heat conduction problem analyzed in [41],

which has a unique solution under simple limitations. However, it is impossible to generalize the method of [41] to an equation with variable coefficients, and the stochastic nature of the perturbations worsens even more the difficulties of a strict mathematical examination of the problem. In view of these reasons (and considering that our main goal is to obtain the parameters of the actual physical process by any means), one has to give up an analytic consideration and reduce the problem to a purely computational one:

1) to solve the direct problem for the "elementary" functions using the difference methods (taking, for example, a white noise source with a rectangular vertical profile);

2) to find the optimum coefficients for the "elementary" functions to adequately describe the observations.

We will not touch on problems about the existence and /91
uniqueness of the solution, about the limitations imposed on the equations and the probability processes, about taking into account the transition from the true to the sample means, and about obtaining an algorithm for constructing the solution of the problem by reducing it to the solution of some integral equation (including the correlation functions), while clearly representing that this is an independent and very difficult mathematical problem.

Such a "practical" approach is justified, for example, in computational mathematics by the successful solution of more complicated problems on the basis of difference methods, although investigations of the existence and uniqueness of the solution, the stability of the methods, etc., are carried out only for the simplest cases. Numerical analysis of the correlation properties of the response of Equation (7a) or (7b) has shown that one can

evaluate only two or three parameters from a correlation analysis of the daily mean fluctuations with an observation volume <200. In this case, the autocorrelation function of the response to a white noise source with an effective width of $\approx H_p$ does not differ significantly from an exponential, and the fluctuations are described by the following system of correlation equations [3, 27]:

$$\begin{aligned}
&\frac{d}{d\tau}R_{12}(\tau)+\lambda R_{12}(\tau)=\beta R_{11}(\tau),\\
&-\frac{d}{d\tau}R_{21}(\tau)+\lambda R_{21}(\tau)=\beta R_{11}(\tau),\\
&\frac{d}{d\tau}R_{22}(\tau)+\lambda R_{22}(\tau)=\beta R_{21}(\tau)+R_{23}(\tau),\\
&-\frac{d}{d\tau}R_{22}(\tau)+\lambda R_{22}(\tau)=\beta R_{12}(\tau)+R_{32}(\tau),
\end{aligned} \tag{33}$$

where

$$\begin{aligned}
&R_{11}(\tau)=\langle\tilde{E}(t)\tilde{E}(t+\tau)\rangle; \quad R_{22}(\tau)=\langle\tilde{P}_A(t)\tilde{P}_A(t+\tau)\rangle;\\
&R_{12}(\tau)=\langle\tilde{E}(t)\tilde{P}_A(t+\tau)\rangle; \quad R_{21}(\tau)=\langle\tilde{P}_A(t)\tilde{E}(t-\tau)\rangle;\\
&R_{23}(\tau)=\lambda\langle\psi(t)\psi(t+\tau)\rangle+\frac{d}{d\tau}\langle\psi(t)\psi(t+\tau)\rangle;\\
&R_{32}(\tau)=\lambda\langle\psi(t)\psi(t+\tau)\rangle-\frac{d}{d\tau}\langle\psi(t)\psi(t+\tau)\rangle;
\end{aligned}$$

$\tilde{E}$ is the variation of the radiation responsible for the two-week fluctuations; ψ are the more rapid fluctuations; $\langle\psi(t)\psi(t+\tau)\rangle/\langle\psi^2\rangle \approx 0$ for $\tau > \tau_*$.

The functions $R_{11}(\tau)$, $R_{12}(\tau)$, $R_{21}(\tau)$, $R_{22}(\tau)$ are evaluated from the observations and the three parameters

$$\lambda, \quad \beta \quad \text{and} \quad \langle\psi^2\rangle/\langle\tilde{E}^2\rangle. \tag{34}$$

are determined. At the same time, the theoretical functions /92

$$\lambda_0(z_{eff}) = \frac{2}{\tau_1+\tau_2}, \quad \beta_0(z_{eff}, \sigma E_x) \tag{35}$$

are evaluated on the basis of Equation (7b) from the effective altitude of the absorption zone z_{eff}. By comparing (34) and (35), one can evaluate the effective altitude of the absorption zone z_{eff} and the amount of absorbed energy.

To determine the vertical absorption profile, it is necessary either to increase significantly the number of observations, or to carry out, in addition to the correlation analysis, evaluations of the moments of the univariate distribution of the fluctuations.

Evidently, better results will be obtained by formulating the inverse problem with analysis of the hourly fluctuations in satellite slowing. According to the observations [42] and the statistical evaluations of [43], small fluctuations with a characteristic time $0^d.2$ were observed in satellite slowing during the 11-year cycle minimum (1963 — 1964) in a period of relatively moderate geomagnetic activity. With the successful development of techniques for such observations, the statistical analysis of fluctuations in satellite slowing and of variations of activity indices could be based on a significantly greater number of observations than for the daily mean data (reaching up to 10,000 two-hour values over three years) and give more reliable estimates.

These fluctuations ought to be described by the three-dimensional parabolic equation. It is proposed subsequently to obtain this equation and to evaluate the parameters of rapid fluctuation sources.

REFERENCES

1. Ozernoy, L. M. and V. Ye. Chertoprud. Astron. zh. (Astronomicheskiy zhurnal), Vol. 46, No. 5, 1969.

2. Chertoprud, V. Ye. Nauchnyye informatsii astrosoveta AN SSSR, No. 9, 1968.

3. Chertoprud, V. Ye. Nauchnyye informatsii Astrosoveta AN SSSR, No. 18, 1970.

4. Chertoprud, V. Ye. Nablyudeniya ISZ, No. 5, 1966, p. 128.

5. Harries, J. and W. Priester. J. Atmos. Sci., Vol. 19, 1962, p. 286.

6. Volland, H. NASA-G.S.F.C. Preprint x-621-69-88, 1969.

7. Blum, W. P. Forschungsber. Astron. Inst. Bohn. Preprint BMwF-FBW, 69-15, 1969.

8. Chertoprud, V. Ye. Space Res., Vol. 11, 1971, p. 929.

9. Chertoprud, V. Ye. Nablyudeniya, ISZ, No. 10, 1970, p. 248.

10. Tikhonov, A. N. and A. A. Samarskiy. Uravneniya matematicheskoy fiziki (Equations of Mathematical Physics). Moscow, "Nauka" Press, 1966, p. 546.

11. Samarskiy, A. A. Vvedeniye v teoriyu raznostnykh skhem (Introduction to the Theory of Difference Methods). Moscow, "Nauka" Press, 1971.

12. Anderson, R. L. Ann. Math. Statist., Vol. 33, 1942, p. 1.

13. Wilkes, S. Mathematical Statistics. Moscow, "Nauka" Press, 1967, Chapter 17.

14. Khennan, E. Analiz vremennykh ryadov (Analysis of Time Series). Moscow, "Nauka" Press, 1964.

15. Bendat, J. and A. Piersal. Izmereniya i analiz sluchaynykh protsessov (Measurement and Analysis of Random Processes). Moscow, "Mir" Press, 1971.

16. CIRA 1965. COSPAR International Reference Atmosphere 1965. Amsterdam, North Holland Publ. Co., 1965.

17. Jacchia, L. G. Space Res., Vol. 2, 1961, p. 747.

18. Slovokhotova, N. P. and V. Ye. Chertoprud. Byulleten stantsiy opticheskikh nablyudeniy ISZ, No. 53 (1), 1969, p. 4. /93

19. Roemer, M. SAO Spec. Report, No. 199, 1966.

20. Jacchia, L. G., J. Slowey and F. Verniani, SAO Spec. Report, No. 218, 1966.

21. Jacchia, L. G. and F. Verniani, SAO Spec. Report, No. 193, 1965.

22. Roemer, M. Space Res., Vol. VII, No. 2, 1967, p. 1091.

23. Jacchia, L. G. SAO Spec. Report, No. 245, 1967.

24. Jacchia, L. G. Nature, Vol. 183, 1959, p. 526.

25. Roemer, M. Forschungsber. Astron. Inst., Bohn, Vol. 2, 1968, p. 68.

26. McDonald, G. J. F. Rev. Geophys., Vol. 1, 1963, p. 305.

27. Chertoprud, V. Ye. Byulleten stantsiy opticheskikh nablyudeniy ISZ, No. 54, 1969, p. 31.

28. Chertoprud, V. Ye. Nablyudeniya ISZ, No. 9, 1969.

29. Mandelstam, S. L. Space Sci. Rev., Vol. IV, 1966, p. 587.

30. Yonezawa, T. Space Sci. Rev., Vol. V, No. 1, 1966, p. 3.

31. Manson, J. E. Astrophys. J., Vol. 147, No. 2, 1967, p. 703.

32. Lespes, J. P. Thesis: Contribution à l'etude de la haute atmosphere entre 350 km et 1500 km, par l'analyse du freinage des satellites artificiels (Contribution to the Study of the Upper Atmosphere between 350 km and 1500 km, for the Analysis of Artificial Satellite Braking). 1969, p. 39.

33. Solar-Geophysical Data (Essa Research Laboratories). Washington, 1965 — 1970.

34. Kreplin, P. W. Space Res., Vol. 5, 1965, p. 951

35. Landini, M., D. Russo and G. Tagliaferri. Planet and Space Sci., Vol. 15, No. 2, 1967, p. 231.

36. Pounds, K. A. Ann. Astrophys., Vol. 28, No. 1, 1965, p. 132.

37. Van Gils, J. N. and W. de Graaff, Solar Phys., Vol. 2, 1967, p. 290.

38. Jacchia, L. G. Space Res., Vol. V, 1965, p. 800.

39. Jacchia, L. G. SAO Spec. Report, No. 332, 1971.

40. Linnik, Yu. V. Metod naimen'shikh kvadratov i osnovy teorii obrabotki nablyudeniy (Method of Least Squares and the Theoretical Principles of Observation Analysis). Moscow, State Physics and Mathematics Press, 1962.

41. Lavrent'yev, M. M., V. G. Vasil'yev and V. G. Romanov. Mnogomernyye obratnyye zadachi dlya differentsial'nykh uravneniy (Multivariate Inverse Problems for Differential Equations). Novosibirsk, "Nauka" Press, 1969, Chapter IV.

42. Jacobs, R. L. LMSC/195700, Traking Note, No. 68, 1965.

43. Chertoprud, V. Ye. and D. I. Irgashev. Nablyudeniya ISZ, 1967, p. 97.

N74-28294

EVALUATION OF THE ACCURACY IN PREDICTING SHORT-PERIOD VARIATIONS OF THE ATMOSPHERIC DENSITY

M. I. Voyskovskiy, I. I. Volkov, N. I. Gryazev,
B. V. Kugayenko, V. M. Sinitsyn, and P. Ye. El'yasberg

ABSTRACT. The possible accuracy in predicting the short-period variations of the atmospheric density correlated with the solar radio emission intensity at 10.7 cm and with the geomagnetic disturbance indices is evaluated in the article. The length of the prediction intervals under consideration ranges from several hours to three days. Tables and graphs are presented, which permit evaluation of the possible errors in calculating the density in the interval of altitudes 150 — 350 km.

The accuracy of operational prediction of the motion of /93
low-orbiting AES is determined to a significant degree by the potentialities of the mathematical descriptions and prediction of the short-term variations of the atmospheric density. In existing models of the atmosphere, the short-period variations of its parameters are, as a rule, in the form of a function of the solar radio emission intensity $F_{10.7}$ and the values of the geomagnetic index a_p (or A_p). Thus, the accuracy in describing the short-term variations of the atmospheric density ρ in a /94
prediction interval for the AES motion depends primarily on the accuracy in predicting the values of $F_{10.7}$ and a_p and on the correspondence of the analytic expressions selected in the models (as a function of these indices) to the actual variations of the atmospheric density. The effect of the first source of

errors, i.e., the effect of errors in predicting the indices $F_{10.7}$, a_p, and A_p, will be evaluated in this work.

We will consider the following versions for assigning the values of these indices in the prediction interval:

Method I — extrapolation of the index values by a method based on the theory of random functions [1, 2];

Method II — use of the last measured value of each index, assuming the index values are constant in the prediction interval [1, 2];

Method III — use of the predicted values of the indices $F_{10.7}$ and A_k instead of A_p from the data of the Institute of Terrestrial Magnetism, Ionosphere and Radiowave Propagation AN SSSR [IZMIRAN].

For the calculations, we will make use of the model of atmospheric density presented in [3]. The prediction interval length of interest to us is no more than three days.

It was shown in [1] that, for steady-state normal sequences, the best extrapolation formula is the following:

$$\bar{\xi}(t_1+\delta)=\sum_{k=1}^{n} a_k\zeta(t_k), \tag{1}$$

where t_1 is the time of the last measurement of the index ζ; $\zeta(t_1 + \delta)$ is the predicted value of the index ζ at the time $t_1 + \delta$; δ is the prediction length; $\zeta(t_k)$ are the observed values of the index at time t_k.

The coefficients a_k are determined by solving the system of n algebraic equations:

$$\sum_{k=1}^{n} a_k R(t_k - t_j) = R[(t_1 - t_j) + \delta], \tag{2}$$

where j = 1, ..., n; $R(t_k - t_j)$, $R[(t_1 - t_j) + \delta]$ are the values of the autocorrelation function of the index ζ corresponding to time shifts equaling $t_k - t_j$ and $(t_1 - t_j) + \delta$, respectively.

To substantiate the possibility of using this algorithm for predicting the indices $F_{10.7}$ and a_p (or A_p), an examination of the steadiness of sequences of these indices and the correspondence of their distribution law to the normal was carried out.

The calculations for verifying the correspondence to the normal distribution law were carried out for the period from 1964 to 1968 for each year individually. The obtained probability of the conformity of the distribution to the normal (by the Pearson criterion) lies in the range 0.75 — 0.90 for all three indices.

The steadiness of the sequences of $F_{10.7}$, a_p, and A_p was investigated by comparing the autocorrelation factors of the corresponding sequences calculated for a number of years (indicated on the graphs) and for a number of origin shifts. The formula was used

$$\hat{R}(\tau) = \frac{1}{(N-M)} \sum_{i=1}^{N-M} [\zeta(t_i) - \bar{\zeta}][\zeta(t_i + \tau) - \bar{\zeta}], \tag{3}$$

where N is the total number of values of the sequence for an interval of one year; $M = \tau/\Delta$; Δ is the sequence step; $\bar{\zeta}$ is the arithmetic average of the index ζ during the interval under consideration.

The obtained normalized autocorrelation functions $K(\tau)$ are presented in Figures 1 — 3. The functions $K(\tau)$ with origin shift for one year are shown in Figures 1a and b; with shift for one month — in Figure 1c.

The shaded region in Figure 3 is the region of variation of the normalized autocorrelation functions of the index a_p for 1965 — 1967. Analogous calculations were also carried out with small origin shifts (up to ten days). However, in this case, the variations of the corresponding normalized autocorrelation functions are insignificant and are not presented graphically.

The variation of the yearly mean values of the indices $F_{10.7}$, a_p, and A_p, and the mean square deviations of the indices $F_{10.7}$, and a_p are shown in Figure 4. This graph can characterize the variability of the mathematical expectation and dispersion of each sequence with the course of time.

Analysis of the curves in Figures 1 — 4 shows that, in the general case, not one of the analyzed sequences satisfies the requirements of steadiness for the considered time intervals. However, by taking the fact into account that short-term prediction of the indices (up to several days) is being examined in this work, one can assume as correct the statement about the steadiness of these sequences for small intervals of time and apply the prediction technique described above.

To select the number of terms n in Formula (1), an analysis of the dependence of the prediction accuracy on the value of n (for $1 \leq n \leq 8$) was carried out. The ratio of the mean square error in predicting for one day the value of the index $F_{10.7}$ with $1 \leq n \leq 8$ to the corresponding error with $n = 1$ for a number of

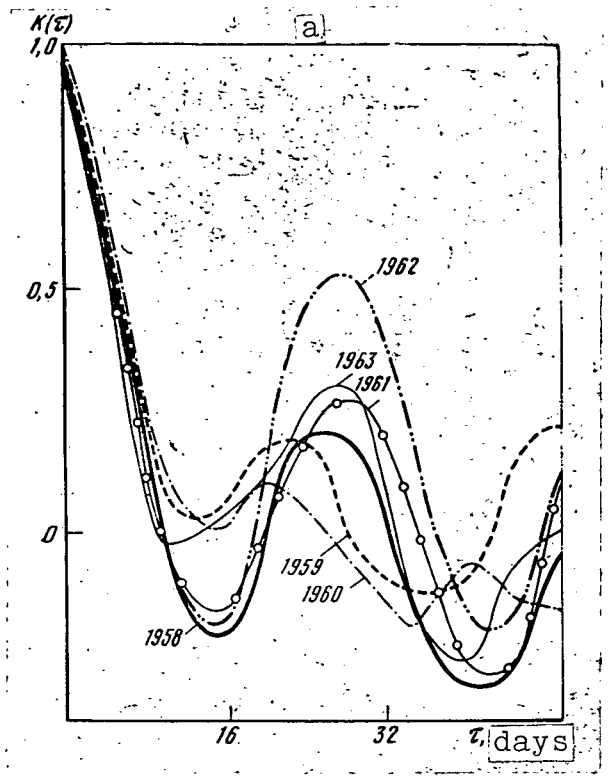

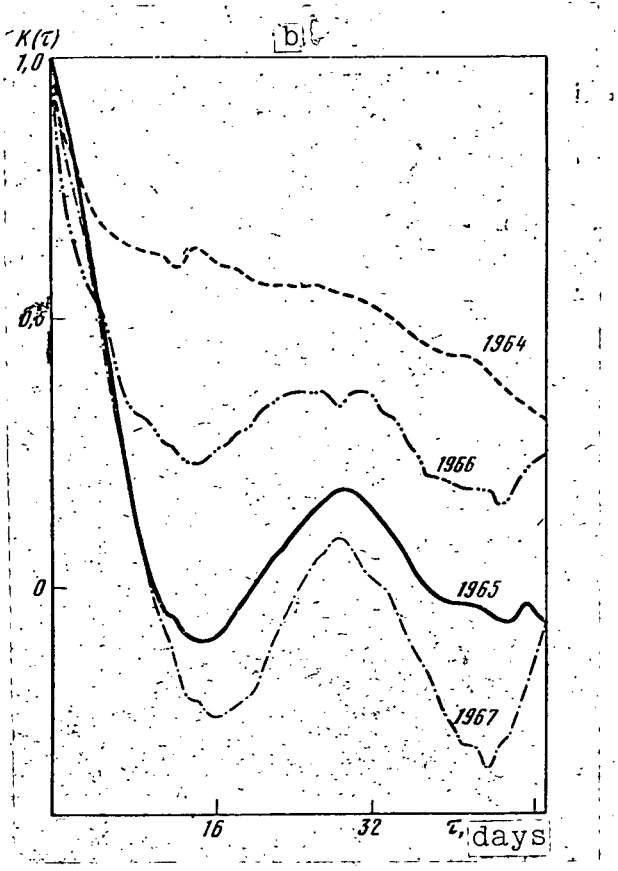

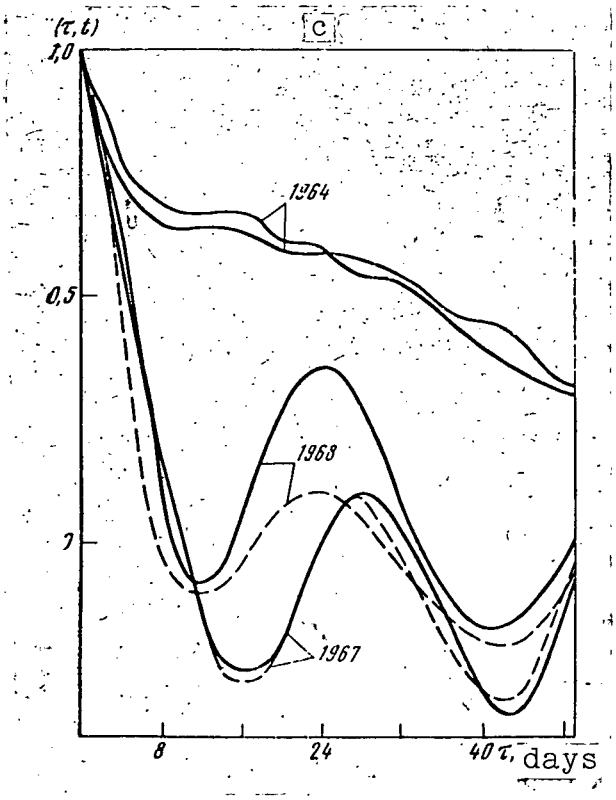

Figure 1. Normalized auto-correlation functions for the solar activity index $F_{10.7}$.

a- 1958 — 1963; b- 1964 — 1967; c- with origin shift for one month.

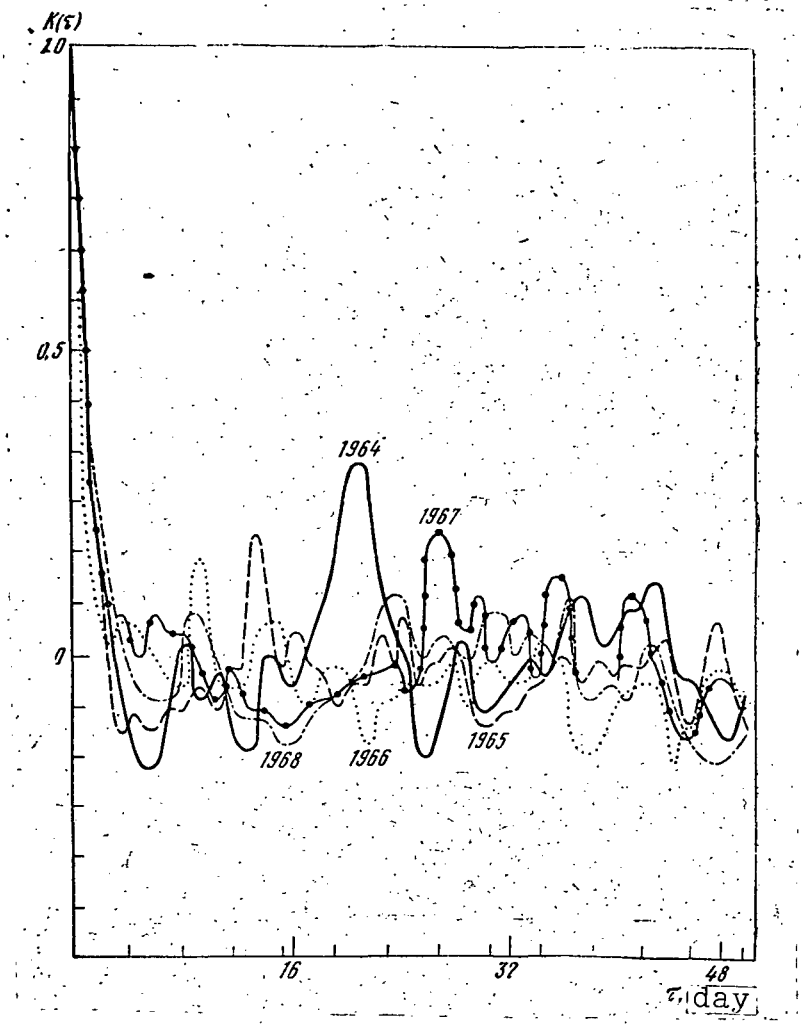

Figure 2. Normalized autocorrelation functions for the geomagnetic disturbance index A_p.

years was calculated for this. All the obtained values occupy the shaded region in Figure 5. It follows from this figure that, to ensure sufficient prediction accuracy, one can take n = 4. Analogous calculations carried out for the sequences of a_p and /97 A_p showed that, in these cases, one can be limited to the same value of n.

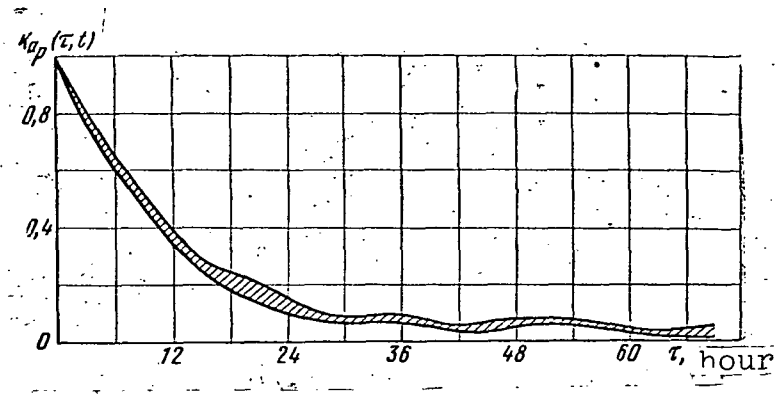

Figure 3. Region of variation of the normalized autocorrelation functions for the index a_p.

An evaluation of the accuracy of Method II for assigning the values of the indices for the prediction interval was carried out by calculating the dispersion of the increments of the indices ζ from the formula

$$D_\zeta(\delta) = M|\zeta(t_1+\delta) - \zeta(t_1)|^2. \tag{4}$$

To evaluate the accuracy of Method III, the arithmetic mean and the mean square deviation of the predicted values of the indices $F_{10.7}$ and A_p were calculated using the predicted values obtained at IZMIRAN for the time interval from 1/1/1969 to 3/31/1970.

Results of the accuracy evaluation of the first two methods /98
for periods from 1964 to 1968 for predicting the index $F_{10.7}$ for 1, 2, and 3 days and the index A_p for one day are presented in Table 1. The ratios of the mean square deviation for the sequence of ζ to its arithmetic mean value $\bar{\zeta}$ are presented for each year in columns 2 and 3 of the table. The corresponding ratios of the prediction errors are given for both methods in columns 5 through 8.

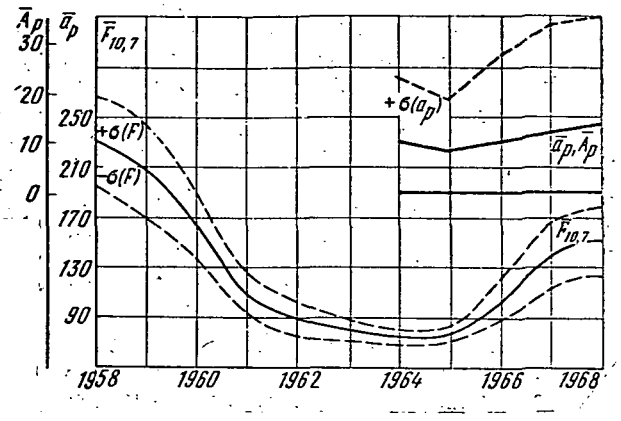

Figure 4. Yearly mean values of the indices $F_{10.7}$, a_p, A_p, and the mean square deviations of the indices $F_{10.7}$ and a_p.

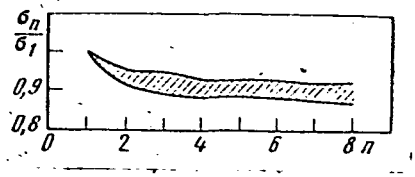

Figure 5. Ratio of the prediction errors for $1 \leq n \leq 8$ to the errors for $n = 1$.

It follows from the data of Table 1 that the prediction Method I is somewhat more accurate than Method II. The relative mean square prediction error of the index $F_{10.7}$ is less than the relative mean square deviation of the sequence of $F_{10.7}$ for the considered prediction interval, whereas these values for A_p are approximately equal when predicting for one day, which attests to the impossibility of predicting the index A_p by these methods (the predicted value of the index A_p differs little from the mathematical expectation of the sequence of A_p). /99 /100

TABLE 1*

Year	$\sigma(F)/\bar{F}$	$\sigma(A_p)/\bar{A}_p$	Method	$\sigma[\bar{\zeta}(t_1+\delta)]/\bar{\zeta}$			
				$F_{10.7}$			A_p
				δ=1	δ=2	δ=3	δ=1
1964	0,05	0,84	I	0,02	0,02	0,02	0,80
			II	0,02	0,02	0,04	0,95
1965	0,06	1,01	I	0,02	0,03	0,05	1,02
			II	0,03	0,03	0,05	1,20
1966	0,18	1,24	I	0,06	0,09	0,13	1,20
			II	0,06	0,10	0,14	1,39
1967	0,18	1,25	I	0,06	0,10	0,15	1,19
			II	0,07	0,10	0,15	1,28
1968	0,15	0,97	I	0,05	0,08	0,12	0,92
			II	0,05	0,08	0,13	0,92

* Translator's Note: Commas in numbers indicate decimals.

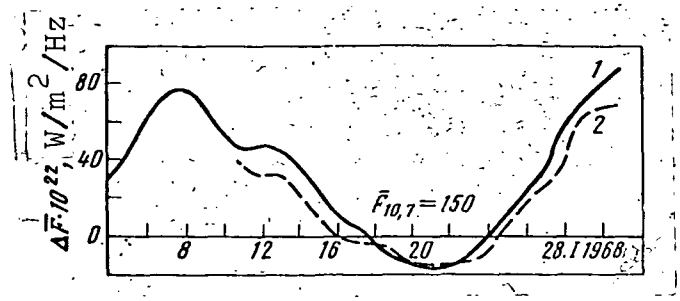

Figure 6. Example of predicting the index $F_{10.7}$ for one day.

1- actual deviation from the mean; 2- predicted deviation from the mean.

An example of predicting the index $F_{10.7}$ for one day by Method I for January, 1968, is presented in Figure 6. It is evident that the predicted values follow approximately the trend of the measured values of the index, while tending to smooth its fluctuations. The error distribution functions for predicting the index $F_{10.7}$ for one and two days, the index A_p for one day, and the index a_p for three hours by Method I are presented in Figure 7 for a number of years.

The relative mean square errors in predicting the indices $F_{10.7}$ and A_p by all three methods for the period from 1/1/1969 to 3/31/1970 are given in Table 2. It is evident from this table that all three methods give approximately the same accuracy when predicting for one and two days. When predicting for three days, Method III is somewhat more accurate. /101

To evaluate the possible accuracy in predicting the index a_p for several hours, the initial part of the average normalized autocorrelation function $K_{a_p}(\tau)$ corresponding to Figure 3 was approximated by an expression of the form

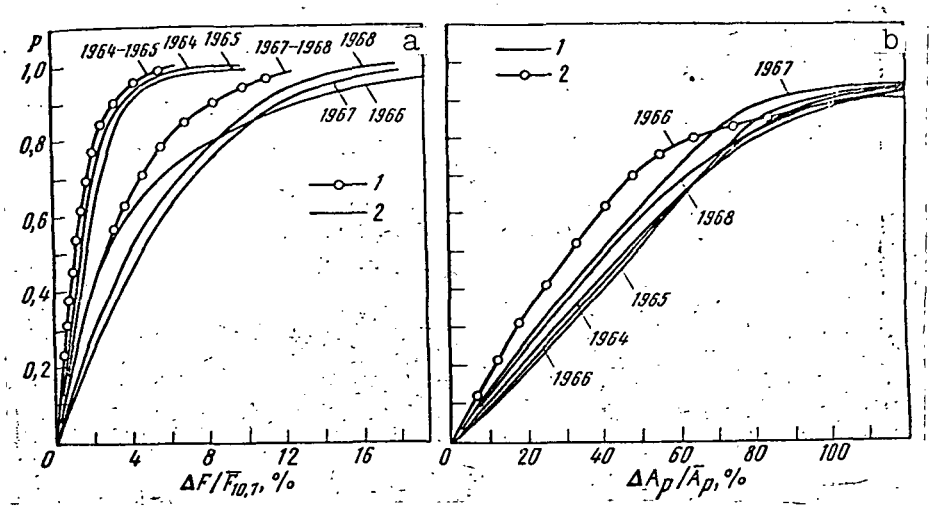

Figure 7. Error distribution functions for predicting the index $F_{10.7}$ and the indices a_p and A_p by Method I:

a- error in predicting the solar activity (1- for one day; 2- for two days); b- predicting (1- A_p; 2- a_p).

TABLE 2*

Method	$\sigma[\bar{\zeta}(t_1+\delta)]/\bar{\zeta}$					
	$F_{10.7}$			A_p		
	δ=1	δ=2	δ=3	δ=1	δ=2	δ=3
I	0,05	0,09	0,13	0,94		
II	0,05	0,10	0,14	0,95	0,96	0,99
III	0,05	0,09	0,11	0,91	0,92	0,90

* Translator's Note: Commas in numbers indicate decimals.

$$K_{a_p}(\tau) = \exp(-\alpha\tau). \tag{5}$$

The value obtained for α ($1/\alpha \approx 12^h$) was substituted into the expressions for the error estimates for predicting by Methods I and II presented in [1]

$$\sigma[\bar{a}_p(t_1+\delta)] = \sigma(a_p)[1-\exp(-2\alpha\delta)]^{1/2} \text{ for Method I,} \tag{6}$$

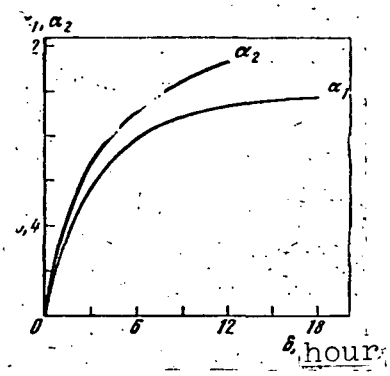

Figure 8. Values of the quantities α_1 and α_2.

$$\sigma[\bar{a}_p(t_1+\delta)] = \sigma(a_p)\{2[1 - \exp(-\alpha\delta)]\}^{1/2} \quad (7)$$

for Method II, where $\sigma(a_p)$ is the mean square deviation of the sequence of a_p.

The dependencies

$$\alpha_1 = [1 - \exp(-2\alpha\delta)]^{1/2} \quad (8)$$

and

$$\alpha_2 = \{2[1 - \exp(-\alpha\delta)]\}^{1/2}. \quad (9)$$

are presented in Figure 8. As follows from Figure 8, predicting the index a_p is valid for a period on the order of twelve hours when using Method I and for a period on the order of six hours for Method II. To calculate the absolute errors in predicting the index a_p, the values of $\sigma(a_p)$ are presented below for a number of years corresponding to low, intermediate, and high solar activity (during the current solar cycle):

Year	1964	1965	1966	1967	1968	1969
$\sigma(a_p)$	12.3	10.0	16.6	20.9	20.3	19.6

One can determine from Relation (7) the value of $\bar{\delta}$ up to which the mean square error in predicting the indices ζ by Method II does not exceed the mean square deviation of ζ. One can see from the graphs for the corresponding normalized autocorrelation functions that $\bar{\delta} \sim 5$ days for the index $F_{10.7}$, $\bar{\delta} \sim 1$ day for the index A_p and $\bar{\delta} \sim 9$ hours for the index a_p.

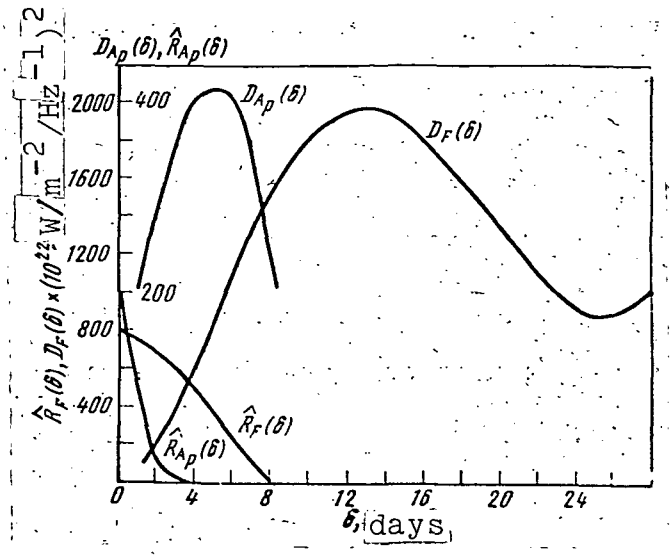

Figure 9. Autocorrelation functions $\hat{R}_F(\delta)$, $\hat{R}_{A_p}(\delta)$ and dispersions $D_F(\delta)$, $D_{A_p}(\delta)$.

Hence, it follows that, without predicted values of $\bar{\zeta}(\bar{t}_1 + \delta)$ corresponding to Methods I or III, it is more suitable for $\delta > \bar{\delta}$ to use not the last measured values of $\zeta(t_1)$ (Method II), but values of the indices ζ averaged for long intervals. The values of the quantity $\bar{\delta}$ for the indices $F_{10.7}$ and A_p are also verified by Figure 9, where graphs of the autocorrelation functions $\hat{R}_F(\delta)$, $\hat{R}_{A_p}(\delta)$ and dispersions $D_F(\delta)$, $D_{A_p}(\delta)$ calculated from Formulas (3) and (4) for 1968 (A_p) and 1969 ($F_{10.7}$) are presented.

Evaluation of the errors in predicting the indices $F_{10.7}$, a_p, and A_p makes it possible to evaluate the corresponding errors in predicting the atmospheric density. By using the density model of [3], we find that the relative error in calculating the density $(\Delta\rho/\bar{\rho})_\zeta$ ($\bar{\rho}$ is the average value of the density) caused by the relative error $\Delta\zeta/\bar{\zeta}$ in specifying the index ζ for the interval of altitudes 160 — 600 km can be described by the relations

TABLE 3

h, km	Method	$F_{10.7}$ δ=1	$F_{10.7}$ δ=2	$F_{10.7}$ δ=3	$\left(\frac{\sigma\rho}{\bar{\rho}}\right)_F$	a_p δ=3h	a_p δ=6h	a_p δ=9h	$\left(\frac{\sigma\rho}{\bar{\rho}}\right)_{a_p}$	A_p δ=1	A_p δ=2	A_p δ=3	$\left(\frac{\sigma\rho}{\bar{\rho}}\right)_{A_p}$
200	I	2	3	5	7	5	7	7	8	6	6	6	6
	II	2	4	5		6	8	9		6			
	III	2	3	4						6	6	5	
300	I	5	8	12	18	12	17	18	21	14	14	15	15
	II	5	9	13		14	19	22		14			
	III	5	8	10						14	14	13	

/103

$$\left.\begin{aligned}\left(\frac{\Delta\rho}{\bar{\rho}}\right)_F &= (-0{,}630 + 0{,}00506h)\frac{\Delta F}{\bar{F}}\\ \left(\frac{\Delta\rho}{\bar{\rho}}\right)_{a_p} &= (-0{,}132 + 0{,}00108h)\frac{\Delta a_p}{\bar{a}_p}\end{aligned}\right\} \text{ for } \bar{F}_{10.7} = 75 \text{ units}, \tag{10}$$

$$\left.\begin{aligned}\left(\frac{\Delta\rho}{\bar{\rho}}\right)_F &= (-0{,}750 + 0{,}00560h)\frac{\Delta F}{\bar{F}}\\ \left(\frac{\Delta\rho}{\bar{\rho}}\right)_{a_p} &= (-0{,}130 + 0{,}00104h)\frac{\Delta a_p}{\bar{a}_p}\end{aligned}\right\} \text{ for } \bar{F}_{10.7} = 100 \text{ units}, \tag{11}$$

$$\left.\begin{aligned}\left(\frac{\Delta\rho}{\bar{\rho}}\right)_F &= (-0{,}710 + 0{,}00562h)\frac{\Delta F}{\bar{F}}\\ \left(\frac{\Delta\rho}{\bar{\rho}}\right)_{a_p} &= (-0{,}128 + 0{,}00095h)\frac{\Delta a_p}{\bar{a}_p}\end{aligned}\right\} \text{ for } \bar{F}_{10.7} = 125 \text{ units}, \tag{12}$$

$$\left.\begin{aligned}\left(\frac{\Delta\rho}{\bar{\rho}}\right)_F &= (-0{,}765 + 0{,}00571h)\frac{\Delta F}{\bar{F}}\\ \left(\frac{\Delta\rho}{\bar{\rho}}\right)_{a_p} &= (-0{,}115 + 0{,}00089h)\frac{\Delta a_p}{\bar{a}_p}\end{aligned}\right\} \text{ for } \bar{F}_{10.7} = 150 \text{ units}, \tag{13}$$

where h is measured in kilometers.

The relative mean square errors in predicting the density (in %) at altitudes of 200 and 300 km are presented for all three prediction methods in Table 3. The mean square deviations of the density values caused by the short-period variations of the indices ζ, which corresponds to the mean square error in /104

predicting ρ taking into account only the long period (11-year) variations of the indices, are presented in the same table for comparison. The errors presented in Table 3 are calculated using Table 2 and correspond to the time interval from 1/1/1969 to 3/31/1970.

As follows from the data of Table 3, all three methods for predicting the density are practically equally accurate at the considered altitudes: the mean square prediction errors do not differ by more than 3 — 4% for the whole prediction interval of interest. It also follows from this table that, when using the considered methods for predicting the index $F_{10.7}$, it is possible to decrease the corresponding error in predicting the density for an interval up to three days; using the prediction of geomagnetic disturbance is valid for an interval up to six hours; predicting the daily mean variation of the geomagnetic disturbance does not produce a decrease of the corresponding error in predicting the density. When solving the question of the suitability of using the predicted values of the indices $F_{10.7}$ and a_p for determining and predicting AES orbits, one must also take into account the delay time present in the variations of atmospheric density, which correspond to the variations of the indices $F_{10.7}$ (the order of one day) and a_p (about six hours).

Graphs of the variations in the magnitudes of the relative mean square errors in predicting the density as a function of altitude when predicting the index $F_{10.7}$ for one, two, and three days and the index a_p for three, six, and nine hours (prediction method I) are presented in Figures 10 and 11. The mean square deviations of the density caused by short-period variations of the indices $F_{10.7}$ and a_p (using only the average long-period values of the indices for predicting the density) are also shown

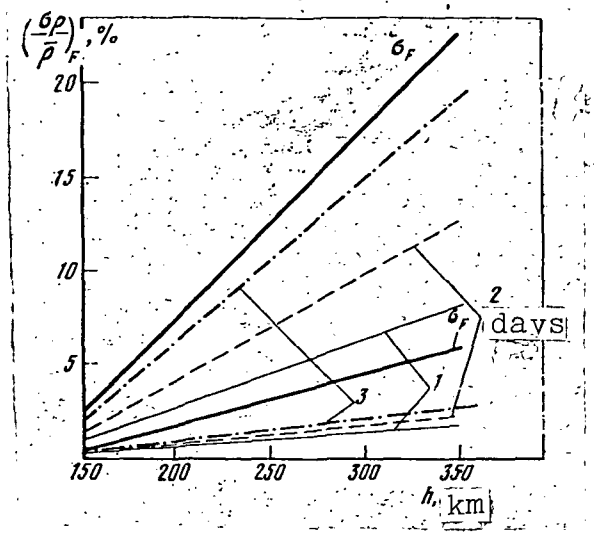

Figure 10. Relative mean square errors in the density values $(\sigma\rho/\rho)_F$ when predicting for one, two, and three days. Lines σ_F — density deviations without prediction.

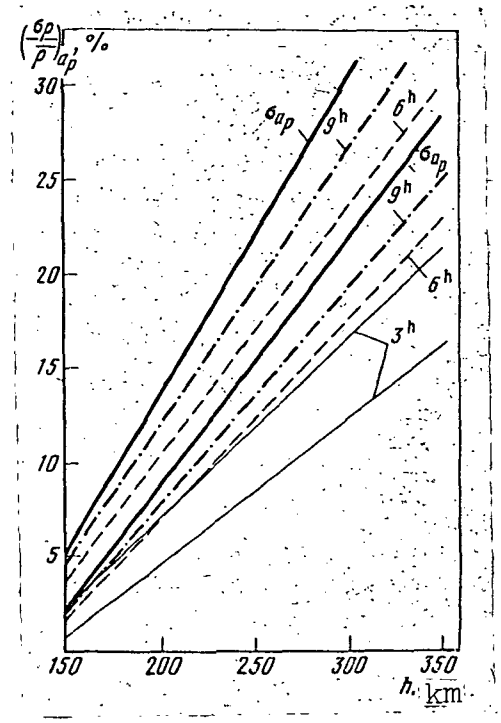

Figure 11. Relative mean square errors in the density values $(\sigma\rho/\bar{\rho})_{a_p}$ when predicting for 3^h, 6^h, and 9^h. Lines σ_{a_p} — density deviations without prediction.

on the same graphs. The lower curves of the graphs correspond to the minimum, and the upper curves — to the maximum errors for the interval from 1964 to 1969. The presented graphs permit /106 one to evaluate the magnitudes of the corresponding errors in the calculated density values for orbit perigees in the altitude interval from 150 to 350 km.

A graph of the total mean square deviations of the daily values of density (line β) constructed from the data of Table 3 and graphs of the mean square variations of density over one, two, and three days (which correspond to the errors in density ρ when predicting orbits for the first, second, and third days and under the condition of refining the average AES slowing between

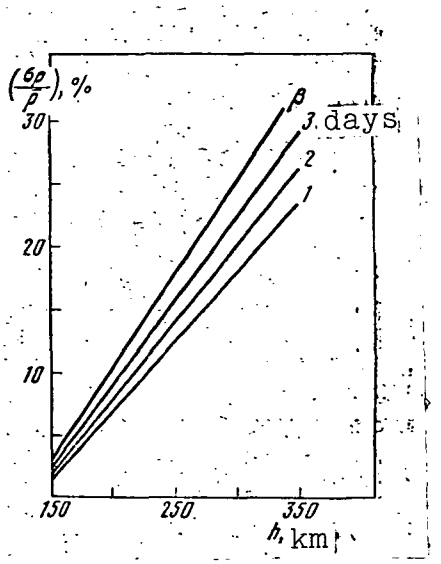

Figure 12. Relative total mean square deviations of the daily values of density (line β) and the relative mean square variations of density over one, two, and three days.

two preceding orbit determinations spaced at one day) are presented in Figure 12 for the same altitude interval. The graphs are constructed assuming the measurements of atmospheric density corresponding to the indices $F_{10.7}$ and A_p are independent.

The small values of the normalized coefficients of the mutual correlation K_{A_pF} calculated for a number of years for different shifts τ can serve as a justification of this. The maximum values of the coefficients K_{A_pF} are presented below:

Year	1965	1965	1966	1967	1968
K_{A_pF}	0.26	0.08	0.07	0.15	0.05

The magnitude of the deviations of ρ presented in Figure 12 depends slightly on the level of solar activity in view of the relatively large effect of the component $(\sigma\rho/\bar{\rho})_{A_p}$, which does not change significantly during the solar cycle.

It is seen from the data of Table 3 and Figures 10 and 11 that predicting the index a_p for three hours permits a decrease of the possible errors by 40 — 45%, for six hours — by about 21%; and for nine hours — by 11 to 12%. It also follows from these figures that the density variations proportional to the flux

$F_{10.7}$ vary over wide limits with variation of the solar activity level. Thus, at an altitude of 200 km, $(\sigma\rho/\bar{\rho})_F$ varies from 2 to 7 — 8%, and at an altitude of 300 km — from 4 — 5 to 17 — 18%. The magnitude of the density variations correlated with the geomagnetic disturbance index a_p is somewhat larger, and its variability within the 11-year cycle is relatively smaller; at an altitude of 200 km $(\sigma\rho/\bar{\rho})_{a_p}$ varies from 8 — 9 to 13 — 14%, and at an altitude of 300 km — from 21 — 22 to 30%.

The use of the predicted values of the index $F_{10.7}$ during the years of the quiet Sun leads to a decrease of the corresponding error in predicting the density by 2 — 3 times for the whole prediction interval. Such a gain occurs in the years of the active Sun when predicting for 1 — 2 days. It follows from Table 3, however, that the part of the total errors selected for this is relatively small because of the significant daily mean variations of density correlated with the index A_p.

REFERENCES

1. Yaglom, A. M. Uspekhi matematicheskikh hauk, No. 5, 1952. /107

2. Vyatkina, V. M. Radioizlucheniye Solntsa. Sb. 1 (Radio Emission of the Sun, Collection 1). Leningrad State University Press, 1969.

3. El'yasberg, P. Ye., B. V. Kugaenko, V. M. Synitsin and M. I. Voiskovsky. Space Res., Vol. XII, 1972, p. 727.

N74-28295

SEMIANNUAL VARIATIONS OF THE ATMOSPHERIC DENSITY AT ALTITUDES OF 200 — 300 km

A. M. Alferov

ABSTRACT. Some results of analyzing density variations of the atmosphere with half-year period obtained from data on "Kosmos" AES drag over the period 1960 — 1970 are discussed. Comparison of the secular variation of the intensity of the semiannual density variations and the 11-year solar cycle indicates that the amplitude and nature of the observed variations depend not only on the level of solar activity but also on the heliolatitude distribution of the activity centers.

In spite of the large amount of data obtained in recent /107
years, the variations with half-year period remain one of the least understood phenomena in the dynamics of the upper atmosphere. These variations first noted by Paetzold and Zschoerner [1] in 1960 from data on the slowing of the third Soviet satellite were subsequently confirmed repeatedly over a wide range of altitudes approximately from the mesosphere (~90 km) to the exosphere (~1500 km). The dependence of the variations with half-year period on altitude, latitude, level of solar activity, and their possible nature have been repeatedly discussed in the literature [2 — 8]. It has been shown that stable maxima occur at the beginning of April and the end of October, and minima — in January and the end of July. The July minimum is always significantly deeper than that in January, and the October maximum exceeds that in April in a majority of cases. A definite periodicity in the amplitude changes of these variations have been observed over a number of years, and it has been established that

they can be commensurable with the density variations depending on the time of day at thermosphere altitudes.

As for the nature of the half-year variations, unfortunately, it has not yet been possible to find the mechanism responsible for their appearance. According to the results of analysis of the slowing of a number of satellites for the period 1958 — 1966, the observed density variations were related to temperature variations in the thermosphere, which originate at the same levels as the variations caused by the effect of solar activity [5]. This result was reflected in the model of Jacchia [1970] in the form of a seasonal correction to the exosphere temperature T_∞. The magnitude of the correction was found in the form of a directly proportional dependence on the smoothed flux of the solar decimeter radio emission. However, data obtained over recent years have shaken the hypotheses relating the nature of the semiannual variations only to thermal origins [2]. It has been shown that the altitude dependence observed in individual years can not be explained in form nor in amplitude within the framework of the /108
proposed model representations. If the agreement is satisfactory for the altitudes of about 600 km, then the large amplitudes in the exosphere and at altitudes below 300 km can evidently be explained only with additional consideration of semiannual variations of the structural parameters close to the turbopause. In addition, it has been found that the observed secular variation of the intensity of the semiannual variations differs greatly from the secular variation of the index $\bar{F}_{10.7}$. Data on the slowing of the "Echo-2" satellite for the period 1964 — 1968 at altitudes of about 1000 km and results obtained for 1960 — 1970 from data on the slowing of "Kosmos" satellites at altitudes below 300 km [8 — 10] have led to this conclusion.

Similar results in the lower thermosphere can no longer be related to the seasonal migration of the helium bulge (as was first done in [5]). All the recent results were taken into account in the new version of Jacchia's model [4], and a correction to the density was introduced, but not to the exosphere temperature as before. The newly obtained empirical relation describes well the intensity of the semiannual variations in the whole thermosphere and lower exosphere observed in 1967 — 1970. However, the conclusion that the semiannual variations are independent of solar activity requires further verification.

The most preferred hypothesis to explain the semiannual variations is the proposal about its connection with the rearrangement of the meridianal circulation system in the lower atmosphere, because of which there should be a great outflow of heat from the lower thermosphere during the solstices, but not during the equinox [6, 8]. Since the lower atmosphere is so much more massive than its upper part, it is quite natural to expect that its strong circulation appears to some degree in its very tenuous upper part. In spite of the lack of systematic data on the global circulation of the atmosphere below 100 km, there is a whole series of circumstantial evidence in favor of this hypothesis, which is examined in [2, 6]. Thus, we will consider subsequently that the formation and stability of the observed semiannual wave in the thermosphere are supported by the basic mechanism connected with the circulation of the lower atmosphere. We will also assume that the lower atmosphere modifies significantly effects of solar origin, in particular, effects related to the interaction of the solar wind with the magnetosphere of the Earth. Although the mechanism of such a relation is not yet clear, many results, in particular, those obtained and generalized recently by E. R. Mustel' [11], permit one to reach the conclusion that the intrusion of corpuscular flux into the magnetosphere leads to intensification of the meridianal type of circulation. In other words,

we will assume that the main background of the semiannual variations in the thermosphere is due to the seasonal circulation of the lower atmosphere; processes related to the effects of the solar corpuscular radiation evidently are able to disturb this background. Thus, the intensity of the semiannual variations cannot depend on the indices of solar activity characterizing the UV-radiation (W, $\bar{F}_{10.7}$). However, this does not mean at all that this phenomenon is completely unrelated to solar activity. The fact that the cyclic changes of the intensity of these variations are caused by the effects of the solar corpuscular radiation is not excluded. It should be kept in mind that the secular variation of the indices of the solar corpuscular activity differs sharply from the cyclic curve of Wolf numbers or $\bar{F}_{10.7}$. In addition, at times close to the equinox, the radially directed corpuscular flux from active regions passes closest to the orbital plane of the Earth, which increases at these times the probability of the effect of the disturbing factor. /109

Attracting attention to this fact is the main goal of the following discussion, in which the semiannual variations observed in the thermosphere, which are derived from analyzing the evolution of AES orbits, and data on solar activity are compared for the period 1960 — 1970.

1. Experimental Results

The actual values of atmospheric density obtained from data on the slowing of Soviet AES were used to study the secular variations of the intensity of the semiannual variations. These data were published in [6, 8, 12 — 14]. Satellites, whose perigees differed from the specified altitude $\bar{Z}$ = 270 km by an amount $|Z - \bar{Z}| < 40$ km (Z is the perigee), were selected to obtain more uniform material for the present investigation.

Besides satellites of the "Kosmos" series, results of the slowing of the first Soviet satellite (1960 ε_2) and its capsule (1960 ε_3) were also used. Analysis of the primary data was carried out with a technique differing somewhat from that described previously [12 — 14]. The running values of the parameters for the osculating ellipse of the AES motion were used as the initial data. Analytic dependences were used to calculate the density, which can be represented in the most general form by the relation

$$\rho_\lambda = k(g_i)\dot{T}, \tag{1}$$

where $\dot{T}$ is the secular acceleration of the orbital period, which reflects to the greatest degree the variations of the satellite drag; $k(g_i)$ is a coefficient as a function of the osculating orbital elements and the ballistic parameters of the object, which is quasi-stationary in successive revolutions of the AES.

The density at an altitude λH_ρ^* above perigee, where H_ρ^* is the preassigned height of the uniform density atmosphere, was determined with relations of the form (1). The form of the coefficients $k(g_i)$ and λ is determined by the known relations [15, 16], whose complexity depends on the orbital eccentricity. The dependencies obtained by King-Hele and Cook [16] give the most precise results, taking into account corrections for rotation, ellipticity, diurnal bulge of the atmosphere, and also change in the scale height of the uniform atmosphere. /110

The aerodynamic drag coefficients of the satellites were calculated with the help of the method of [17] (with the use of the free molecular flow theory with diffuse reflection of molecules).

The running values of density calculated with relations of the form (1) and related to conditions in the region of the orbit perigee depend significantly on many variables:

$$\rho_\lambda = \rho_\lambda(Z, t, \varphi, Y, \overline{F}_{10.7}, F_{10.7} - \overline{F}_{10.7}, A_p),$$

where Z is the altitude; t is the local time; φ is the geographic latitude; Y is the calendar time (the day number measured from January 1); $F_{10.7}$ is the value of the solar radio emission flux (shortwave radiation index) at the wavelength 10.7 cm [in units of 10^{-22} W/(m^2/Hz)] taken a day before the measurement; $\overline{F}_{10.7}$ is the same flux smoothed with a period T = 3 months* (reflecting the 11-year variation of the solar activity level); A_p is the geomagnetic disturbance index.

The study and separation of the characteristic variations were carried out by the following method:

a) The short-period (27-day and irregular) variations related to changes of the solar shortwave and corpuscular radiation were separated out. Relations of the following form were used for this:

$$\frac{\delta\rho_1}{\rho} = [a_1 + a_2(Z-270)]\left[1 + a_3\cos\left(\frac{\pi}{12}t - 3\right)\right]\frac{F_{10.7} - \overline{F}_{10.7}}{\overline{F}_{10.7}}, \qquad (2)$$

$$\frac{\delta\rho_2}{\rho} = [b_1 + b_2(Z-270)]\left[1 + b_3\cos\left(\frac{\pi}{12}t - 3\right)\right] \times \left[(85,2\sin|\varphi| + 71,2)\log\frac{A_p}{2,3}\right]^{1,1}, \qquad (3)$$

*The value T = 3 months was determined in our case by the fact that over the period 1960 — 1970, the average time for the existence of solar activity centers (a complex of interrelated solar activity appearances in various layers of the solar atmosphere and localized within bounded regions) was 3.0 ± 1.5 solar rotations.

were ρ is the running value of the density reduced to the smoothed value $\bar{F}_{10.7}$; $\delta\rho_1$ is the change in density related to the variations of $F_{10.7}$ relative to $\bar{F}_{10.7}$; $\delta\rho_2$ is the change in density caused by geomagnetic effects. The coefficients a_1, a_2, a_3, b_1, b_2, b_3 were determined using multiple regression equations. /111

b) For each yearly interval with a shift of two months, the maximum day (ρ_{max}) and minimum night (ρ_{min}) values of the density were approximated by polynomials of the form

$$\log \rho_{max} = \sum_0^4 A_I (Z-270)^I, \tag{4}$$

$$\log \rho_{min} = \sum_0^4 B_I (Z-270)^I. \tag{5}$$

The selection of the maximum and minimum values of density was carried out for this under the assumptions

$$\text{for} \quad \rho_{max}: \quad |\varphi - \delta_\odot| < 10^0, \quad |t - 14^h| < 2^h,$$
$$\text{for} \quad \rho_{min}: \quad |\varphi + \delta_\odot| < 10^0, \quad |t - 3^h| < 3^h,$$

The coefficients A_j, B_j were determined using multiple regression equations, the coefficients with indices j = 3, 4 being taken as constant and the coefficients with indices j = 1, 2 also reflecting the effect of the variable $\bar{F}_{10.7}$.

c) Under the assumption that in the interval of altitudes $|Z - 270| < 40$ km, the semiannual variations do not depend on the latitude and local time and that the diurnal bulge has exactly the same form, the running values of density were approximated by relations of the form

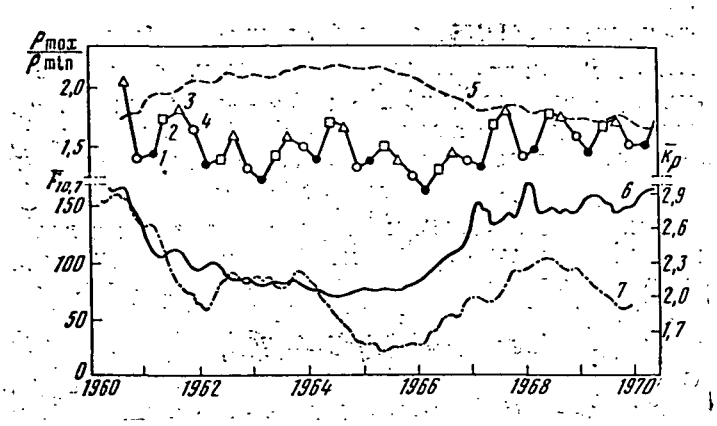

Figure 1. Values of the intensity of the diurnal and semiannual variations at an altitude $\bar{z}$ = 270 km observed during 1960 — 1970.

1- ρ(IV)/ρ(I); 2- ρ(IV)/ρ(VII); 3- ρ(X)/ρ(VII); 4- ρ(X)/ρ(I); 5- ρ_{max} (day/ρ_{min} (night); 6- $\bar{F}_{10.7}$ x 10^{-22} w/(m^2/Hz); 7- $\bar{K}_p$-index.

$$\log \rho = [C_1(Y) + C_2(Y)(Z - 270)]\,[\log \rho_{max} - \log \rho_{min}]\, q(t, \varphi). \qquad (6)$$

The coefficients $C_1(Y)$, $C_2(Y)$ were represented in the form of a Fourier series expansion. The values of the coefficients averaged over two-month intervals $\bar{C}_{1i}$, $\bar{C}_{2i}$ (i = 1, 2, ..., 6) were first determined, which were then represented in the form of a superposition of annual and semiannual terms with statistical provision by the method of least squares. The actual amplitudes of the semiannual variations were restored with consideration of the averaging period used. The expression g(t, φ) characterizing the diurnal density distribution was represented in the form of an expansion in spherical harmonics to fourth order inclusively. The coefficients of this expansion were found for each two-month interval by the Gauss method.

The results obtained for the period 1960 — 1970 are presented in Figure 1. The diurnal variations are expressed in the form of the ratio of the maximum day and minimum night density. The

intensity of the semiannual effect was evaluated by the ratio of the maximum density in October or April to the preceding or following density minimum in January or July. The smoothed values of the index $\bar{F}_{10.7}$ and geomagnetic index $\bar{K}_p$ are also presented in Figure 1 for comparison. /112

Since only the secular variation of the semiannual variations of density will be of interest to us in the following, results concerning the form of the diurnal bulge and the reaction of the thermosphere to short-period and cyclic changes of the solar activity level will not be considered in this article.

2. Solar Data

As characteristics of the solar corpuscular activity near the Earth one usually uses, as is well known, data on geomagnetic disturbances, for which various indices such as C_p, A_p, K_p, etc., are a quantitative measure. It is known that these characteristics depend very significantly on the state of the solar wind. However, there are also strong arguments for assuming that the indices derived by terrestrial magnetic observatories also depend on processes in the upper atmosphere of the Earth (principally on the atmospheric circulation at the level of the ionosopheric E layer) [18]. Thus, we have used direct solar data.

The monthly total of sunspots passing the central meridian of the Sun (CMS) was used as a characteristic of solar activity. The fact was used that all the remaining active formations in all /113 layers of the Sun, in particular sources of quasi-steady-state corpuscular flux, close to sunspots both in position on the solar surface and in time of appearance are proportional on the average in quantity and intensity to the number of the spots in the group. The direction of the corpuscular flux was also taken into account.

Keeping in mind the change in heliographic latitude of the Earth related to the direction of sometimes the northern, sometimes the southern hemisphere of the Sun toward the Earth, it is advisable to conduct the study of solar activity for each hemisphere of the Sun separately.

The following quantities were calculated for the northern (N) and southern (S) hemispheres of the Sun from data of the bulletin "Solar Data" for the period 1960 — 1970: Σf_{Ni}, Σf_{Si} are the monthly total of spots passing through the CMS; φ_N, φ_S are the monthly mean latitudes of the activity centers, which were calculated from the formulas

$$\varphi_N = \frac{\Sigma \varphi_{Ni} f_{Ni}}{\Sigma f_{Ni}}, \varphi_S = \frac{\Sigma \varphi_{Si} f_{Si}}{\Sigma f_{Si}},$$

where φ_{Ni} is the latitude of the i^{th} spot group; f_{Ni} is the number of spots in the group at CMS passage.

The quantities $\Sigma(f_{Ni} + f_{Si})$ and $\bar{\varphi}_{av} = (\varphi_N + \varphi_S)/2$ were used to characterize activity development on the whole solar disk. All /114 these indices smoothed with a period of six months are presented in Figures 2 and 3. The hemisphere average value of the centroid of the spot groups $\bar{\varphi}_{av}$ is placed in Figure 2 in accordance to each value of the index $\bar{F}_{10.7}$. The year designations denote the values occurring in the first month of each year. It should be noted that, in spite of the simplicity of the selected indices (Σf_{Ni}, Σf_{Si}), their summed value $\Sigma(f_{Ni} + f_{Si})$ reflects sufficiently well the level of solar activity on the whole disk. This is seen by comparing the indices $\Sigma(f_{Ni} + f_{Si})$ and $\bar{F}_{10.7}$ in the upper part /115 of Figure 3.

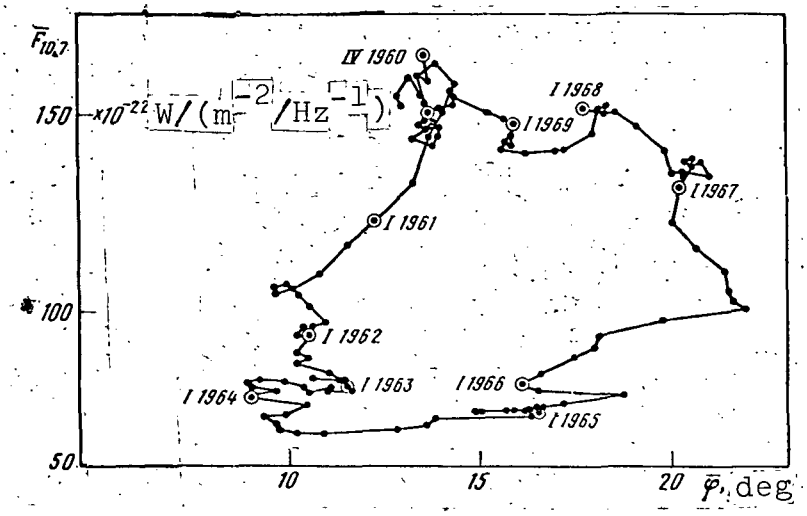

Figure 2. Comparison of the monthly mean values of the solar radio emission flux at the wavelength 10.7 cm ($\bar{F}_{10.7}$) and the average helioatitudes of spot groups for the period 1960 — 1970 ($\bar{\varphi}_{av}$).

It is known that the terrestrial effect is a more stable property of the active formations of the Sun than their ability to be accompanied by the visible elements of solar activity. In other words, the frequency or the degree of development of visible active formations is not yet a comprehensive characteristic of the terrestrial effect of a given active region of the Sun. In order to take this property into account if only on the average over the considered 11-year period, one can make use of the 27-day recurrence diagrams for the index C9, which are published annually by J. Bartels in the journal, "Solar Geophysical Data." Such a diagram for the period 1963 — 1964 is presented in Figure 4 as an example. As is seen in this figure, it contains the following. The horizontal line contains 27 places corresponding to the synodic period of solar rotation. The rotation numbers according to Chapman and Bartels, and the dates of the corresponding first days, are assigned on the left of each line. The state of the field on any day of the period under consideration

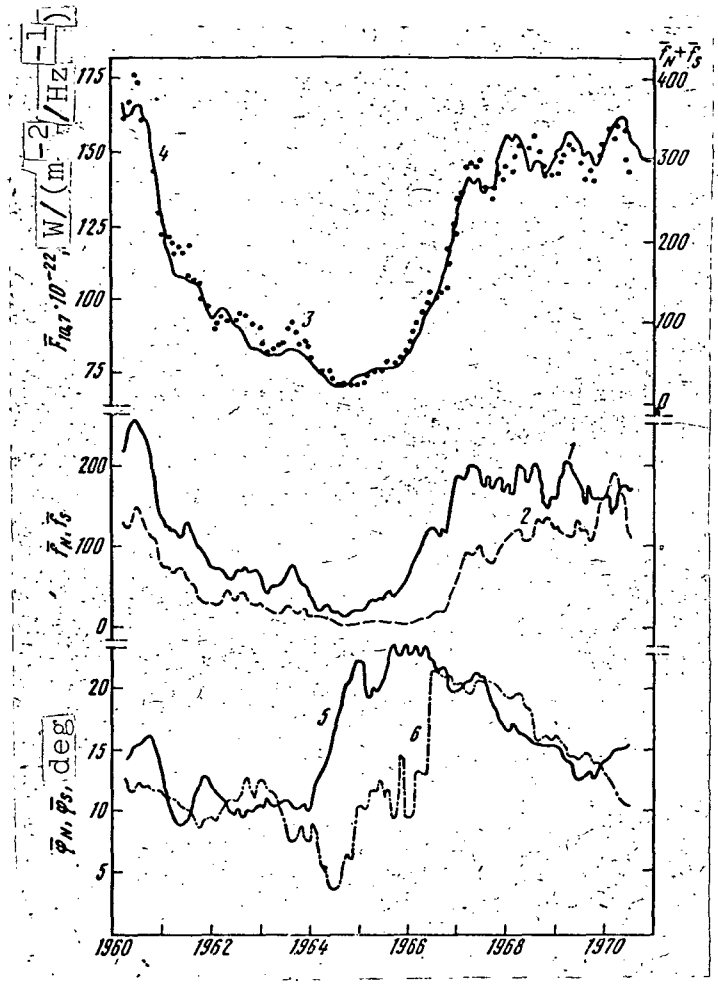

Figure 3. Cyclic curves of solar activity development in the northern (N) and southern (S) hemispheres of the Sun.

1- $\bar{f}_N = \Sigma f_{Ni}$; 2- $\bar{f}_S = \bar{\Sigma} f_{Si}$ — monthly sums of spots passing the CMS in the northern and southern hemispheres of the Sun; 3- $\bar{f}_N + \bar{f}S$; 4- $\bar{F}_{10.7}$; 5- $\bar{\varphi}_N$; 6- $\bar{\varphi}_S$ — monthly mean heliolatitudes of activity centers (all indices smoothed with a period of six months).

can be characterized by special marks. However, in our case, the presence of a mark in the corresponding position indicates that, on the given day, the magnetic disturbance was characterized by the index C9 equaling 4 and greater (which also corresponds to /116 $A_p \geq 14$). For the period 1960 — 1970, the 27-day diagram contained 1500 magnetically disturbed days characterized by the

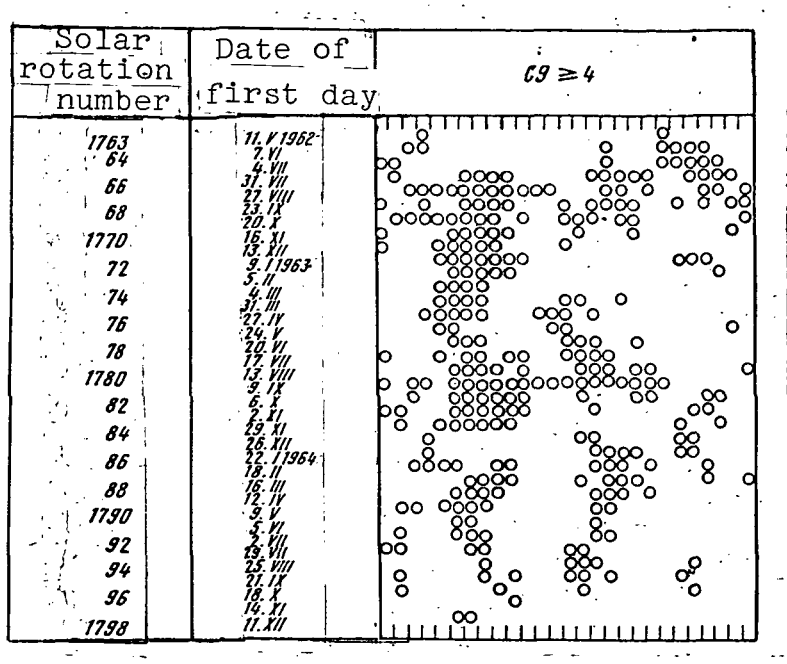

Figure 4. Example of the 27-day recurrence diagram for the index C9 ≥ 4 for the period 1963 — 1964.

index C9 ≥ 4 ($A_p \geq 14$). Of this number, 1053 days appeared in 27-day sequences beginning with triple and more. The multiplicity of the sequence designates the number of recurrences of disturbed days after two, three, etc., solar rotations beginning with the first disturbed day in the sequence. Double sequences were not taken into account, since they are the least reliable events. We will subsequently take the ratio $\alpha = 1053/1500 = 0.702$ as the mean statistical coefficient of the recurrence (in the first approximation). The quantity α can be considered as characterizing the stability of solar corpuscular flux in the physical sense and in the sense of maintaining its direction and position with respect to the solar surface.

The data of Figure 5 illustrate a semiannual variation in the magnetic disturbance indices, the semiannual wave being more clearly expressed for the recurrent disturbances, i.e., those appearing in 27-day sequences (curve 2).

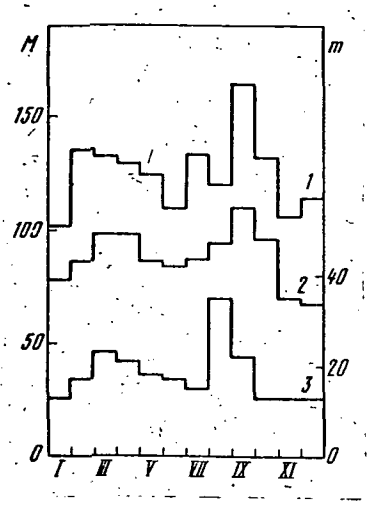

Figure 5. Seasonal dependence of the total annual distribution (over 1960 — 1970).

1- number of all disturbed days with indices C9 ≥ 4; 2- number of magnetic disturbances appearing in 27-day sequences; 3- number of times of first turbulent days in sequences beginning with triple [left scale (M) for curves 1, 2; right scale (m) for curve 3].

3. Analysis of the Results Obtained

The variations with half-year period experimentally determined from the analysis of AES orbits, as seen in Figure 1, have a significant secular dependence. This dependence differs sharply from the secular variation of the index $\bar{F}_{10.7}$ (solar activity level). Actually, in 1964, the semiannual variations at an altitude $\bar{Z}$ = 270 km exceed by 1.5 times the variations obtained for 1966 and reached the 1961 levels in 1967 — 1970. At the same time, the solar activity level in 1964 was minimum ($\bar{F}_{10.7}$ = 70 — 75) /117 and in 1967 — 1970, was in the range $\bar{F}_{10.7}$ = 125 — 160. It is evident from a comparison of the presented data with the geomagnetic K_p index that the secular variation of the semiannual variations at altitudes below 300 km depends more on the state of the solar wind than on the UV radiation. When comparing an observed phenomenon with solar data, it is very important to take into account the phase of the 11-year solar cycle. This is related in particular to the minimum of solar activity. It is in this period that such fundamental phenomena as the shift of the low-latitude belt of solar activity to high-latitude are observed, and a change in the nature of the magnetic field polarity in the sunspots of bipolar groups also occurs. The

manifestation of Spoerer's law indicating that the spots of the new cycle appear at high latitudes ($\bar{\varphi}_{av} > 20°$) and then gradually descend toward the solar equator ($\varphi_{av} \sim 10°$) is clearly seen in Figure 2. With consideration of the remarks noted previously, one can assume that the secular variation of the intensity of the semiannual effect should depend not only on the level of solar activity, but also on the average heliolatitude of the activity centers. Since the same value of the index $\bar{F}_{10.7}$ on different branches of the solar cycle correspond to different values of $\bar{\varphi}_{av}$, a certain phase of the 11-year cycle cannot be characterized by only one index.

Figure 3 clearly illustrates the importance of considering separately the solar activity of each hemisphere. It follows from the presented data that, during the whole period under consideration, the southern hemisphere of the Sun was 80% more active on the average than the northern. Within the framework of the explicit assumptions, the observed stability of the inequality of the autumn and spring maxima in the seasonal variation of the thermospheric density can be explained completely by the hemispherical asymmetry of the solar activity existing for the period under consideration. It is also seen in Figure 3 that the solar hemispheric asymmetry was characterized not only from the quantitative aspect, but also with the phase divergence, most significant in 1964 — 1966. If the high latitude band of activity (i.e., active formations of the new, $20\frac{th}{}$ cycle) already predominated at the end of 1964 in the northern hemisphere of the Sun, then this occurred in the southern hemisphere with almost a two-year lag. This (within the framework of our initial assumptions) can explain the presence of the sharp anomalies observed in 1965 and 1966 in the seasonal variation of the density in comparison to the distribution averaged over many years [10].

Comparison of the secular variation of the semiannual variations (Figure 1) and the data of Figures 2 and 3 shows that the minimum of the secular variation of these variations (end of 1965 — beginning of 1966) coincides with the maximum in the secular variation of the index $\bar{\varphi}_{av}$. This also verifies our initial assumptions. /118

The average (over the period 1960 — 1970) dates of the extrema of the semiannual variations (January 24, April 3, July 28, November 1) [6] at first glance disagree significantly from the times of the extrema of the quantity expressing the difference of the heliolatitude of the maximum solar activity zones and the heliolatitude of the Earth (or the center of the visible Sun $|B_0|$). The quantity $|B_0|$ takes its maximum value, as is well known, on March 5 and September 7. In connection with this, we have analyzed the semiannual variations from the point of view of the recurrence of the corpuscular flux. S. K. Vsekhsvyatskiy [19] first pointed out the possibility of explaining the properties of the annual variation by the effect of the 27-day recurrence. Actually, the data presented in Figure 5 (curve 3) show that the onset of stable sequences is related mainly to times when the Earth has the greatest heliographic latitude. Then, with consideration of the 27-day recurrence, the effect of the perturbing factor (the corpuscular radiation affecting the Earth) should be maximum at times somewhat shifted with respect to the extremum dates for $|B_0|$. With consideration of the mean statistical recurrence coefficient α and with a number of additional simplifying assumptions [19], the following expression can be obtained for the times for the maximum effect of the corpuscular radiation in the plane of the ecliptic

$$\operatorname{tg}\vartheta = -\frac{1+\alpha\cos\tau+\alpha^2\cos 2\tau+\ldots}{\alpha(\sin\tau+\alpha\sin 2\tau+\ldots)}, \qquad (7)$$

where $\tau = \frac{2\pi\cdot 27,2}{365,25}$.

It should be noted that the relation (7) is valid if the field of the solar radiation affecting the Earth is proportional to $\sin \bar{\varphi}_{av}$, the possible variations with solar activity phase are neglected, and the effect of the eccentricity of the Earth's orbit and the asymmetry of the northern and southern hemispheres of the Sun are not taken into account [19]. By considering, in Expression (7), terms up to $6^{\underline{th}}$ order inclusively with the use of the actual data on 27-day recurrence (Figures 4 and 5), one can calculate the times of the extreme effect of radiation on the terrestrial magnetosphere. The evaluations carried out have shown that, with changes of α within the range from 0.5 to 0.8, the consideration of recurrence can provide a phase shift (in the sense of a lag) of 20 to 50 days with respect to the dates of the extrema of the quantity $|B_0|$. Thus, the observed phase of the semiannual variations can be explained by the effect of the 27-day recurrence, if more than half of the corpuscular flux appearing in the formation of the sinusoidal wave of the annual curve are repeated after solar rotation.

Conclusion

/119

We will summarize the discussed results briefly. Data on the evolution of "Kosmos" AES orbits over the period 1960 — 1970 have made it possible to track the behavior of the basic characteristic variations at different phases of solar activity.

The intensity of the observed semiannual variations has a significant secular variation. The cyclic nature of the development of the semiannual density wave is not uniquely related to the level of solar activity. This ambiguity can be eliminated by assuming a relation of the semiannual variation intensity with the corpuscular radiation affecting the Earth. It is necessary

to use solar activity indices which relate the experimental data to a certain phase of solar activity in the 11-year cycle.

All the known properties (form, averaged over many years, and phase of the semiannual variations, and the sharp anomalies of these characteristics present in individual years) can be explained qualitatively with consideration of solar activity differentiated according to its hemispheres, 27-day recurrence, and with the use of one of the indices characterizing the heliolatitude distribution of the solar activity centers.

The author thanks M. Ya. Marov for constant interest in the work and discussion of the results.

REFERENCES

1. Paetzold, H. K. and H. Zschorner. Space Res., Vol. 1, 1960, p. 24.

2. Cook, G. E. Ann. Geophys., Vol. 25, 1969, p. 451.

3. CIRA 1965. COSPAR International Reference Atmosphere. Amsterdam, North Holland Publ. Co., 1965.

4. Jacchia, L. G. Smithsonian Astrophys. Obs. Spec. Rept., No. 332, 1971.

5. Jacchia, L. G. Smithsonian Astrophys. Obs. Spec. Rept., No. 313, 1970.

6. Marov, M. Ya. and A. M. Alpherov. Space Res., Vol. XII, 1972, p. 803.

7. Cook, G. E. Planet Space Sci., Vol. 18, 1970, p. 387.

8. Marov, M. Ya. and A. M. Alferov. Report presented at XIII COSPAR Session, 1970.

9. Voiskovskiy, M. I., B. V. Kugaenko, V. M. Synitsin and P. Ye. El'yasberg. Space Res., Vol. XI, 1971, p. 953.

10. El'yasberg, P. Ye., B. V. Kugaenko, V. M. Synitsin and M. I. Voiskovskiy. Paper presented at XIV COSPAR Meeting, Seattle, 1971.

11. Mustel', E. R. Nauchnyye informatsii astrosoveta AN SSSR, No. 10, 1968, p. 98.

12. Marov, M. Ya. Space Res., Vol. VIII, 1968, p. 811.

13. Marov, M. Ya. and A. M. Alpherov. Space Res., Vol. IX, 1969, p. 487.

14. Marov, M. Ya. and A. M. Alpherov. Space Res., Vol. 10, 1970, p. 419.

15. King-Hele, D. Teoriya orbit iskusstvennykh sputnikov v atmosfere (Theory of Artificial Satellite Orbits in the Atmosphere). Moscow, "Mir" Press, 1966.

16. Cook, G. E. and D. G. King-Hele. Philos. Trans. Roy. Soc., Vol. 259A, 1965, p. 33.

17. Kameko, V. F., M. Ya. Marov and E. P. Yaskevich. Kosmicheskiye issledovaniya, Vol. 7, No. 4, 1966, p. 607.

18. Krasovskiy, V. I. Geomagnetizm i aeronomiya, Vol. IX, No. 1, 1969, p. 29.

19. Vsekhsvyatskiy, S. K. Publikatsiya kiyevskoy astronomicheskoy observatorii, No. 1, 1946, p. 86.

N74-28296

AERODYNAMICS OF SATELLITES AND THE DETERMINATION OF THE SURFACE-FLUX INTERACTION PARAMETERS FROM AES "KOSMOS-166" AND "KOSMOS-230" DRAG IN THE UPPER ATMOSPHERE OF THE EARTH

G. I. Zmiyevskaya

ABSTRACT. The possibility of refining atmospheric density variations determined from satellite drag of complex configurations is examined. The actual surface orientation of the satellites "Proton-2," "Proton-4," "Kosmos-166" and "Kosmos-230" with respect to the velocity vector of the oncoming flux with their motion in the Earth's atmosphere is taken into account. The results of a numerical simulation of the surface-flux interaction are used for calculating the aerodynamic drag coefficients C_D of these satellites. The simulated momentum accommodation coefficients depend on the incident angle, velocity and composition of the oncoming flux and on the properties of the satellite coating material. Evaluations of the accuracy in calculating C_D are presented. The proposed technique for refining the aerodynamic drag of satellites from the known actual orientations can increase the accuracy of determining the atmospheric density from drag. The surface-flux interaction parameters can be found by the method of least squares from data on the orbital drag attenuation of the satellites "Kosmos-166" and "Kosmos-230" assuming the reliability of the atmospheric model.

The determination of the atmospheric density variations from /120 orbital drag has been carried out in many works under the assumption of constant aerodynamic drag coefficient C_D of the satellite. It is well known that, for satellites of complex configuration, C_D

depends on the orientation of the surface elements of the satellite with respect to the velocity vector of the oncoming flux of gas molecules, on the interaction mechanism of the gas molecules with the satellite surface with consideration of the covering material properties, on the configuration of the satellite surface, and the relative arrangement of the structural elements.

Two cases of satellite motion will be considered.

1) Free rotation of the "Proton" AES about its center of mass, the total triaxial orientation of the angular momentum vector L being determined from the reading of an orientation indication system.

2) Motion of the "Interkosmos" type AES with one of the satellite axes stabilized in space, whose orientation gradually changes, depending on the angular position of the Sun in absolute space; such a known orientation of AES can be called incomplete uniaxial orientation.

Aerodynamic simulation of the coefficient C_D for AES takes into account the dependence of this coefficient on the angle of attack between the normal to the surface element of the satellite and the direction of the velocity vector of the oncoming flux [1] and some model of the interaction of the oncoming flux with the surface based on numerical experiments on the flow of neutral molecules around a smooth surface with velocities of the satellite flight [2].

Following are the initial data for calculating C_D.

1. The osculating elements of the satellite orbits ("Proton-2," "Proton-4," "Kosmos-166," "Kosmos-230"), which determine the

position of the flux velocity vector with respect to the satellite.

2. Information on the position of the normals to the structural surface elements (determined from data on the satellite orientation and on the arrangement of the surface elements of the satellite).

3. Data on the coating materials, on the crystal structure, on the velocities and composition of the molecules in the oncoming flux, which are necessary for the direct integration of the equations of motion for the gas molecules and the atoms of the solid, as a result of which the exchange coefficients of the momentum components are determined. /121

The use of these data permits one to determine the aerodynamic characteristics in the free molecular approximation for satellites moving in the atmosphere of the Earth. Comparison of the results for various types of satellite motions and accumulation of actual data will subsequently lead to recommendations on the use of variable and constant values of the aerodynamic drag coefficient of a satellite in calculations of the atmospheric density variations from drag depending on the type of motion of the object under consideration.

The values of C_D from the determination of [3] equal

$$C_D = \sum_j C_D^j = \frac{2}{\rho v^2 S_M} \int_{S_j} (\bar{F}_j \cdot \bar{e}_v) dS_j, \qquad (1)$$

where j is the number of the satellite structural element; F_j is the element of force acting on the surface resulting from the effect of the incident and reflected flux; ρv^2 is the velocity head; S_M is the median cross section; S_j is the area of the $j^{\underline{th}}$ element over which the magnitude of the projection of the force

in the direction of the oncoming flux velocity is integrated. It can be written in a form suitable for analysis of its behavior, depending on the orientation and interaction parameters. As a result of this, a method is proposed for determining C_D (surface-flux interaction parameters) from the attenuation of orbital drag $\dot{T}$ under the assumption of a known atmospheric density model and of measured orientation angles.

1. Satellite Orientation

Total triaxial orientation of the "Proton" satellites. The theory of satellite motion relative to its center of mass was developed by Beletskiy [4]. Results of statistical analyses of the readings of orientation indication systems established on satellites are presented in [1, 5]. We will briefly enumerate the basic premises for solving the problem of determining the actual satellite orientation. The model of the motion: the satellite moves in an elliptic orbit unperturbed everywhere except for the portion in the vicinity of the perigee, where the satellite is under the effect of significant aerodynamic torques arising as the result of the rotational propeller effect of the planes of the solar batteries.

Data on the satellite motion beyond the perigee portion were used to analyze magnetometric data. For this, the motion was assumed to be unperturbed and described by the Euler-Poisson equations. The magnitude and position of the angular momentum vector L were determined.

The evolution of the "Proton" satellite motion includes long /122
period transitions from the axial rotation mode to a somersault mode with a period of about three days [1], i.e., $T_0 \sim 40 - 60$ revolutions of the satellite around the Earth. The rapid rotation

of the satellite with respect to the angular momentum vector is superimposed on this motion: the precession period T_ψ - 2' and the natural rotation period T_φ - 15'.

The complex precession-nutation motion of the satellite is a quasiregular precession, i.e., the main orientation parameters are constant on each revolution of the satellite around the Earth, and their change occurs at a constant rate at the time of perigee passage under the effect of the aerodynamic torques.

To determine C_D, it is necessary to know values of this quantity averaged over one orbit. Since the regular precession model is valid, knowing the C_D^0 element

$$C_D^0 = \frac{2}{\rho v^2 S_M} \int_S (F \cdot e_v)\, dS, \tag{2}$$

one can, in accordance with [4], average C_D over the fast periods of AES rotation:

$$\bar{C}_D = \frac{\int_{2\pi}\int_{2\pi} C_D^0 d\varphi d\psi}{(2\pi)^2}, \quad T_\varphi, T_\psi \ll T_{\text{orbit}}, \quad T_{\text{orbit}} \approx 90'. \tag{3}$$

Uniaxial orientation of "Interkosmos" type satellites. If, for the motion of satellites provided with an orientation indication system, we obtain as a result some values of C_D averaged over the rapid rotations per turn, then for stabilized satellites having the solar battery panels oriented toward the Sun, the change in the attack angle and C_D occurs slowly and is determined by finding the projections of the velocity vector (v_x, v_y, v_z) of the orbital motion on the direction vector toward the Sun (S_x, S_y,

S_z). Calculation of the attack angle α = arc cos (v, s) is carried out with consideration of the peculiarities of the uniaxial orientation of the satellite.

2. Surface-Flux Interaction Model

The free molecular model of the flow of rarified gas around the surface is used to calculate the aerodynamic drag of a satellite, the flux consisting of monoatomic neutral molecules for which the Maxwellian molecular velocity distribution function is valid. The orbital velocity of the satellite is much greater than the thermal velocity.

Calculation of the characteristics of the reflected flux in the oncoming flux is a complex problem, since the distribution function of the reflected particles should take into account the interaction law of the gas molecules with the crystal lattice of the coating. Experimental data for the energy range from 1 to 10 eV corresponding to space flight velocities are isolated and contain peculiarities not permitting them to be used as a reliable model. The traditional scheme of diffuse reflection contains constant accommodation coefficients of the normal and tangential momentum components: /123

$$\sigma_n = \frac{p_i - p_r}{p_i - p_w}, \quad \sigma_\tau = \frac{\tau_i - \tau_r}{\tau_i - \tau_w}, \tag{4}$$

where p_i, τ_i characterizes the incident flux, p_r, τ_r, p_w, τ_w — the reflected flux. For diffuse reflection $\tau_w = 0$ by definition, and $p_w = p_r$ for reflection with a temperature T_w equal the temperature of the satellite surface. Then, $\sigma_n = \sigma_\tau = 1.0$. Such a model does not take into account the actual scattering

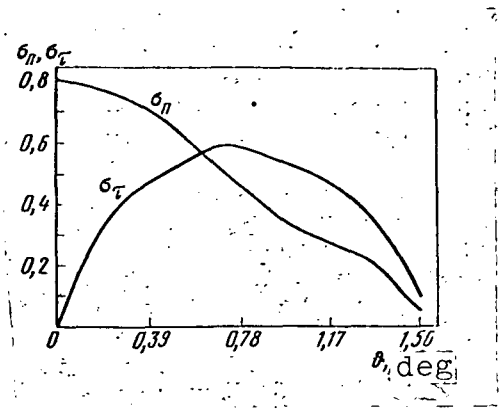

Figure 1. Accommodation coefficients for the normal (σ_n) and tangential (σ_τ) components of momentum obtained in [6] for calculating the interaction of a nitrogen flux with the ceramic coating of a satellite.

properties of the reflected flux and the dependence of p_r and τ_r on the reflection direction. Formal introduction of σ_n and σ_τ differing from 1 is sometimes used by authors, but without explanation by the model.

Numerical experiments [6] carried out on the scattering of molecules at a three-dimensional crystal lattice with consideration of coating material and gas composition of the oncoming flux do not take into account the surface microroughness and the possible presence of adsorbed atoms on the surface. But A. A. Pyarnpuu obtained curves for the dependence of the momentum accommodation coefficients on the angle of attack of the oncoming flux to the surface assumed smooth (Figure 1).

Investigations (2) have shown that these characteristics depend on the ratio of the atomic (molecular) mass of the gas and surface μ, the impact velocity v, the lattice constant, and the interaction potential both between the gas and surface atoms as well as inside the lattice. For numerical simulations of the interaction process, the system of equations for the motion of the gas atoms and some limited block of atoms of the solid with /124 given interaction parameters μ, v, α and the angle of incidence of the molecules is solved. In the reference block of the interacting lattice, $5 \times 5 \times 3 + 1$ atoms participate. The interaction forces depend linearly on the shift from the equilibrium position. Each atom interacts only with its nearest neighbors. The Lenard-Jones potential is taken for the surface-gas interaction according

to (6) — (12) of [2], whose parameters correspond to the properties of the actual atoms. The momentum accommodation coefficients are calculated as quantities averaged over a unit area.

3. Aerodynamic Approximation of the Coefficient C_D

The forces acting on the element of satellite surface were calculated taking into account the actual orientation of the surface elements and for the surface-flux interaction model based on the numerical simulation:

$$\boldsymbol{F}_j = p\boldsymbol{n}_j + \tau\boldsymbol{\tau}_j = (p_i + p_r)\boldsymbol{n}_j + (\tau_i - \tau_r)\boldsymbol{\tau}_j, \tag{5}$$

where p_i, τ_i are the normal and tangential momentum components of the incident flux; p_r, τ_r are the corresponding quantities for the reflected flux; $\mathbf{n}_j = n_x\mathbf{e}_1 + n_y\mathbf{e}_2 + n_z\mathbf{e}_3$ is the value of the local normal to the surface element given by the satellite structure.

For the "Proton" satellite, the normals to the four solar battery panels can be written (j = 1 — 4):

$$\begin{aligned} \boldsymbol{n}_1 &= (-\boldsymbol{j} + \boldsymbol{k})n_0, \quad \boldsymbol{n}_2 = (\boldsymbol{j} + \boldsymbol{k})n_0, \\ \boldsymbol{n}_3 &= (\boldsymbol{i} + \boldsymbol{k})n_0, \quad \boldsymbol{n}_4 = (-\boldsymbol{i} + \boldsymbol{k})n_0, \end{aligned} \tag{6}$$

where $n_0 = 0.707$.

For the satellites "Kosmos-166" and "Kosmos-230" having uniaxial orientation, the directions of the normals to the solar battery plates coincide with the direction vector toward the Sun.

In calculating C_D, it is necessary to determine the projection of $\mathbf{F}_j$ in the direction of the velocity of the satellite orbital motion $\mathbf{v}$, i.e., $(\mathbf{F}_j \cdot \mathbf{e}_v)$. The velocity vector components and the vector components of the local surface normals are given in different coordinate systems. For example, for the calculation of C_D for the "Proton-2" and "Proton-4" AES, v_x, v_y, v_z were known in an absolute system and the normal vector $\mathbf{n}$ — in the satellite coordinate system. Calculating the attack angle required transforming v_x, v_y, v_z into the coordinate system in which the components n_x', n_y', n_z' are determined. By using the transformation matrix from one coordinate system to the other (from the absolute x, y, z to x', y', z' fixed to the satellite), we determine in accordance with [3]:

$$v_x' = v_x\alpha_1 + v_y\beta_1 + v_z\gamma_1, \quad v_y' = v_x\alpha_2 + v_y\beta_2 + v_z\gamma_2, \quad v_z' = v_x\alpha_3 + v_4\beta_3 + v_z\gamma_3. \tag{7}$$

/125

The unit velocity vector has the direction cosines

$$\frac{v_x'}{v}, \quad \frac{v_y'}{v}, \quad \frac{v_z'}{v}, \quad e_v = i\frac{v_x'}{v} + j\frac{v_y'}{v} + k\frac{v_z'}{v}. \tag{8}$$

The scalar product $(\mathbf{e}_v\mathbf{n})$ permits the use of the orientation measurements and data on the orbit for simulating C_D:

$$(e_v n) = \frac{n_x v_x' + n_y v_y' + n_z v_z'}{|v| \cdot |n_k|}, \tag{9}$$

where k = 1 — 4 is the plate number. The normal $\mathbf{n}_k$ can be represented in the form $\mathbf{n} = \mathbf{n}_0$ sign $(n_0 e_v)$, where $\mathbf{n}_0$ is the normal to one fixed side of the plate. Then:

$$(e_v n) = (e_v n_0)\,\mathrm{sign}\,(n_0 e_v) = |e_v n_0|. \tag{10}$$

By substituting $|\mathbf{e}_v\mathbf{n}| \to (\mathbf{e}_v\mathbf{n})^2$, we obtain formulas for C_D convenient for integration over the fast periods (for analysis of data from the satellites "Proton-2" and "Proton-4").

When the thermal spread in the oncoming flux is neglected:

$$p_i = \rho v^2 (e_v n)^2, \quad \tau_i = \rho v^2 (e_v n)(e_v \tau). \tag{11}$$

Then, for the $k^{\underline{th}}$ element of the satellite structure approximated as a plate, C_D^k can be written in the form

$$C_D^k = \frac{2}{\rho v^2 S_M} \int_{S_k} (F_k e_v)\, dS_k = \frac{2}{\rho v^2 S_M} \{a (e_v n_k)^4 + b (e_v n_k)^2\}\, S'_{pl}, \tag{12}$$

where $a = \sigma_\tau - \sigma_n$, $b = 2 - \sigma_\tau$, and σ_n, σ_τ are calculated taking into account the ceramic composition of the solar battery panel coating and the interaction of nitrogen atoms with this material for an oncoming flux velocity of 8 km/sec. For the cylindrical casing of the satellite, C_D is calculated according to the approximation

$$C_D = \pi^{-1} \left(\int_0^{\pi/2} C_D(\delta)\, d\varphi \right)^2 (\rho v^2 S_M)^{-1},$$

then

$$C'_{Dcyl} = \frac{2}{\rho v^2 S_M} [0{,}375 (\sigma_\tau - \sigma_n)(e_v \tau)^4 + 0{,}5 (2 - \sigma_\tau)(e_v \tau)^2]\, S'_{cyl}. \tag{13}$$

The results of the calculations of C_D are presented in Figures 2a and b. For satellites having free rotation relative to their centers of mass ("Proton-2" and "Proton-4"), an averaging of C_D over the fast periods (precession and natural rotation) was carried out; use of the variable momentum accommodation coefficients was reduced in the calculations to smoothing the C_D /126

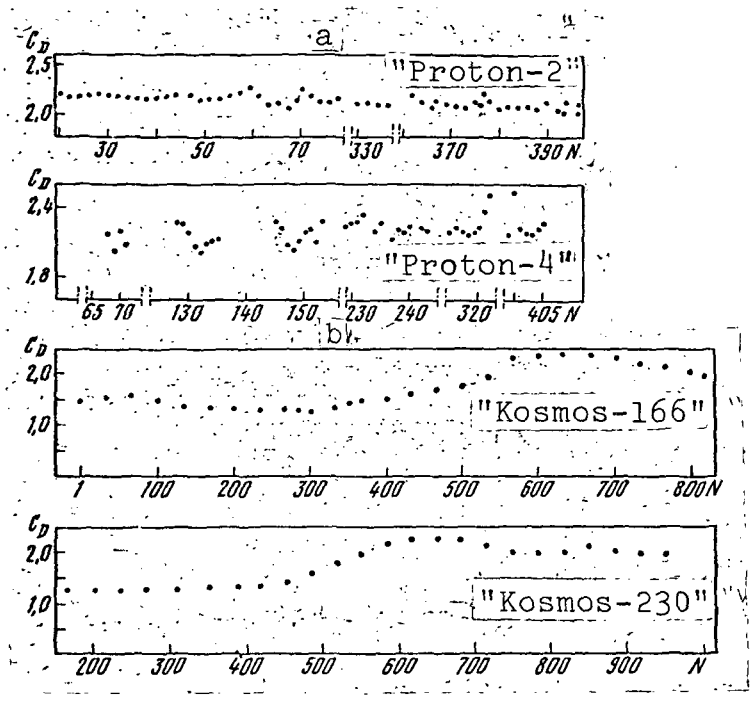

Figure 2. Variation of the aerodynamic drag coefficient C_D of satellites over a time interval measured by the number of revolutions N about the Earth.

a- for "Proton-2" and "Proton-4"; b- for "Kosmos-166" and "Kosmos-230."

variation curve in periods with uniform motion. Small deviations from a constant value are observed, when the long period shift from the axial twist mode to the somersault mode occurs, but on the whole C_D for satellites of such types can be considered constant for determining the atmospheric density. The values of C_D of the satellites "Kosmos-166" and "Kosmos-230" for several months of flight are presented in the same figure. Change of the position of the Sun and the orbital elements leads to a significant change in the satellite position with respect to the incident flux. The value of C_D undergoes significant changes over this interval of time. Thus, consideration of the orientation of such a satellite is necessary when determining the variations of atmospheric density from its drag.

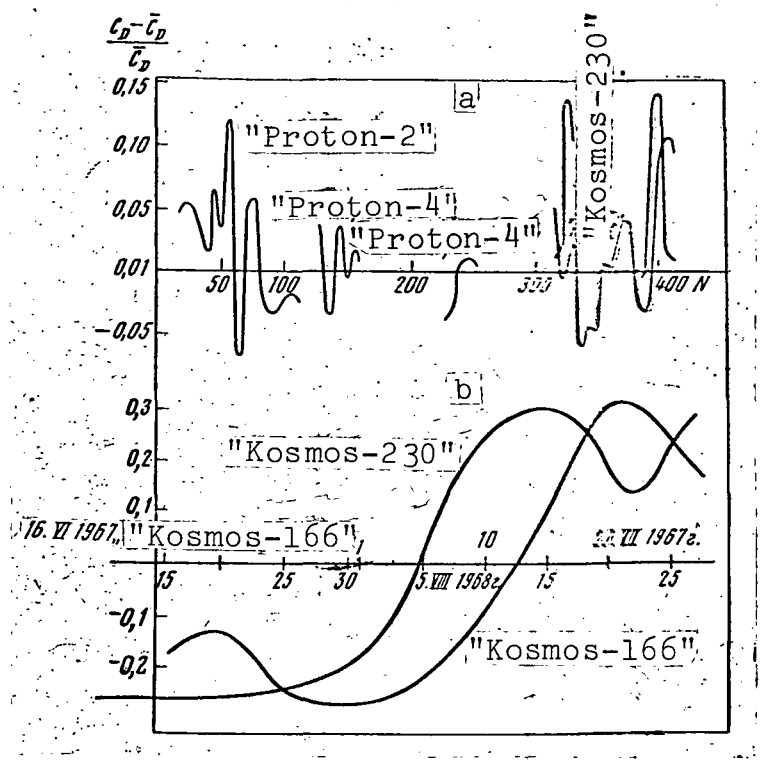

Figure 3. Probabilities of the deviation of C_D calculated by the proposed technique from the average value of C_D for the satellites.

a- "Proton-2" ($\bar{C}_D$ = 2.108), "Proton-4" ($\bar{C}_D$ = 2.167); b- "Kosmos-166" ($\bar{C}_D$ = 1.77), "Kosmos-230" ($\bar{C}_D$ = 1.75).

The magnitudes of the errors contributed when calculating C_D for the satellites of the "Proton" and "Kosmos" series without taking into account their actual orientation, are shown in Figure 3. An analysis of the errors in C_D due to errors in the orientation parameters and errors in the numerical simulation of the interaction parameters was carried out in [7]. A comparison of /127 the aerodynamic approximation method for simulating C_D with the numerical simulation method using the scattering curves for the reflected particles from the satellite surface was carried out in [8]. Thus, the possibilities of determining the aerodynamics of

satellites with complex configurations have been investigated, which increase the reliability of determining the variations of atmospheric density from drag.

4. Determination of the Surface-Flux Interaction Parameters from AES "Kosmos-166" and "Kosmos-230" Drag

Data on the orbital motion of the satellite are used as the initial data for determining the unknown parameters. For its motion in a rectangular geocentric coordinate system, the state of the satellite at each instant of time is characterized by the /128
radius vector $\mathbf{R}(x, y, z)$ and velocity vector $\mathbf{v}(v_x, v_y, v_z)$ measured by tracking the satellite. From the set of observations, one can find $Q_1, Q_2, \ldots, Q_m$ of the independent trajectory parameters for a specified atmospheric density model and constant C_D. We specify M parameters defining the satellite orbit and extrapolate data about the atmospheric density according to a model (using data on satellite drag for the simplest configuration, for which neither the reflected flux model nor the orientation relative to the center of mass is significant), then $C_D = f(t_j, \delta_j, a_m)$, the aerodynamic drag coefficient (δ_j is the angle of attack to the surface element measured at time t_j, a_m are the unknown 1, 2, ..., m parameters) will be the unknown quantity. The method for determining the constant momentum accommodation coefficients (two-parameter model) was proposed by the author [9] and is developed here for a large number of unknown parameters describing the surface-flux interaction model. Let there be, at time t_j, some measured function Φ_j of the trajectory parameters. It is assumed that the measurement errors are principally random in nature and satisfy a multivariate normal distribution law with zero mathematical expectation and known dispersion. An excess of

measurements (in comparison with the number of parameters to be determined) and the random nature of their errors permit the use of the method of maximum probability for processing the available information. The minimum of the sum is needed

$$Q = \sum_{j}^{n} \frac{[\Phi_j - f(\rho_\pi, t_j, \delta_j, a_m)]^2}{\sigma_j^2}, \qquad (14)$$

where (j = 1, 2, ..., n) is the number of experimental points; m is the number of varied parameters; $w_j = \sigma_j^{-1}$ is the weight. The set of parameters $a_1, a_2, \ldots, a_m$ is found, for which the function $f(\delta_j, a_1, \ldots, a_m)$ corresponds best to the experimental values Φ_j (the errors in the measurements of coordinate δ_j equal σ_j). It is known that $\dot{T}_j$, the attenuation of the orbital period of satellite revolution measured at some time t_j, can be expressed as

$$\dot{T}_j = \rho(h_\pi + \lambda H^*) K(\omega_j) C_{Dj}(\delta_j, a_m), \qquad (15)$$

where $K(\omega_j)$ are the values of the function of the osculating orbital elements and some constant ballistic parameters of the satellite (weight, area), which are quasi-constant on neighboring portions of the trajectory; $\rho(h_\pi + \lambda H^*)$ are the values of atmospheric density in some neighborhood λH^* of the orbit perigee h_π; $C_{Dj}(\delta_j, a_m)$ is the aerodynamic drag coefficient of the satellite depending on the orientation (δ_j) of the surface elements with respect to the velocity vector of the oncoming flux and the unknown parameters a_m characterizing the interaction of the flux /129 with the coating material.

The results of the orbital measurements for the satellites "Kosmos-166" and "Kosmos-230" [10]

$$\Phi_j = \dot{T}_j K^{-1}(\omega_j) \tag{16}$$

are taken as the function Φ_j, and the function $f(t_j, \delta_j, a_1, \ldots, a_m)$ can be represented in the form

$$\rho_\pi (h_\pi + \lambda H^*) C_D(\delta_j, a_m), \tag{17}$$

where t_j is the perigee transit time of the satellite; δ_j is the angle between the velocity vector **v** and **n**, the normal to the surface element at time t_j.

The orientation of the "Kosmos" satellites is uniaxial — toward the Sun. The coefficient C_D is determined according to the formulas presented in Paragraph 3. This relation is an approximation formula. We assume that the momentum accommodation coefficients appearing in the expression for C_D depend on the attack angle δ_j such that

$$\sigma_n = a_1 \cos a_2 \delta_j, \ \sigma_\tau = a_3 \sin a_4 \delta_j. \tag{18}$$

With minimization of the sum (14), we obtain a system of nonlinear equations with respect to the parameters a_m, $\partial Q/\partial a_m = 0$ ($m = 1 — 4$), which is solved by the method of steepest descent. The values of the momentum accommodation coefficients obtained from the drag of the satellites "Kosmos-166" and "Kosmos-230" with the atmospheric model CIRA-71 are presented in Figure 4. Comparison of these values with the data on σ_n, σ_τ obtained by A. A. Pyarnpuu as a result of numerical simulation of the smooth surface flux interaction shows a difference, which can be explained by the roughness and adsorbed atoms present on the actual surface.

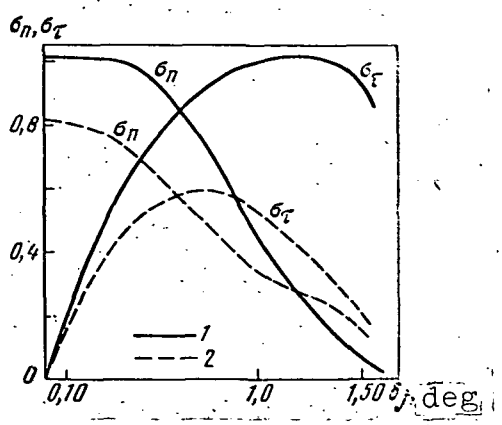

Figure 4. Comparison of the momentum accommodation coefficients σ_n and σ_τ obtained by numerical simulation [2] with the quantities σ_n, σ_τ found by the method of least squares from drag of the satellites "Kosmos-166" and "Kosmos-230." Values of the parameters a_1 — a_4 obtained for minimum Q are presented on the figure.

a_1- 1.084 ± 0.04; a_2- 1.951 ± 0.03; a_3- 1.73 ± 0.04; a_4- 0.735 ± 0.105.

1- from drag; 2- numerical simulation.

Conclusion

/130

Consideration of the problem of simulating the aerodynamic drag coefficient C_D of a satellite taking into account its actual orientation for the case of a freely rotating satellite and the case of satellite motion stabilization with respect to its center of mass indicates a difference of these characteristics for the different types of motion. Deviations from the average value of C_D can distort the analysis of density variations when calculating the atmospheric density from drag. Refining the plan of the interaction (taking into account adsorption, microroughness) of the molecular flux with the satellite surface permits a more reliable evaluation of the absolute value of the aerodynamic drag coefficient and, consequently, the determination of the atmospheric parameters.

The author considers it a pleasant obligation to thank M. Ya. Marov for the suggested topic of investigation and interest in the work, V. V. Beletskiy and M. V. Maslennikov for valuable comments and discussions, A. A. Pyarnpuu for useful creative collaboration, A. M. Alferov and V. F. Kameko for consultation, V. M. Sinitsyn and I. G. Khatskevich for the use of data on the orientation and motion of the satellites "Proton-2," "Proton-4," "Kosmos-166" and "Kosmos-230."

REFERENCES

1. Beletskiy, V. V., V. V. Golubkov, Ye. A. Stepanova, and I. G. Khatskevich. Kosmicheskiye issledovaniya, Vol. 7, No. 4, 1969, p. 522.

2. Pyarnpuu, A. A. PMTF, No. 2, 1970, p. 162.

3. Beletskiy, V. V., G. I. Zmiyevskaya and M. Ya. Marov. Kosmicheskiye issledovaniya, Vol. 8, 1970, p. 6.

4. Beletskiy, V. V. Dvizheniye iskusstvennovo sputnika otnositel'no tsentra mass (Motion of an Artificial Satellite Relative to Its Center of Mass). Moscow, "Nauka" Press, 1965.

5. Khatskevich, I. G. Opredeleniye oriyentatsii iskusstvennykh sputnikov Zemli po magnitometricheskim izmereniyam (Orientation Determination of Artifical Earth Satellites from Magnetometric Measurements). Preprint IPM AN SSSR, No. 46, 1970.

6. Marov, M. Ya., G. I. Zmiyevskaya and A. A. Pyarnpuu. Space Res., Vol. 11, 1971.

7. Zmiyevskaya, G. I., M. Ya. Marov and A. A. Pyarnpuu. Space Res., Vol. 12, 1972.

8. Pyarnpuu, A. A. and G. I. Zmiyevskaya. Fluid Dyn. Trans., Part 2, Vol. 6, 1971.

9. Zmiyevskaya, G. I. Trudy 3-y Vses. konf. po dinamike razrezhennovo gaza (Works of the Third All-Union Conference on Rarified Gasdynamics). Novosibirsk, 1969.

10. Zmiyevskaya, G. I. Fluid Dyn. Trans., Part 2, Vol. 6, 1971.

N74-28297

MODIFICATIONS OF JACCHIA'S STATIC DIFFUSION MODELS OF THE UPPER ATMOSPHERE

M. A. Degtyarev

ABSTRACT. Modifications of Jacchia's static diffusion models of the upper atmosphere are obtained. Algorithms for determining the density of the upper atmosphere, which satisfy the conditions of compactness and speed, are constructed with the help of these modifications. The suitability of considering various types of density variations is evaluated for problems in predicting AES motion. The density and temperature profiles of Jacchia's static models are compared.

A model of the upper atmosphere of the Earth, which describes /131 as completely and accurately as possible its properties, is necessary for predicting AES motion or determining its existence time. For such problems, it is important to know the values and behavior of one of the structural parameters of the upper atmosphere, its density. Such factors, as the speed and compactness of the algorithm for calculating the density, acquire great value for the problem of predicting AES motion.

At present, the models of the upper atmosphere most widespread and developed in aeronomy are the CIRA-65 model [1] and Jacchia's static diffusion models [2, 3]. But both the international standard model of the upper atmosphere CIRA-65, which is represented in tabular form, and Jacchia's models, which are given in the form of differential equations, do not satisfy the requirements of compactness and speed.

In order to eliminate these deficiencies of Jacchia's models, modifications of Jacchia's static diffusion models of the upper atmosphere [2, 3] have been obtained. Following Jacchia, we introduce the notation for his models, for convenience of examination. The model produced in 1965 [2] is the J65 model and the model proposed in 1970 [3] is the J70 model.

1. Modification of the J65 Model of the Upper Atmosphere

The diffusion equation in the case of Jacchia's static models [2, 3] (assuming diffusion equilibrium of the atmospheric components) for each i^{th} component of the atmosphere has the form

$$\frac{dn_i}{n_i} = -\frac{m_i g(z)}{kT(z)}dz - \frac{dT}{T(z)}(1+\alpha_i) \tag{1}$$

and a solution of the form

$$n_i(z) = n_i(z_0)\left\{\left[\frac{T(z_0)}{T(z)}\right]^{1+\alpha_i}\exp\left(-\int_{z_0}^{z}\frac{m_i g(z')}{kT(z')}dz'\right)\right\}, \tag{2}$$

where n_i is the concentration; m_i is the molecular or atomic mass; k is the Boltzmann constant; z is the altitude above the surface of the Earth; α_i is the thermal diffusion coefficient; g(z) is the gravitational acceleration.

Cook [4], by using the results of Bates [5] and Walker [6] /132
for the temperature profile $T_K(z)$, integrated Equation (1) and obtained a solution of the form

$$n_i(z) = n_i(z_0)\left\{\frac{1-a}{1-a\exp(-\tau\zeta)}\right\}^{1+\alpha_i+\gamma_i}\exp(-\tau\gamma_i\zeta), \tag{3}$$

where the "quasigradient" τ and the temperature profile equal

$$\tau = \frac{1}{T_\infty - T(z_0)} \left(\frac{dT}{dz}\right)_{z=z_0}, \quad T_K = T_\infty \{1 - a \exp(-\tau\zeta)\},$$

the geopotential altitude ζ is given by the relation

$$\zeta = \frac{(z - z_0)(R + z_0)}{(R + z)},$$

and the coefficients equal

$$\gamma_i = \frac{m_i g(z_0)}{\tau k T_\infty}, \quad a = 1 - \frac{T_K(z_0)}{T_\infty},$$

R is the radius of the Earth; T_∞ is the exospheric temperature.

Cook took the temperature gradient at the lower boundary z_0 = 120 km from the J65 model

$$\left(\frac{dT}{dz}\right)_{z=z_0} = [T_\infty - T(z_0)]\, S, \tag{4}$$

where

$$S = 0{,}0291 \exp\left(-\frac{1}{2} X^2\right), \quad X = \frac{T_\infty - 800}{750 + 1{,}722 \cdot 10^{-4} (T_\infty - 800)^2}. \tag{5}$$

The boundary conditions at the altitude z_0 = 120 km and the values of the constants were also taken from the J65 model.

The assertion by Cook that his solution (3) of the diffusion Equation (1) differs from Jacchia's numerical solution by no more than 2% in the interval of altitude 120 — 1000 km was verified by checking.

A more precise solution of the diffusion Equation (1) is proposed in the form

$$n_i(z) = n_i(z_0)\left\{\left[\frac{T(z_0)}{T(z)}\right]^{1+\alpha_i+\nu_i}\exp\left[-\gamma_i\tau\frac{(z-z_0)(R+z_0)}{(R+z)}\right]\right\}, \quad (6)$$

where the temperature profile is given by the expression

$$T(z) = T_\infty - [T_\infty - T(z_0)]\exp[-\tau(z-z_0)], \quad (7)$$

and the coefficients equal /133

$$\gamma_i = \frac{m_i g(z_0)}{\tau k T_\infty}, \quad \tau = S,$$

S being determined by the relation (5). We note that the temperature profile T(z) (7) is that of the J65 model. Walker [6] made a comparison of the temperature profile of Cook's model $T_K(z)$ and of the J65 model (7). He found that these temperature profiles differ by less than 1% over the whole range of altitudes and temperature under consideration.

The atmospheric density ρ is determined by an expression of the form

$$\rho = \sum_i n_i(z) m_i.$$

The solution (6) is an approximate analytic solution of the diffusion Equation (1). Comparison of the solution (6) with Jacchia's numerical solution has shown that the difference in densities does not exceed 1% in absolute value for the intermediate and maximum temperatures T_∞ = 1200 and 2100° K (for the altitude interval 200 — 1000 km). For the minimum temperature T_∞ = 650° K, this difference does not exceed 2% in absolute value. The following results are obtained for the altitude interval 120 — 200 km: the difference in densities does not exceed 1, 1.6, and 1.7% for T_∞=650, 1200, and 2100° K, respectively.

Thus, an approximate analytic solution (6) is obtained, which gives a difference from Jacchia's numerical solution two times smaller than from Cook's solution for maximum and intermediate levels of solar activity. This decrease in approximation error is due to taking the precise temperature profile of the J65 model.

The following model of the upper atmosphere is constructed. The density profile is given with the help of the solution (6) taking (5) into account. Variations of the density ρ of the upper atmosphere are taken into account with the help of the variations of the exospheric temperature given by the empirical equations of the J70 model. To decrease the number of free parameters of the model, it is proposed to take into account the following variations of density of the upper atmosphere:

— variations related to the 11-year solar cycle;

— diurnal variations;

— semiannual variations [4, 7].

We note that the diurnal variations of density and exospheric temperature depend on the solar hour angle, geographic latitude and declination of the Sun.

The following algorithm for determining these variables is proposed.

As is known [8, 9], the solar hour angle H and solar declination δ_C equal: /134

$$H = \alpha_0 - \alpha_C$$

$$\delta_C = \operatorname{arctg}\left\{\operatorname{tg} 23,^\circ 5 \sin\left[\frac{2\pi}{365}(d - 80)\right]\right\},$$

where α_0 is the right ascension of the AES, α_C is the right ascension of the Sun.

On the other hand, α_C is given by the formula [9]

$$\alpha_C = \arcsin\left(\frac{\delta_C}{23,^\circ 5}\right).$$

Let the AES position in space be defined by the osculating elements (p, q, k, i, Ω, u), then, in accordance with [10], the right ascension of the AES is determined by the formula

$$\alpha_0 = \Omega + \operatorname{arctg}(\operatorname{tg} u \cdot \cos i),$$

where Ω is the longitude of the ascending node of the orbit; i is the orbital inclination; u is the argument of the latitude.

The altitude z above the surface of the Earth and the geographic latitude are determined from the following expressions:

$$z = r - a(1 - \varepsilon \sin^2 u \cdot \sin^2 i)$$

and

$$\varphi = \arcsin(\sin i \cdot \sin u),$$

where r is the distance from the center of the Earth to the satellite; a is the semimajor axis of the international terrestrial ellipsoid; ε is the flattening of the Earth.

The distance r is determined by the known expression

$$r = \frac{p}{1 + q\cos u + k \sin u},$$

where p is the focal parameter; q, k are the components of the Laplace vector [11].

To satisfy the requirements of compactness and speed of the algorithm for determining the density and to decrease the number of free parameters in the model of the upper atmosphere, such density variations were not considered, as the seasonal-latitude variation of ρ in the lower thermosphere — which is easily taken into account by the formulas of the J70 model and the value of which in our estimations does not exceed 3% of the total density of the upper atmosphere for an altitude of about 200 km — rapidly decreases with increasing altitude and equals zero above 300 km. The seasonal-latitude variation of the helium concentration (or the so-called winter helium bulge) [3, 12] was also not taken into account, but should be considered for AES in /135
polar orbits for altitudes above 500 km.

Since there is no sufficiently good prediction of the diurnal variations of geomagnetic and solar activity, then it is obviously not possible to take them into account in practice, unless one uses the relations for them recommended by the J70 model. Thus, these variations were also not taken into account.

2. Modifications of the J70 Model of the Upper Atmosphere

In recent years, works have appeared (for example, [13 — 15]) on determining the density of the upper atmosphere on the basis of studying the parameters of AES drag for altitudes below 200 km.

Jacchia, considering the deficiencies of the J65 model (examined in detail by him in [16]) and the timeliness of the altitudes below 200 km, proposed the static diffusion model of the upper atmosphere J70 [3], which represents more reliably the density at altitudes below 200 km and the densities in the whole altitude interval under consideration during the solar activity maximum.

For this purpose, the lower boundary conditions in the J70 model were specified at an altitude of 90 km (instead of 120 km in the J65 model), a higher ratio $n(O)/n(O_2)$ at 120 km than in the J65 model was taken, and a new atmospheric component — argon — was introduced. The temperature profile T(z) and the temperature gradient G_x (at an altitude z_x = 125 km) were given in the J70 model by the following

$$T(z) = T_x + A \operatorname{arctg}\left\{\frac{G_x}{A}(z - z_x)[1 + B(z - z_x)^n]\right\} \tag{8}$$

and

$$G_x = 1{,}9\frac{T_x - T_0}{z_x - z_0}, \tag{9}$$

where

$$A = \frac{2}{\pi}(T_\infty - T_x),$$

and the coefficients equal: T_0 = 185° K, n = 2.5, B = $4.5 \cdot 10^{-6}$ (for z in kilometers), the value of the temperature T_x at the altitude z_x equaling T_x = 444.3807 + 0.02385 T_∞ − 392.8292 exp (0.0021357 T_∞).

The diffusion Equation (1) and its solution (2) were used in the range of altitudes under consideration. To satisfy the conditions cited above on the compactness and speed of the algorithm for determining the density, we will construct a number of models of the upper atmosphere, which approximate the numerical solution of the J70 model, and compare them.

Model I - Modification of Cook's Model. Cook's temperature profile $T_K(z)$ [4] and the exact solution (3) of the diffusion Equation (1) are used, taking the parameter τ in this case equal to /136

$$\tau = \frac{G_x}{T_\infty - T_x}. \qquad (10)$$

Model II - Modification of the J70 model. The approximate analytic solution (6) of the diffusion Equation (1) is used, the temperature profile is taken from the J70 model (8), and the parameter τ is determined from the relation (10).

Model III - Approximate analytic solution of the J70 model. The approximate analytic solution (6) and the temperature profile (8) are used, the parameter τ is taken as

$$\tau = \frac{2}{\frac{1}{S} + \frac{T_\infty - T_x}{G_x}},$$

where S is taken from (5).

Model IV - The approximate analytic solution (6) with the temperature profile (8) is used, and the parameter τ = S, where S is obtained from the relation (5).

A comparison of the density profiles of Models I — IV with the numerical density profiles (for the same exospheric temperatures) obtained by Jacchia [3] was carried out for four values of exospheric temperatures T_∞ equaling 2000, 1700, 1200, 600° K, which encompass the whole range of variation of T_∞, and for the altitude interval 125 — 500 km, most interesting from the practical point of view.

The lower boundary conditions at the altitude z_x = 125 km for each exospheric temperature T_∞ from the four under consideration were taken from the tables of the J70 model.

COMPARISON OF THE MODEL PROFILES OF DENSITY AND TEMPERATURE WITH THE PROFILES OF DENSITY AND TEMPERATURE OF THE J70 MODEL

$T\infty$,°K	Model	$\max_z\left(\frac{\rho_{70}-\rho}{\rho_{70}}\right)100\ \%$		$\max_z\left(\frac{T_{70}-T}{T_{70}}\right)100\ \%$	
		(200, 500 km	(125, 200 km	(200, 500 km	(125, 200 km
2000	I	+20	− 4	+10	+9
	II	+25	+20	0	0
	III	+10	± 5	0	0
	IV	−10	±15	0	0
	J65	+30	+25	± 1	−5
1700	I	+13	− 3	+ 6	+7
	II	+18	+15	0	0
	III	+ 2	− 4	0	0
	IV	−18	−18	0	0
	J65	+15	+18	− 4	−8
1200	I	+ 5	± 4	+ 1	+4
	II	+ 5	+ 8	0	0
	III	−10	− 7	0	0
	IV	−25	−30	0	0
	J65	± 5	± 5	− 6	−7
600	I	− 5	± 3	− 2	−2,5
	II	−11	+ 6	0	0
	III	± 5	+ 8	0	0
	IV	+10	+16	0	0
700	J65	± 8	−16	− 2	±6

The results of the comparison are presented in the table, where the quantities

$$\max_z\left(\frac{\rho_{70}-\rho}{\rho_{70}}\right)100\,\% \quad \text{and} \quad \max_z\left(\frac{T_{70}-T}{T_{70}}\right)100\,\%$$

give the deviations of the model values of density ρ and temperature T from the profile ρ_{70} and from the temperature profile T_{70} obtained by the numerical solution of the J70 model by Jacchia himself.

By using the relations of the J70 model describing the semi-annual, diurnal, and solar cycle variations, the maximum values of the exospheric temperatures T_∞ are evaluated for three levels

of solar activity considering average geomagnetic conditions. For the minimum solar activity level $\bar{F}_{10.7} = 70$, the exospheric temperature $T_\infty \simeq 900°$ K, for the intermediate level $\bar{F}_{10.7} = 160$, $T_\infty \simeq 1300°$ K, and for the maximum level, $\bar{F}_{10.7} = 240$, $T_\infty \simeq 1700°$ K.

Thus, the temperature interval (600 — 1700°) encompasses /137
the whole range of variation of solar activity, if we do not take into account the geomagnetic disturbances and diurnal variations of solar activity.

Examination of the results in the table lead to the following conclusions. For the altitude range (200 — 500 km), the densities of the J70 model exceed the densities of the J65 model for maximum exospheric temperature $T_\infty = 2000°$ K and for high exospheric temperature $T_\infty = 1700°$ K by 30 and 15%, respectively.

Although the temperature profiles of these models differ by no more than ±1 and -4%, respectively, increasing the concentration ratio $n(O)/n(O_2)$ at 120 km in the J70 model has also led to the density divergence discussed above. For intermediate and minimum solar activity, the deviations of the model density profiles (in the case of J65) do not exceed 5 and 8%, respectively.

For the range of altitudes (200 — 500 km) and in the /138
temperature interval (600 — 1700° K), Model III gives a maximum approximation error, not exceeding 10% in absolute value, and Model I — a maximum approximation error no more than 13% in absolute value, this error reaching the maximum for $T_\infty = 1700°$ K. Model I in the same altitude range and for $T_\infty = 1200$ — 600° K gives a maximum approximation error no more than 5%. Model I — maximum error of 4% — and Model III — maximum error of 8% —

give a good approximation for the altitude range (125 — 200 km) and for the temperature interval T_∞ = 1700 — 600° K.

As is well known, a large portion of the data (according to [17] about 90%) on density is obtained from AES drag. Therefore, both in the case of the J65 model and evidently in the case of the J70 model, Jacchia used density data obtained from AES drag in constructing these models, in which case the errors in the densities (standard deviation) is about ±10% [13 — 15, 18, 19]. Consequently, the approximation errors given by models I and III are probably within the error limits (standard deviations) of the densities of the J65 and J70 models.

The use of the following constructed models is recommended for predicting AES motion: Model III for the altitude interval 200 — 500 km and Model I for the altitude interval 125 — 200 km with consideration of the semiannual, diurnal and solar cycle variations (for an average level of geomagnetic activity).

The use of the obtained modification of the J65 model, in which case the lower boundary conditions are specified simply, is also recommended for the altitude range 200 — 1000 km. The model values of density given by it have been verified by many authors in comparison with density data from AES drag. For example, the comparison carried out by Marov [20] of the density values obtained by him (during the intense solar activity minimum) from Soviet AES drag with the J65 model for T_∞ = 700° K indicated good agreement, which would be worse with the J70 model.

The author thanks F. D. Petrovskiy for interest in the work.

REFERENCES

1. CIRA-1965. COSPAR International Reference Atmosphere. Amsterdam, North Holland Publ. Co., 1965.

2. Jacchia, L. G. Smithsonian Contribs. Astrophys., Vol. 8, 1965, p. 215.

3. Jacchia, L. G. Smithsonian Astrophys. Spec. Rept., No. 313, 1970.

4. Cook, G. E. Ann. Geophys., Vol. 25, No. 2, 1969, p. 451.

5. Bates, D. R. Proc. Roy. Soc., Vol. A253, 1959, p. 451.

6. Walker, J. C. J. Atmos. Sci., Vol. 22, No. 4, 1965, p. 462.

7. Jacchia, L. G., et al. Smithsonian Astrophys. Obs. Spec. Rept., No. 265, 1968. /139

8. Scott, D. W. Planet. Space Sci., Vol. 15, No. 12, 1967, p. 1895.

9. Stubbe, P. J. Atmos. and Terrest. Phys., Vol. 32, No. 5, 1970, p. 865.

10. El'yasberg, P. Ye. Vvedeniye v teoriyu poleta ISZ (Introduction to the Theory of AES Flight). Moscow, "Nauka" Press, 1965.

11. Yevtushenko, Yu. G., et al. Dvizheniye iskusstvennykh sputnikov v gravitatsionnom pole Zemli (Artificial Satellite Motion in the Earth's Gravitational Field). Moscow, Computer Center AN SSSR Press, 1967.

12. Jacchia, L. G. and J. W. Slowey. Smithsonian Astrophys. Obs. Spec. Rept., No. 242, 1967.

13. King-Hele, D. G. and J. Hingston. Planet. Space Sci., Vol. 16, No. 5, 1968, p. 675.

14. King-Hele, D. G. and J. Hingston. Planet. Space Sci., Vol. 15, No. 12, 1967, p. 1883.

15. King-Hele, D. G. and D. W. C. Walker. Planet Space Sci. Vol. 17, No. 8, 1969, p. 1539.

16. Jacchia, L. G. Space Res., Vol. 9, 1969.

17. Moe, K. AIAA Paper, No. 69 - 50, 1969.

18. Roemer, M. Ann. Geophys., Vol. 25, No. 2, 1969, p. 419.

19. King-Hele, D. G. and D. W. C. Walker. Planet Space Sci., Vol. 17, No. 12, 1969, p. 2027.

20. Marov, M. Ya. Kosmicheskiye issledovaniya, Vol. 6, No. 1, 1968, p. 110.

Translated for National Aeronautics and Space Administration under contract No. NASw-2483 by SCITRAN, P. O. Box 5456, Santa Barbara, California, 93108.